NASA TECHNICAL MEMORANDUM

NASA TM X-73489

NASA TM X-73489

SPACE-TO-EARTH POWER TRANSMISSION SYSTEM

by Grady H. Stevens and Richard Schuh
Lewis Research Center
Cleveland, Ohio 44135
November 1976

1. Report No.	2. Government Accession No.	3. Recipient's Catalog No.
NASA TM X-73489		

4. Title and Subtitle	5. Report Date
SPACE-TO-EARTH POWER TRANSMISSION SYSTEM	6. Performing Organization Code

7. Author(s)	8. Performing Organization Report No.
Grady H. Stevens and Richard Schuh	E-8885
	10. Work Unit No.

9. Performing Organization Name and Address	11. Contract or Grant No.
Lewis Research Center National Aeronautics and Space Administration Cleveland, Ohio 44135	13. Type of Report and Period Covered
	Technical Memorandum
12. Sponsoring Agency Name and Address	14. Sponsoring Agency Code
National Aeronautics and Space Administration Washington, D.C. 20546	

15. Supplementary Notes

16. Abstract

A preliminary analysis was conducted to establish the requirements of a space-to-earth microwave power transmission system. The need for accurate phase control on the transmitter was established and methods for assessing the impact of power density and thermal constraints on system performance were demonstrated. Potential radio frequency interference was considered. The sensitivity of transmission system scale to variations in power source, transportation and orbital fabrication and assembly costs was also determined.

17. Key Words (Suggested by Author(s))	18. Distribution Statement
Power transmission Microwaves Solar power Space industrialization	Unclassified - unlimited

19. Security Classif. (of this report)	20. Security Classif. (of this page)	21. No. of Pages	22. Price*
Unclassified	Unclassified		

* For sale by the National Technical Information Service, Springfield, Virginia 22161

SPACE-TO-EARTH POWER TRANSMISSION SYSTEM

by Grady H. Stevens and Richard Schuh

Cleveland, Ohio

ABSTRACT

A preliminary analysis was conducted to establish the requirements of a space-to-earth microwave power transmission system. The need for accurate phase control on the transmitter was established and methods for assessing the impact of power density and thermal constraints on system performance were demonstrated. Potential radio frequency interference was considered. The sensitivity of transmission system scale to variations in power source, transportation and orbital fabrication and assembly costs was also determined.

SPACE-TO-EARTH MICROWAVE POWER TRANSMISSION SYSTEM

CONTENTS

SPACE-TO-EARTH MICROWAVE POWER TRANSMISSION SYSTEM

by Grady H. Stevens and Richard Schuh

Lewis Research Center

Cleveland, Ohio

SUMMARY

A preliminary analysis was conducted to establish the requirements of a space-to-earth microwave power transmission system. The need for accurate phase control on the transmit antenna was established. A total rms phase error, from all causes, of no more than 10 degrees is required to insure scattering losses will be less than 3 per cent.

Calculations were performed to determine the sensitivity of the system to variations in geometry and antenna illumination. These analyses included variations of the transmitter and receiver diameters, beam interception efficiency and illumination taper. The impacts on system design of constraints imposed by microwave power density and antenna heat dissipation limitations were also determined. In addition, the sensitivity of microwave system scale to variations in power source, transportation and orbital fabrication and assembly costs was determined using values of cost parameters obtained from a literature survey.

The RFI impact was assessed, including the effects of DC-RF converter noise emissions and harmonic radiation. It was shown

STAR category 07

that with suitable filtering, an exclusion band can be defined outside of which interference is unlikely for other spectral users. The impact of harmonic radiation is more uncertain than that of the noise emissions since the assessment is very sensitive to various assumptions used in conducting the analyses. Typically, 10-40 db of rejection of each harmonic will be necessary to prevent interference with satellite-to-earth communications. This is in addition to 80 db of rejection assumed to be provided by the fundamental filter and waveguide circuitry.

1.0 INTRODUCTION

It has been demonstrated that when a receive antenna fills a significant portion of the main beam of a transmitter, efficient transfer of power can occur. Tests at Raytheon (Waltham, Mass.) and at JPL (Goldstone) have demonstrated high efficiency transmission and long range transmission respectively. Raytheon has demonstrated a DC-DC link efficiency of 54 per cent while recovering 495 watts DC (reference 1). A recent test at the NASA-JPL complex at Goldstone, Calif. demonstrated the transfer of power over a range of 1.54 Km. The NASA-JPL test realized a recovery of up to 30.4 Kw (reference 2).

The tests noted above were small scale tests intended to make preliminary evaluations of the feasibility of long distance power transmission by microwaves on a large scale. One application of this technique would be the collection and conversion of solar energy at synchronous orbit and transmission of this collected energy to earth via microwave link as in the Satellite Solar Power Station (reference 3). There are also possible terrestial applications including underground waveguide links and above ground point-to-point free space links (references 4,5). Another application is the use of a reflector in geosynchronous orbit to relay power from one point on earth to another (reference 6).

The Satellite Solar Power Station (SSPS) concept was

originated by Peter Glaser of A. D. Little, Inc. This concept makes use of photovoltaic solar converters for energy conversion. A study of this concept was conducted under contract NAS 3-16804. The results were published as NASA CR-2357 (reference 3). The study focused primarily on the feasibility of constructing and controlling large structures in space and the feasibility of obtaining very low cost, light weight, and efficient photovoltaic converters. In addition, preliminary estimates were made of the requirements of the microwave link.

The results of the SSPS study indicated that the orbital system would weigh on the order of 10 million Kg and that the appropriate antenna sizes for reasonable interception efficiency were 1 Km and 7.4 Km for the transmitter and receiver respectively. The study also indicated that a space-to-earth power transmission system could be made competitive with terrestial systems, given suitable technology developments.

Subsequently, an effort was undertaken to further define the Microwave Power Transmission System (MPTS). The study reported herein and an effort undertaken by Raytheon (reference 7) focused on the microwave link. However, in order to optimize the MPTS in the context of the application, it was necessary to include additional SSPS parameters in the analysis. Estimates of prime power costs and weights were taken from references 8 and 9. The impact of transportation and orbital assembly cost was examined in a parametric fashion with reference values being taken from reference 9.

2.0 MPTS SYSTEM MODEL

2.1 TRANSMITTER

A typical geometry arrangement for a space-to-earth microwave power transmission system is shown in Figure 1. As was shown in the SSPS study (reference 3) and verified in this study, the required transmitter diameter is nominally 1 Km and the receiver is sized to intercept nominally 90 per cent of the beam power. More beam interception can be realized by increasing the transmitter or receiver diameter or both. As will be shown later there is no cost advantage to using beam interception efficiencies beyond 90-95 per cent.

The SSPS study also indicated good aperture efficiency and good DC-RF conversion efficiency could be obtained with the combination of slotted waveguide radiating elements and integral amplitrons as converters. In this study, several alternatives to the slotted waveguide were examined. Table I lists the options considered. Of those listed, the combination suggested in the SSPS study seems to be the best choice in the frequency range of 2-3 Ghz. The circularly polarized system would likely be the best choice if the transmission frequency were less than 2 Ghz. In addition aspects of the illumination function, phase control, energy distribution on the transmit antenna, losses, and RFI impact were examined to establish sensitivity of the system to changes in these parameters. Also, critical areas in need of

technology development were identified.

2.1.1 ILLUMINATION FUNCTION

In regard to antenna illumination, it is well known that the field pattern at a receive site can be somewhat arbitrarily shaped by a suitable choice of the transmitter illumination function. Since the purpose of MPTS is the transmission of power and since the fraction of the beam intercepted by the receiver significantly affects overall system efficiency, one could pose the following question. Given a particular transmit/receive geometry, what should the transmitting antenna illumination be in order to maximize the interception at the receive site? This particular question has been resolved by others (references 10,11,12) for a lossless, unconstrained antenna system.

Generally, these optimal illuminations have a spherical phasing to focus the transmitted beam on the receiver and they have an amplitude distribution which depends on transmit/receive geometry. For typical geometries associated with space-to-earth power transmission, the Fresnel approximation is valid. Consequently, the spherical focusing factor can be approximated quite accurately by a quadratic focusing factor. Therefore, for the MPTS the optimal illumination function, $g_t(r)$, would have the form

$$g_t(r) = f(r) \exp\left(j\frac{\pi r^2}{\lambda z}\right) \qquad (2.1.1)$$

where r is the radial position of interest, f(r) is the appropriate amplitude factor and the exponential term is the quadratic focusing factor (reference 13).

Since the focusing term is already specified, one need only be concerned with identifying a suitable amplitude function, f(r). This study made use of the method developed in reference 12 to obtain f(r).

These optimal illuminations can conveniently be described with the use of the geometric parameter given by,

$$\tau = \frac{\sqrt{A_t A_r}}{\lambda z} \qquad (2.1.2)$$

where A_t and A_r are the transmitter and receiver aperture areas respectively, z is the separation of the two antennas and λ is the wavelength of the microwave radiation.

Generally, for small τ, the receive antenna intercepts only a small portion of the main beam. Therefore, the best collection efficiency is obtained when the axial power density at the receive site is a maximum. This maximum occurs for uniform illumination on the transmit antenna. In this region of τ, the optimal amplitude illuminations are (reference 12)

$$f(r) \doteq 1 - \frac{(r\tau/R_t)^2}{2}, \quad \frac{r}{R_t} \leq 1 \qquad (2.1.3)$$

where R_t is the radius of the transmitter. The fraction of

available energy enclosed by the receive antenna is

$$\eta(\tau) \doteq \tau^2 \tag{2.1.4}$$

For large τ, the receive antenna fills or nearly fills the main beam and possibly the near sidelobes. For this case, the best collection efficiency is obtained with a gaussian illumination (reference 12) and in this range of τ,

$$f(r) \doteq \exp\left[-\tau\left(\frac{r}{R_t}\right)^2\right] \tag{2.1.5}$$

and the fraction of collected energy is,

$$\eta(\tau) \doteq 1 \tag{2.1.6}$$

For intermediate values of τ, the optimal illumination ranges between the quadratic form (2.1.3) and the guassian form (2.1.5).

Therefore using methods such as that in reference 12 one can obtain the minimum value of τ and the corresponding unique illumination which will provide a given interception efficiency.

Note that these optimal illuminations are obtained without consideration of physical constraints. As a result, these illuminations can lead to systems with unrealizable requirements. For example, consider the trend of system scale as a function of

interception efficiency shown in Figure 2. If one were willing to build large enough antennas such a system can be made to arbitrarily approach unity interception. To the extent that system scale reflects cost, there may be severe cost penalties associated with high beam interception.

As another example, consider the peak power density trend on the transmitter. The growth in peak power density relative to average power density is shown as a function of beam efficiency in Figure 3. As will be shown in section 2.3.3 thermal and other constraints place an upper limit on this peak density.

Inclusion of constraints such as these can lead to systems with parameters significantly different than those disregarding constraints. Therefore, it is necessary to provide a means of analyzing the impact of departing from the optimal illuminations whenever it is desired to accommodate constraints.

There are a variety of ways one could provide for such a departure. In reference 7 the impact of a departure was assessed by simply altering the decay rate and truncation point of a gaussian illumination function. In this study, the method of reference 12 was used to establish the optimal illuminations for nominal interceptions and perturbations were obtained by varying the receiver antenna size from the unconstrained optimum and calculating the new interception efficiency. This method provided results similar to reference 7 and had the advantage that the illumination function was optimal for at least one

selection of system geometry even for uniform illumination.

For convenience in plotting, the new combination of antenna sizes were normalized using equation 2.1.2. Illumination functions were selected from the optimal set which exhibited edge power densities of 0,5,10, and 15 db below the peak power density. These corresponded to interception efficiencies of 0,68,90, and 96 per cent (using optimal geometries) respectively. Higher tapers (ratio of peak density to edge density) were considered but the results are not included here since the system costs for the higher tapers were unfavorably high.

Figure 4 shows the trends in system scale with interception efficiency for various fixed tapers. Note that at high interception efficiency, very dramatic increases in τ may be required to realize a given interception efficiency if a suitable taper is not used. These contours are similar to the Goubau relation in Figure 2, however they differ in that the taper is fixed for each contour whereas the taper varies continuously along the Goubau relation. The need for this display will become more apparent when the cost model is introduced in section 2.3.

Figure 5 shows contours of constant efficiency as a function of taper. Also shown is the locus of minimum τ as a function of taper. This locus, τ_{opt} , is an alternative display of the Goubau relation previously displayed in Figure 2. At low interception efficiency the τ required for a given interception efficiency is relatively insensitive to taper. At high

interception efficiency, 98 per cent and above, the required geometry factor, τ, becomes sensitive to taper and increases dramatically if the taper is less than that required for optimal illumination. At intermediate efficiency, 80-96 per cent, tapers significantly less than optimum can be used and the actual required τ would not be much different than τ_{opt}.

By reducing the taper below optimum an increase in throughput power can be realized for a fixed peak transmitter power density which may result in a decrease in the cost of delivered ground power. Therefore, although a selected illumination is nonoptimal with respect to antenna sizes, it may be optimal in the sense that power costs are a minimum within the constraint framework. In this study, when such an illumination is identified it will be designated a cost effective illumination.

In addition to the previous comments regarding a cost effective choice of τ, it should be made clear that many choices of transmit/receive geometries will yield the same value of and hence the same interception efficiency. In section 2.3 the trade between the transmit antenna size and the receive antenna size is developed in detail and will not be covered here.

2.1.2 FOCUSING AND PHASE CONTROL

It was mentioned in section 2.1.1 that a specific phase distribution was required in order to focus the transmitted power

at the receive site. Not mentioned, but implicit in the requirement for focusing, is the need for additional phase adjustment to steer the beam onto the target. Of course, a portion of this last task can be accomplished mechanically. However, the final steering will require accuracies of an arc-second or less. At this time, it seems more appropriate to accomplish this last task electronically.

Figure 6 shows the per cent loss of recovered power as a function of pointing error of the main beam. This data was calculated by allowing the beam to be offset slightly and performing a two dimensional integration to establish the change in recovered power. Obviously, this pointing precision can be relaxed somewhat by oversizing the receive antenna. However, this could prove to be very expensive since the increment in area at large radii for a small change in radius is large.

There are proven methods for accomplishing both the steering and focusing task simultaneously (references 15, 16,17). For the purposes of this study, these methods will be grouped into two classes, adaptive and retro-directive. These terms have been used interchangeably in the literature but herein are distinguished as specified below.

The adaptive class will consist of all those methods that perform an iteration on the improvement of antenna performance. That is, at regular intervals, the antenna performance and state are measured or estimated and adjustments are made to maximize

the antenna performance given the current antenna state.

The retro-directive class will consist of all those methods that perform a conjugation and amplification of an incident reference beam. That is, an incident wavefront is reversed in direction and curvature and also increased in power level. This method instantaneously corrects for antenna deformations and motion and it can compensate for some atmospheric disturbances (references 15,16).

Retro-directive methods have been examined independently by both JPL and Raytheon (reference 7) for feasibility as a prime phase control method in a MPTS type system. Raytheon also considered adaptive methods, as possible competitors for the prime phase control function and also as a backup system in case of failure of the retro-directive system.

The key to the retro-directive approach is the precise distribution of a phase reference to all the subarrays of the transmit antenna. JPL is investigating one distribution method that essentially measures and compensates for changes in path length of interconnecting phase reference distribution buses. This method is similar to that demonstrated as part of the supersynthesis radio telescope of the Dominion Radio Astrophysical Observatory (reference 18). That demonstration achieved phase control to an accuracy of 1 degree rms over a baseline of 600 meters. Therefore, this method has promise but more in-depth analysis and experimentation is required to

determine the performance of the retro-directive and the phase distribution systems operating in concert.

From the point of view of beam acquisition, the retro-directive approach seems to be the only realistic method for performing this function. The adaptive approach requires the beam to be within a sensor field in order to perform the adaptive task. In start-up (obviously at low beam power), the main beam might only be pointed generally in the direction of the receive site and will likely be very broad. Given enough time and computational capability it would be possible to acquire the beam in the adaptive mode. On the other hand, the retro-directive method will provide almost instantaneous beam acquisition (again, at low beam power). After acquisition the retro-directive system could remain functional and the adaptive system brought on line. The adaptive system could then act as a parallel system with the goal of improving performance or as a stand-by in case of failure in the retro-directive system.

Another possibility with the retro-directive scheme is the use of multiple beams (reference 15). This would allow simultaneous distribution of power to several locations, or it might be used to obtain beam shaping at one location.

In section 2.3 it is shown that when the transmitter is thermally limited, the specific cost of the system can actually be made to decrease by simultaneously increasing the transmitter diameter and power throughput. This effect is bounded, however,

by the maximum allowable peak density at the receiver. Using multiple beams would enable the use of larger transmitters since the peak density of the individual beams could be set below a specified level and the total transmitted power could be several times more than that permissible with a single beam.

Such methods have not been examined in this study but they could be a point of departure in any future efforts.

2.1.3 ENERGY DISTRIBUTION ON TRANSMITTER

In section 2.1.1 it was shown that the optimal illuminations have a large peak power density requirement at high interception efficiency. The maximum possible power density on the transmit antenna depends on several factors. In this study, the DC-RF converters were assumed to be passively cooled. Hence, the peak RF power density cannot exceed that obtained when the converters are packed to the point where the thermal radiators touch.

Using equation (2.1.1) the RF power distribution can be written as

$$p_t(r) = p_t(0)\, f^2(r) \qquad (2.1.7)$$

where $p_t(0)$ is the peak power and f(r) is normalized so that

$$f(0) = 1$$

Figure 7 shows how the RF power is distributed for a typical

MPTS geometry. Various tapers are included to display the effect of this variable. This figure was plotted for a constant power throughput. Also indicated are the maximum power densities obtained when the thermal radiators of the DC-RF converters touch. This maximum achievable RF power density is a function of thermal radiator size which is in turn a function of the heat rejection requirements and the assumption of passive thermal control.

In reference 7 this maximum RF power density, designated k_{tube}, is given for passively-cooled DC-RF converters:

$$k_{tube} = \begin{cases} 21{,}000 \text{ watts/m}^2 & \text{amplitron} \\ 14{,}000 \text{ watts/m}^2 & \text{klystron} \end{cases} \qquad (2.1.8)$$

In the klystron the collector can be separate from the tube body. Such a geometry has higher temperature capabilities than one where the collector is integral to the tube as in the amplitron. From this, one might expect the packing density to be greater for the klystron, since the collector radiator can be smaller for the same thermal rejection requirement. Although this point is correct, preliminary calculations (reference 7) indicate the packing density for the klystron to be smaller. The reason for this is that the dominant thermal limitation is not the collector but the output cavity. The waste heat generated by beam interception and RF power dissipation as well as heat radiated toward the tube body from the collector, combine to

place a requirement for an additional radiator to cool the tube body which is much larger than the collector radiator. This larger radiator is then responsible for the lower packing density for the klystron.

It is apparent from Figure 7 that decreasing the taper will decrease the peak power density and will therefore allow a corresponding increase in power throughput. To be cost effective, the costs incurred by increasing γ (to maintain interception) should be more than compensated for by the revenues obtained with the increased throughput power, i.e. where

$$\frac{\partial Cost}{\partial \gamma}\frac{\partial \gamma}{\partial Taper} < \left|\frac{\partial Cost}{\partial P_{RDC}}\frac{\partial P_{RDC}}{\partial Taper}\right| \qquad (2.1.9)$$

where P_{RDC} is the delivered ground power.

Alternatively, one could simply increase the transmitter diameter. For a fixed peak power density and taper the throughput power would increase as the square of the diameter. To be cost effective, the costs incurred by increasing the transmitter diameter must be more than offset by the revenues obtained with the increased throughput power and the decrease in receiver cost (receiver diameter is inversely related to transmitter diameter). In terms of the system derivatives, this is stated as,

$$\frac{\partial Cost}{\partial A_t} < \left|\frac{\partial Cost}{\partial P_{RDC}}\frac{\partial P_{RDC}}{\partial A_t} + \frac{\partial Cost}{\partial Ar}\frac{\partial Ar}{\partial A_t}\right| \qquad (2.1.10)$$

These considerations are discussed in greater detail in section 2.3.

One other alternative is to pursue a technology program which will permit an increase in DC-RF converter packing density. This could be achieved for example by increasing converter efficiency, and/or, using improved forms of heat transfer devices such as heat pipes. The impact of improved thermal capabilities is evaluated parametrically in section 2.3.

Using equation (2.1.7) the thermal power distribution, $q_t(r)$, can be written as,

$$q_t(r) = \left(\frac{1-\eta_t}{\eta_t}\right) p_t(0)\, f^2(r) \qquad (2.1.11)$$

where η_t is the DC-RF converter efficiency.

Figure 8 shows the thermal power distribution for a typical MPTS geometry. As discussed above, the minimum thermal requirement is exhibited by a uniform illumination. As the taper increases, the structure at the center of the antenna will be subjected to a more severe thermal environment. The maximum thermal capabilities of several materials is indicated for comparison. These capabilities were arrived at in the Raytheon study (reference 7) from a thermal analysis of a rectangular grid approach to the transmitter structure. As shown, the maximum allowable structural temperature could also place a limitation on the allowable power density on the transmitter. However,

using the same approach as above, the throughput power can be increased with a corresponding decrease in system specific cost.

Letting the converter packing density, expressed in terms of RF power density, assume a general value, k_{tube} , the resultant peak thermal load is

$$q_t(\omega) = \left(\frac{1-\eta_t}{\eta_t}\right) k_{tube} \qquad (2.1.12)$$

This thermal flux will raise the temperature of the surrounding structure. The maximum allowable temperature depends on the material used for construction. In turn, the maximum allowable temperature will dictate the maximum allowable thermal flux, k_{mat} . In reference 7 this thermal flux limitation was identified for three materials:

$$k_{mat} = \begin{cases} 3600 \text{ watts/m}^2 \text{ Aluminum} \\ 3600 \text{ watts/m}^2 \text{ Epoxy Composites} \\ 8100 \text{ watts/m}^2 \text{ Polyimide Composites} \end{cases} \qquad (2.1.13)$$

Equating equation (2.1.12) and k_{mat} identifies that tube efficiency which will permit the radiators to touch. These results are tabulated as Table II.

In reference 7 it is suggested the amplitron has a potential for exceeding 85 per cent efficiency and the klystron possibly 80 per cent. Given these efficiencies, amplitrons can be packed to

touching, providing significant flexibility in transmitter design. In contrast it appears that the klystron cannot be packed to the point of touching, limiting somewhat the flexibility of transmitter design.

Due to the uncertainty in k_{mat} and k_{tube}, it is appropriate to consider the possibility that either the structural-thermal or the converter packing limitation may dominate. A suitable non-dimensional parameter for locating this transition is

$$\gamma = \left(\frac{\eta_t}{1-\eta_t}\right) \frac{k_{mat}}{k_{tube}} \qquad (2.1.14)$$

where for

$$\begin{aligned} &\gamma > 1 \quad \text{tube packing dominates} \\ &\gamma < 1 \quad \text{structural limit dominates} \end{aligned} \qquad (2.1.15)$$

Given k_{tube}, k_{mat}, and η_t the required antenna diameter and net RF transmitted power can be related as follows:

$$\begin{aligned} D_t &\geq 2\frac{V}{f}\sqrt{\frac{(1-\eta_t)P_t}{\pi\,\eta_t\,k_{mat}}}, \quad \gamma > 1 \\ D_t &\geq 2\frac{V}{f}\sqrt{\frac{P_t}{\pi\,k_{tube}}}, \quad \gamma < 1 \end{aligned} \qquad (2.1.16)$$

where V, f are parameters that result from calculation of the optimal illuminations. Approximations to these parameters are given in Table III for illuminations corresponding to tapers of

0-20db. The ratio of ∇ and $\mathcal{F}$ is identically equal to the peak to average power ratio for that particular optimal illumination. For minimum cost at a given throughput power, the diameter that satifies the equality would be selected.

2.1.4 LOSSES ASSOCIATED WITH TRANSMITTER

There are many sources of power loss within a MPTS. The more significant losses are identified and estimated in this section. For example, estimates have been made (reference 7) of power losses incurred through bussing and switch gear. The total loss, excluding that at the rotary joint, is estimated to be 2.2 per cent.

Also, a preamplifier will be required to bring the reference signal to a level sufficient to drive the first RF converter. This is a high gain application and therefore either a TWT or klystron will be used. The loss contributed by this element is given by the approximate relation

$$\eta_{pre} = \frac{1}{(1 + \eta_t/NG\eta_p)} \qquad (2.1.17)$$

where η_{pre} is a multiplying factor to be applied to overall system efficiency, η_t is the RF converter efficiency, η_p the preamplifier efficiency, N the number of RF converters in cascade, and G the power gain of the first RF converter. This loss is typically 1 per cent.

The RF converter losses have already been mentioned. Associated with the converters is another loss, the filter loss. Constraining the bandwidth of the emissions requires a filter for each converter and the loss is expected to be about 1-2 per cent. The waveguide losses are expected to be 0.2-1 per cent.

Another loss will be the scattering losses associated with imperfections of the subarray surface. For a particular subarray it is not economical to electronically compensate for deformations or imperfections. The phasing and amplitude adjustments will be made only on a subarray to subarray basis and not within a subarray. That is, the mean amplitude and phase of each subarray will be controlled. Consequently, any errors within a subarray will be uncorrected and there will be some resulting scattering loss.

For a particular subarray the distribution of the surface deformations is equivalent to a phase error distribution. For a given rms surface error, σ , the efficiency associated with each subarray is (reference 20),

$$\eta_\sigma = \exp\left[-\left(\frac{2\pi\sigma}{\lambda}\right)^2\right] \qquad (2.1.18)$$

This can be manipulated into a form including subarray size. Defining, σ/L_{SA} , as the rms surface error fraction, equation (2.1.18) becomes

$$\eta_\sigma = \exp\left[-\left(\frac{2\pi L_{SA}}{\lambda}\right)^2\left(\frac{\sigma}{L_{SA}}\right)^2\right] \qquad (2.1.19)$$

where L_{SA} is the length of one side of the subarray.

Current fabrication accuracies for large structures are such that the rms surface error fraction is typically 10^{-4} (reference 20). It is reasonable to assume such accuracies can be obtained or exceeded for the MPTS subarrays. At a frequency of 2.45 Ghz an antenna with a 20 meter side and $\sigma/L_{SA} = 10^{-4}$, would have a 1 per cent scattering loss.

Choice of subarray size involves consideration of several factors. Figure 9 shows an optimization that trades phase control costs against prime power costs. As the subarrays are made larger the phase control costs decrease since fewer components are required (number of subarrays decreasing). However, with a fixed surface error fraction, the subarray efficiency decreases as its size increases. Therefore, maintaining a constant delivered DC power requires additional prime power which becomes a penalty to system cost. Eventually this penalty overrides the decrease in phase control costs.

There is an additional inefficiency not included in this analysis. As the subarray size increases, the phase quantization becomes more coarse and scattering of energy into grating lobes occurs. This effect would cause the optimum size to be slightly less than that shown in Figure 9.

Figure 10 shows the sensitivity of the optimum subarray size to unit phase control costs and prime power costs.

Other considerations determining subarray size have been examined (reference 7). Among these are pointing accuracy requirements and ionospheric and atmospheric turbulence. These analyses suggest the use of a subarray less than 30 meters in size.

It should be mentioned that the mechanical subarray and electrical subarray need not be the same size. In fact, one mechanical subarray may be organized as several electrical subarrays. This allows flexibility in construction of the MPTS.

With large subarrays it is important that each subarray axis be directed at the receive site. Otherwise the contribution of each subarray will not be a maximum and some loss will be incurred. For a uniformly illuminated square subarray, the power density, $p_r(W)$, along one axis of the receive antenna is given by

$$p_r(W) = p_r(0)\left[\frac{\sin(W)}{W}\right]^2 \qquad (2.1.20)$$

where,

$p_r(0)$ = contribution of subarray to axial power density

$$W = \left(\frac{\pi L_{sa}}{\lambda}\right)\sin\theta \qquad (2.1.21)$$

θ = pointing error of subarray

For a 20 meter antenna at 2.45 Ghz, the ratio $p_r(W)/p_r(0)$ can be made to exceed 0.99 provided θ is controlled to better than 1 min

of arc. This requirement varies inversely with L_{SA} .

To be exact, one would have to account for the correlation between the pointing errors of all the subarrays before one could compute the exact losses due to subarray misalignment. However, for the purposes of this study, the above analysis will be used to estimate required pointing accuracies.

Even with this approximation, it is clear that for large subarrays some form of mechanical adjustment will be required to position each subarray. Further, this adjustment will likely be required at regular intervals. For subarrays approaching 20 meters, some form of auto-track should be included for each subarray. Very little would be added in the way of complexity since electrically driven positioners and receivers for the reference beam would be required anyway to perform the retro-directive function.

Previously, the loss due to surface imperfections of the subarrays was discussed. The same analysis applies to the random phase errors which will occur between subarrays. The retro-directive system will remove the major errors. However, the residual errors due to errors in distribution of the reference, aging and thermal cycling of components, etc, will contribute significant losses.

At this time, only estimates can be made of these residual errors. These estimates depend on the phase control system assumed. Estimates of phase control accuracies of 10 degrees and

15 degrees rms have been made for particular retro-directive and adaptive schemes respectively (reference 7).

Using equation (2.1.18) and replacing the quantity in parenthesis with the rms radian phase error for each case, the losses would be 3 per cent and 6.6 per cent for the respective phase control schemes. These are considered optimistic at this time and technology development is required to insure such accuracies can be obtained.

Another loss will be incurred by quantizing the amplitude and phase distribution. However, 5-10 quantization steps are sufficient to remove the associated losses as a significant factor (reference 7).

Since the retro-directive system will accomplish beam steering electronically, some flexibility is obtained regarding mechanical pointing control of the transmitter. If the subarrays are mechanically aligned by means of auto-track systems, then squint losses would not be significant even if the mechanical pointing of the transmitter was relaxed to 1 degree. Beyond this, the subarrays would begin to shadow one another and the losses in this regime have not been estimated.

Alternatively, if the subarrays were positioned only at very infrequent intervals, then the pointing accuracy of the transmitter must be that required of the individual subarrays as defined above, i.e. about 1 arc-min. This appears readily achievable so that either option would be available.

2.1.5 LOSSES DUE TO IONOSPHERE AND ATMOSPHERE

Generally, atmospheric attenuation becomes more severe as frequency is increased above 1 Ghz. When effects of rain are included, this attenuation can be severe indeed.

Figure 11 shows the expected atmospheric losses for various rain rates. Clearly the atmosphere would tend to force the system to the lower frequencies. However, another effect, polarization loss, has the opposite trend with frequency.

The polarization effect can be avoided by using circularly polarized transmit and receive elements, but the current concept of MPTS uses linear polarization.

It would be possible to calculate a frequency for minimum loss due to these two effects. However, such a calculation would ignore other spectral users. Therefore, the effects of the atmosphere and ionosphere will impact the frequency selection for an MPTS in only a macroscopic sense. The specific assignment will probably be based on minimizing impact to other spectral users.

For this study 2.45Ghz was selected as a nominal system frequency simply as a focal point. This frequency is low enough to obtain good atmospheric transmission (>98 per cent) (reference 21,22), high enough for minimal polarization losses (<0.5 per cent) (reference 22,23), and coincides with the microwave

industrial/medical frequency assignment (minimum spectral impact) and appears to be a cost-effective assignment (see section 2.3.4).

Potentially, the peak power density in the ionosphere could be sufficient to cause nonlinear effects (reference 22). At this time it is not clear what significance these phenomena will have. Ionospheric modification experiments have been performed at HF (reference 28) and significant physical changes observed. For example, heating the ionosphere with HF emissions near the plasma frequency has produced regions highly reflective to HF as well as other frequencies including UHF. In addition, this HF heating has produced other effects such as small scale (3 meter) electron density fluctuations.

Preliminary analyses of the MPTS application (reference 7) indicate that a power density of 230 watts/m (typical for MPTS) in the ionosphere at 2.45 GHz will produce similar effects. However, these analyses also indicate these effects will not significantly degrade the beam. These conclusions should not be regarded as final, however. Ionospheric modification and its effects on the beam and environment are likely to be a continual issue. Also, if one were interested in a demonstration of insignificance of ionospheric effects, a question would arise as to whether the test must be performed at 2.45 GHz or whether it would be sufficient to do the test at HF. Costs for HF testing are expected to be less since less power would be needed. It is not clear that current theory can resolve such questions.

Therefore, it seems appropriate to support more theoretical development and possibly more experimental work to augment the HF tests.

2.1.6 RFI IMPACT

When transmitting gigawatts of power, the power density in sidelobes and grating lobes can be significant. In principal, these densities can be adjusted to nearly any level. However, this adjustment has a direct impact on system cost and performance. That is, the lower the sidelobe level the greater the peak to average power ratio on the transmit antenna and, consequently, the lower the achievable throughput power. Also the lower the grating lobe level, the greater the complexity of the transmit antenna resulting in an increase in assembly and component cost. These levels will be adjusted to fall below some, currently unspecified, limit. Therefore, these limits will have a significant impact on system costs.

For the purposes of this study peak ground power densities as high as 1000 watts/m^2 were considered for the on-axis radiation. For the sidelobes, peak densities as high as 1 watt/m^2 were considered. Access to near sidelobes was assumed to be controlled by a protective fence.

As was mentioned in section 2.1.4 imperfections in the phase control system and imperfections in the subarrays will cause a scattering loss. This energy will appear as a relatively diffuse

power pattern about the main beam. For MPTS, the greater portion of this scattering will be due to errors in phase and amplitude control. If one were to assume the N subarrays to be identical and only the mean amplitude and phase of each subarray was controlled, the expected power pattern at the receive site would have the form (reference 24),

$$\mathcal{P}(x_o,y_o) = \frac{\bar{P}_t}{4\pi Z^2}\left[G(x_o,y_o)\exp(-\sigma_{\bar{\phi}}^2) + [1-\exp(-\sigma_{\bar{\phi}}^2)]\,G_{SA}(x_o,y_o) + K^2 G_{SA}(x_o,y_o)\right] \qquad (2.1.22)$$

where,

$G(x_o,y_o)$ = Overall array gain with mean illumination

$G_{SA}(x_o,y_o)$ = Subarray gain

$\bar{P}_t$ = Mean power in illumination field

$\sigma_{\bar{\phi}}^2$ = Mean square phase error

K^2 = Fractional mean square amplitude error (2.1.23)

This equation was arrived at by using an analysis similar to that used in reference 19 and reference 25. However, because of the quantization of the aperture and assuming no correlation of the random errors between subarrays, the resulting equation was considerably simpler.

The first term is simply the power pattern that would result if there were no phase or amplitude errors, but, decremented by

an exponential factor which depends on the rms phase error. The first term is also known as the diffraction pattern. Added to this pattern are two terms which can be interpreted as scattered power.

In the second and third terms the pattern shape is controlled by the subarray size through the factor $G_{sa}(x_o, y_o)$. It can be shown that this factor is the subaperture gain and is given by,

$$G_{sa}(x_o, y_o) = 4\pi \frac{L_{sa}}{\lambda} \operatorname{sinc}^2\left(\frac{\pi L_{sa} x_o}{\lambda z}\right) \operatorname{sinc}^2\left(\frac{\pi L_{sa} y_o}{\lambda z}\right) \qquad (2.1.24)$$

Therefore, the resulting power density pattern is the sum of a diffraction pattern, controlled by the large array, and two scattered patterns shaped by the subarray. The form of these two latter terms is equivalent to one subarray driven by the total scattered power, P_S, given by

$$P_S = \left[1 + K^2 - \exp(-\sigma_\phi^2)\right] \bar{P}_t \qquad (2.1.25)$$

Figure 12 shows how these component patterns combine to produce an overall radiated pattern for a typical MPTS geometry.

It may not be apparent in equation (2.1.22), but any mean or deterministic quantization is not considered an error. The process used to calculate the error free pattern should account for the quantization of the aperture. Equation (2.1.22) is used

to account for the random errors about this mean pattern, whatever form the mean pattern might take.

In areas remote from the receive site these scattered fields can exceed the diffraction pattern. Therefore, in estimating interference impact, the scattered pattern should be used to determine affected spectral users within the MPTS assigned bandwidth. As currently envisoned, there will be no spectral users operating communication services or radio astronomy within the band assigned to the MPTS. However, it is expected that there will be users with such applications near the MPTS assignment. For these users, the out-of-band interference is of interest.

The RF emissions from each subarray will be coherent with the transmitted reference signal. However, each device used for processing this signal will degrade the signal to noise ratio. The degraded signal to noise ratio can result in residual phase modulation which can generate otf frequency components. The greatest offenders will be the DC-RF converters.

With gigawatts of power being transmitted, the noise emissions associated with that transmission can be significant. The DC-RF converters currently being considered are estimated (reference 7) to have noise levels of -130db/Hz and -150db/Hz for the amplitron and klystron respectively. How this noise radiates and impacts other spectral users depends on how the radiating elements are excited and how much filtering is

provided.

For this study, the converters were assumed to be driven in a cascade arrangement.

For the cascaded amplitrons, two possible models for estimating noise impact are discussed in Appendix A. The model used for this study predicts a radiated noise power density, $P_n(0)$, of

$$P_n(0) = \frac{\pi \Delta (N+1)(2N+1) D_t^2}{48 \lambda^2 z^2} P_n \qquad (2.1.26)$$

where P_n is the noise power produced by each of the converters and $\Delta < 1$ is a factor which accounts for partial coherency of the noise sources. That is, in a series cascade of converters, the output noise of one tube will excite the input of the following converter and cause a partially coherent noise component to appear at the output (this argument is made clearer when the model in Appendix A is examined). The coherence is only partial since there is a finite separation between converters. There is a correspondence between spatial correlation lengths and time correlation lengths. Not knowing exactly how the converters would be arranged nor the precise noise properties of the converters some assumptions regarding correlation must be made.

As a worst case of coherence(as regards interference), it will be assumed the converters are very close in proximity and $\Delta = 1$. The amplitron will be treated as a 5kw RF device having a

bandwidth of 20Mhz and -130db/Hz noise level. In-band noise levels for different cascade configurations are tabulated in Table IV. Compare these with the CCIR reccomendations of -188dbW/m^2/Hz for satellite to earth emissions. Given the above amplitron and assuming a filter on each device having a 24db/octave rolloff away from 10Mhz, the required spectral assignment would span approximately 3 octaves or 80Mhz for a 20 tube cascade configuration. However, this is only for proximity to one class of service. The required spectral assignment for proximity to several typical services is given in Table V. At the expense of greater losses a more narrow bandwidth filter could be used to reduce the spectral impact.

At this time, data on harmonic generation of MPTS type amplitrons and klystrons is not available. However, Table VI (reference 26) provides data on harmonic levels for typical devices used in ground applications.

The magnetron is similar to the amplitron in operation and is often used to infer amplitron characteristics. Consequently, for lack of better information, these levels for the magnetron will be assumed indicative of what might be expected of an amplitron.

To estimate the radiation pattern for each of the harmonics, equation (2.1.22) can be used. It remains to estimate the mean square phase error, mean square amplitude error, and region of complete coherence for each harmonic.

It is conceivable that if all the converters were identical and installed in identical waveguide circuits, as in MPTS, their harmonic outputs might be coherent. The fundamental of each converter is, by design, coherent with the reference signal. Each converter nonlinearity results in harmonics with a fixed phase relationship with the fundamental. Since the fundamental is coherent over the array, then the harmonics could, conceivably, be coherent. If the nonlinearity of each converter is identical and not significantly affected by the small variations in the circuit in which it is placed, then there is a very good chance that this could occur.

However, it is expected that small differences in converters and their circuits will introduce random deviations from this trend. It seems reasonable, though, to assume that partial coherency of the harmonics would occur.

If there were complete coherence over a subarray, then the mean square phase error for harmonic n, $\sigma_{n\phi}^2$, would be,

$$\sigma_{n\phi}^2 = n^2 \sigma_\phi^2$$

where σ_ϕ^2 is the mean square phase error of the fundamental.

The mean square amplitude error for the harmonics is expected to be considerably larger than that for the fundamental. In Table VI the range on the harmonic level for various harmonics was shown. For example, with the magnetron, the range on the harmonic level for the 2nd, 3rd, and 4th harmonics was

approximately 50db. Unfortunately, the cited reference did not indicate if these variations were for identical magnetrons in identical waveguide circuits.

As a "worst case" (regarding interference) this study assumed that the amplitude variation of the harmonics was proportional to that of the fundamental and that the fractional change in the harmonics was no more than one order of magnitude larger than that of the fundamental. That is,

$$K_n = 10K \tag{2.1.27}$$

where K_n is the rms variation in the Nth harmonic. Also, it was assumed that complete coherence of the harmonics existed over each subarray. Then equation (2.1.22) for the Nth harmonic becomes,

$$p_n(x_o,y_o) = \frac{\overline{P}_{nt}}{4\pi Z^2}\left\{G_n(x_o,y_o)\exp(-\sigma_{n\phi}^2) + [1+K_n^2-\exp(-\sigma_{n\phi}^2)]\,G_{san}(x_o,y_o)\right\} \tag{2.1.28}$$

where,

$\overline{P}_{nt}$ = Mean harmonic power in illumination field at harmonic n.

K_n^2 = Fractional mean square amplitude error at harmonic n.

G_{san} = Subarray gain at harmonic n.

G_n = Large array gain at harmonic n. (2.1.29)

It is expected that the frequency dependent characteristics

of the converter filters and slotted waveguide will reduce the harmonic content considerably. However, without being specifically designed for harmonic rejection, the reduction is expected to be no more than 60-80db.

Using the stated assumptions and the data in Table VI, the interference level for harmonics through the 8th are tabulated in Table VII for a typical MPTS geometry. In each case, calculations are made at the first sidelobe of the scattered field. The calculations assume the converter filter and waveguide provide 80db rejection of the harmonics, a rms phase error of 10 degrees at the fundamental, a rms amplitude error of 5 per cent at the fundamental, and that equations (2.1.26) and (2.1.27) as well as the data of Table VI apply.

Previously, it was mentioned that the CCIR recommended interference level for satellite to earth communications was $-188 dbW/m^2/Hz$. Therefore, in a 4KHz bandwidth this recommendation is $-152 dbW/m^2$. It can be seen from Table VII, that only the fundamental is sufficient for interference with this service. However, for radio astronomy, the typical interference level is $-240 dbW/m^2/Hz$. To avoid interference with this application, additional filtering may be required for each harmonic. At this time, it is uncertain how accurate the estimates in Table VII might be. However, this data indicates that 10-40db of additional filtering of each harmonic may be required, assuming 80db would already be provided by the fundamental filter and waveguide circuitry.

2.2 RECEIVER

As currently envisoned, the MPTS receiver or rectenna will consist of an array of dipoles, each with a rectifying diode and filter circuit, with the dimensions of the array nominally 9km x 13km. Means will be provided for interconnecting all the rectifying circuits to yield high voltage DC suitable for interconnects to DC utility grids or perhaps some form of high efficiency conversion for interconnects with AC utility grids.

Tests have been made by JPL at the NASA-JPL complex at Goldstone, Calif. to evaluate this form of RF-DC conversion. A recent test at JPL (reference 2) on a prototype array recovered up to 30.4 Kw at a distance of 1.54km. This was a small scale test, by design, so that the rectenna did not fill the transmitted beam. The conversion efficiency was therefore inferred from field measurements over the surface of the rectenna. The calculations indicate a maximum efficiency of about 80 per cent was obtained. Recent measurements at Raytheon (reference 1) using an improved rectenna realized a DC-DC transmission efficiency of 54 per cent and a recovery of 495 watts. The calculated efficiency for the improved rectenna was 85 per cent.

For the purposes of this study, a frequency dependent model for rectenna efficiency was used (reference 7) and is given by

$$\eta_r = 1.92 - \exp(.022f), \quad f < 6\ \text{GHz} \qquad (2.2.1)$$

where f is system frequency in GHz. At 2.45GHz, this model predicts an efficiency of 86 per cent.

There is also an efficiency dependency on power density. Figure 13 shows the results of measurements made by Raytheon giving conversion efficiency as a function of power density. This variation was not accounted for in this study. Instead, the rectenna efficiency was assumed constant over the receive array and given by equation (2.2.1).

It was also assumed that the receive array was surrounded by a protective fence so that only authorized personel could enter. The fence was sized so that the flux outside it was equal to or less than 1 watt/m^2.

It is reasonable to assume that the maximum power density on axis will be subject to environmental regulation. Details on the impact of such regulations appear in section 2.3.

There are alternatives to the dipole-diode receiver scheme. For example, it is conceivable to use high gain receive elements and high power converters for this application. However, it will be ditficult to provide high power tube type converters that will match the proven efficiency of the rectenna element. If, however, the peak power density is restricted to lower power levels than examined in this study, high gain receivers may be

required.

Since the power on the rectenna tapers off to low values at the edge, it may be desirable to use high gain elements in this region. The diode converter could be driven by several dipoles interconnected as a phased array. This array must not be too large or pointing losses will cancel the gain advantages offered by the array (auto-tracking receive elements would be much too costly). The maximum array size can be determined from equation (2.1.20) and the expected station-keeping error for the orbital system.

Figure 14 shows the maximum phased array size as a function of station-keeping error for 1 and 2 per cent pointing error loss. The station-keeping accuracy of the orbital system is expected to be no better than one degree to avoid excessive propellant resupply. Therefore, the maximum aperture size of any rectifying phased arrays can be no larger than 40-50 cm on a side. With 0.62λ spacing of the dipoles this would permit arraying approximately 5x5 or 25 elements therefore providing an increase in the power delivered to a single diode by a factor of 25.

Shielding the rectenna from the environment is essential but must be done with care. Figure 15 shows the transmission efficiency of a wet radome for various frequencies as a function of water layer thickness (reference 27). This would indicate that radomes would be unsatisfactory from an efficiency

viewpoint. It would be appropriate to experimentally determine dielectric or conductive coatings or other means of protecting the rectenna elements to insure long life and efficiency.

2.3 CAPITAL COSTS

2.3.1 COST MODEL

In section 2.1.1 it was mentioned that there were many combinations of transmitter and receiver sizes that would provide the same interception efficiency. There is an inverse relationship between the two antenna diameters as shown in Figure 16 for various interception efficiencies. This relation shows that if one used a 1 Km transmitter then one could obtain 80-98 per cent interception by using receivers of diameter 8.2-12.5 Km. Of course, either a smaller or larger transmitter could be used with a corresponding inverse change in receiver diameter.

To determine the best combinations of antenna sizes, this study made use of a cost model which is essentially the same as that suggested by Raytheon (reference 7). The model is developed in detail in Appendix B. Using this model, the total system cost can be written as,

$$Cost = F_1 A_t + F_2 A_r + F_3\sqrt{P_{RDC}} + F_4 P_{RDC} + F_5 \qquad (2.3.1)$$

where A_t is the transmit antenna area, A_r is the beam area normal to the beam axis at the receive site, P_{RDC} is the delivered

ground DC power, and F_1 -F_5 are expressions involving system parameters and are defined in Appendix B.

When optimizing system cost, it is appropriate to consider the optimization of the ratio,

$$\Gamma = \frac{Cost}{P_{RDC}}$$

This ratio, the system specific cost in $/kw, is given by

$$\Gamma = (F_1 A_t + F_2 A_r + F_5)/P_{RDC} + F_3/\sqrt{P_{RDC}} + F_4 \qquad (2.3.2)$$

2.3.2 OPTIMIZATION OF SYSTEM CAPITAL COST WITH NO CONSTRAINTS

When there are no constraints, it is possible to use equation (2.3.2) for system specific cost and optimize system parameters to minimize system cost. This model has minima with respect to some parameters such as:

1) Transmit antenna area (and hence rectenna area)

2) Subarray size (see section 2.1.4)

3) Beam efficiency

4) Frequency

Other minima exist but are not included here.

There are other parameters for which the model exhibits no

minima. Examples of these parameters are:

1) Total delivered DC power at receiver, P_{RDC}

2) Peak power density at the receive site, $p_r(0)$

3) Transportation and assembly costs

4) Prime power costs

System specific costs monotonically decrease as P_{RDC} and peak power density increases. System specific cost decreases almost directly with transportation and assembly costs and prime power costs. This is primarily the result of these costs being the dominant system costs.

With no constraints other than constant P_{Roc}, equation (2.3.2) can be minimized with respect to transmit antenna area with the result

$$A_t^{opt} = \lambda z \tau \sqrt{\frac{F_2}{F_1}} \qquad (2.3.3)$$

where the ratio F_2/F_1 is essentially the ratio of rectenna costs to transmitter costs(excluding prime power costs).

This derivation made use of equation (2.1.2) to relate A_t and A_r. Therefore, (2.3.3) indirectly identifies an optimum rectenna area.

Since equation (2.3.2) monotonically decreases with

increasing P_{Roc}, no optimum P_{Roc} exists other than $P_{Roc} \to \infty$. The asymptote which system specific cost approaches is

$$\Gamma(P_{Roc} \to \infty) = F_4 \tag{2.3.4}$$

The peak power density, $p_r(0)$, at the receive site can be related to the delivered DC power with the expression,

$$p_r(0) = \frac{A_t P_{Roc}}{\eta_{BM} \eta_r (\lambda z f)^2} \tag{2.3.5}$$

where η_r is the rectenna collection and conversion efficiency and η_{BM} is the beam efficiency corresponding to the system geometry.

Substituting equation (2.3.5) into (2.3.2) the system specific cost as a function of peak power density is given by

$$\Gamma = F_6/p_r(0) + F_7/\sqrt{p_r(0)} + F_4 \tag{2.3.6}$$

where,

$$F_6 = \frac{(F_1 A_t + F_2 A_r + F_5) A_t}{\eta_{BM} \eta_r (\lambda z f)^2} \tag{2.3.7}$$

$$F_7 = \frac{F_3}{\lambda z \tau} \sqrt{\frac{A_t}{\eta_r \eta_{BM} \eta_{DC}}} \tag{2.3.8}$$

and η_{DC} is the MPTS total link DC-DC efficiency and F_4 is defined in Appendix B.

Now the system specific cost, as modeled by equation (2.3.6), decreases monotonically with $p_r(0)$. Therefore, no optimum is exhibited by this model other than the case where $p_r(0) \to \infty$ for which

$$\Gamma[p_r(0) \to \infty] = F_4$$

These trends for A_t, $p_r(0)$, and P_{RDC} are shown for no constraints in Figures 17, 18, and 19.

Figure 17 shows the system relative cost as a function of ground power density for various levels of delivered DC ground power. In calculating the relative cost, the specific cost in \$/Kw of a 5Gw space power station with the reference cost parameters given in Appendix C was used as a normalization factor. The variation in peak density is generated for a fixed DC ground power by varying the transmit antenna area from 1/2 to 2 times optimum (no constraints). Also shown is the locus of minimum system specific cost. The locus approaches the asymptote, F_4, as peak density increases. Note that very little is gained by increasing the power density above 300-500 watts/m^2 or increasing the delivered DC power above 8-10 Gw. This conclusion is sensitive to costs of prime power, assembly, and transportation. An indication of this sensitivity is given in Figure 18. System costs are shown as a function of power density for various rectenna cost assumptions. Peak power densities that are optimum for each rectenna cost level are indicated.

Figure 19 shows the system specific cost as a function of

transmit antenna diameter for various levels of delivered DC ground power. Note that, for no constraints, the optimum antenna diameter is the same for all power levels. The locus of minima, for the particular geometry shown, passes through approximately 1 Km diameter. Also it was found that this optimum was relatively insensitive to assumptions regarding costs. Figure 20 shows this sensitivity for a 4:1 range of power and transportation costs. Note the diameter only changes by about 20 per cent.

2.3.3 OPTIMIZATION OF SYSTEM CAPITAL COST WITH CONSTRAINTS

When constraints such as maximum thermal loading of the transmit antenna structure, maximum converter packing, or peak allowable flux density are included, system optimization can change radically.

As the delivered DC ground power is increased, for fixed A_t, the peak power on the transmit antenna will eventually be limited by the maximum converter packing density, or, the waste heat from the converters will raise the structural temperature to its rated limit. At this point more throughput power can be realized only if the transmit antenna is made larger than the unconstrained optimum.

It is shown in Appendix B that the system specific cost, A_t, and the peak allowable power density on the transmit antenna can be related as

$$\Gamma = \frac{F_8}{A_t^2 p_{thm}} + \frac{F_9}{A_t p_{thm}} + \frac{F_{10}}{\sqrt{A_t p_{thm}}} + \frac{F_{11}}{p_{thm}} + F_4 \qquad (2.3.9)$$

where p_{thm} is the maximum allowable power density on the transmit antenna, F_4 is defined in Appendix B, and

$$F_8 = \frac{F_2 (\lambda Z \tau V/E)^2}{\eta_r \eta_{rf} \eta_{om}} \qquad (2.3.10)$$

$$F_9 = \frac{F_5 (V/E)^2}{\eta_r \eta_{rf} \eta_{om}} \qquad (2.3.11)$$

$$F_{10} = \frac{F_3 (V/E)}{\eta_r \eta_{oc} \eta_{om}} \qquad (2.3.12)$$

$$F_{11} = \frac{F_1 (V/E)^2}{\eta_r \eta_{rf} \eta_{om}} \qquad (2.3.13)$$

The RF efficiency in (2.3.13), η_{rf}, includes effects of phase errors, subarray losses, pointing losses, and atmospheric loss.

Equation (2.3.9) indicates the system specific cost decreases monotonically with transmit antenna area when the system is thermally constrained. Therefore, no optimum exists other than the extreme, $A_t \to \infty$. However, since equation (2.3.9) assumes the throughput power is increasing as the antenna area is increasing, the peak power density at the receive site will rise very rapidly with transmit antenna diameter. At some point, the peak ground density will equal some, as yet unspecified, biological limit.

When the system is constrained to a particular peak power density at the receiver, throughput power can be increased only if the transmit antenna is made smaller.

It is shown in Appendix B that the system specific cost, A_t, and the peak allowable power density at the receive site, p_{bio1}, can be related as

$$\Gamma = F_{12}\sqrt{\frac{A_t}{p_{bio1}}} + F_{13}\frac{A_t}{p_{bio1}} + F_{14}\frac{A_t^2}{p_{bio1}} + \frac{F_{15}}{p_{bio1}} + F_4 \qquad (2.3.14)$$

where,

$$F_{12} = \frac{F_3}{\lambda z \xi \sqrt{\eta_r \eta_{BM}}} \qquad (2.3.15)$$

$$F_{13} = \frac{F_5}{\eta_{BM}\eta_r(\lambda z \xi)^2} \qquad (2.3.16)$$

$$F_{14} = \frac{F_1}{\eta_{BM}\eta_r(\lambda z \xi)^2} \qquad (2.3.17)$$

$$F_{15} = \frac{F_2(z/\xi)^2}{\eta_r \eta_{BM}} \qquad (2.3.18)$$

For a fixed peak power density, p_{bio1}, equation (2.3.14) indicates system specific cost monotonically increases with transmit antenna area. Therefore, no optimum exists other than the trivial case, $A_t \to 0$. This equation was derived assuming the throughput power would increase as the antenna area decreases. Therefore, the peak power density on the transmit antenna will

rise very rapidly as the antenna area is decreased. Eventually, a thermal limit will be encountered.

With either the biological or thermal constraints alone, A_t has no optimum value. However, taken together, the two constraints do yield an optimum A_t for certain geometries.

Figure 21 shows the system specific costs for both the thermally limited case and the biologically limited case. The thermally limited contours are shown for three values of thermal capability which span estimates of structural and converter packing limits. The contours for limits on peak receiver power density are also shown for three values. The level of 100 watts/m^2 is currently accepted as a level of continuous exposure in the U.S. Although not shown, 2700 watts/m^2 would be on the order of that used in microwave ovens.

Whatever these constraints might be, the minimum cost system is obtained when it is designed to achieve the thermal and biological limits simultaneously. Using the lower range on thermal capability a 5 Gw system would require about a 1 Km transmitter and would produce about 270 watts/m^2 at the center of the receiver. This is higher than the continuous level, but should be acceptable since this only occurs in a restricted area. Outside the protected area the density would drop below 1 watt/m^2.

At each intersection the optimum transmit antenna area that satisfies both constraints is given by (Appendix B)

$$A_t = \sqrt{\frac{f_{bi}\, l}{\eta_{rf}\, p_{thm}}}$$

It was mentioned in section 2.1.1 that for high interception efficiency, the system scale, as indicated by τ, can be very large. The effect on the required transmitter diameter, including thermal constraints, is shown for a 5GW system in Figure 22.

The required transmitter diameter is shown as a function of beam interception efficiency for various tapers. Note the slope discontinuities of the 10 and 15 db contours. These discontinuities indicate a shift to a thermally limited system which forces the transmitter diameter to actually increase as the interception decreases.

Also note that each contour rises very rapidly above some interception fraction. These breaks correspond to interception of sidelobes and are geometrically as well as cost inefficient. The thermal condition at the low values of interception is forced by requiring a fixed delivered DC ground power, while simultaneously decreasing the system efficiency. This combination of constraints forces the peak power density on the transmit antenna to equal the maximum allowable at the break points. And, as discussed in section 2.3.3, the required antenna diameter increases to allow the higher transmitted power demanded by the decreasing interception efficiency and constant DC delivered ground power.

In the thermally constrained range, the rectenna diameter must decrease rapidly since these two diameters are inversely related for a given interception efficiency.

Increasing the system scale, of course, increases system cost. Depending on the power level and system parameters, these increased costs may or may not be balanced by the increase in system efficiency.

Figure 23 shows the system specific costs for a thermally constrained system as a function of interception efficiency for various tapers. As in Figure 22, these data are for a 5GW system.

System costs rise at low interception efficiency, for a fixed delivered ground power, because a greater prime power is required for the same delivered ground power. Also, because of the thermal constraints encountered, the costs will experience an additional rise since the antenna diameter is larger than optimum. At higher interception, the costs rise because system scale and microwave costs increase much more rapidly than the modest increase in power interception. All the previous figures were generated for a 5 db taper and 90 per cent interception. Actually, as can be seen here, the cost contours have a very broad minimum with the lowest cost occuring for the combination of 10 db taper and 93 per cent interception. The difference between the two cases is relatively insignificant. Therefore, either would be acceptable. It can be seen in Figure 22 that the

required transmitter diameter is the same as the unconstrained optimum in both cases.

These results are sensitive to the assumptions regarding the costs of prime power, transportation, and assembly. This sensitivity is illustrated in Table VIII. Minimum cost parameters are presented for both 5 and 10 db illuminations. The corresponding cost advantage of the 10 db contour is indicated in the last column. If the cost parameters are low so that the microwave system dominates total system cost, the system optimizes at low interception and small values of taper. Conversely, if the microwave system is not a significant cost factor, the system optimizes at high interception and large values of taper.

With a 10 Gw system the system specific costs vary as shown in Figure 24. Again, above some interception fraction system costs rise rapidly for each contour. However, the rise is less dramatic in this case since the microwave system is less of a factor in total system costs. For the 10Gw system specific costs optimize for the combination of 10 db taper and 95 per cent interception.

For the 10GW case the system specific costs optimize for the combination of 10db taper and 95 per cent beam efficiency. This cost is about 10 per cent less than the 5GW system.

The data in Figures 22, 23, and 24 are shown for the combination of amplitron converters, aluminum structure, a

southwest location, and a frequency of 2.45GHz. Other geometries were not included here because this combination appears to be the lowest technical risk combination at this time.

2.3.4 COST CONSIDERATIONS IN FREQUENCY SELECTION

If there were no thermal or biological constraints and if the atmosphere were lossless at all frequencies, the best transmission frequency, from the viewpoint of minimizing cost, would be the highest that technology would allow. Such a strategy would minimize the size of both the receiver and transmitter and hence the required capitalization to construct the microwave system. However, upon introducing constraints into the analysis, the applicable frequency range is narrowed to 1-5 GHz.

In Figure 25 the required transmitter diameter as a function of frequency is shown for various received DC power levels. Without constraints, the transmitter diameter decreases with frequency as shown by the lower curve decreasing from left to right. This curve represents the locus of the optimum transmitter diameter for an unconstrained system (section 2.3.2). As the diameter decreases the peak transmitter power density increases (for a fixed throughput power). The curves branching from this locus indicate the frequency where the resulting thermal load equals the maximum allowed by the selected structural technology (3600 watts/m^2 was assumed for this case). The diameter continues to rise beyond this point in order to

support the required increase in transmitter power to offset the decreasing efficiency of the atmosphere and subsystems. As indicated, at 2.45GHz, a 5GW system would lie on the unconstrained contour and would have a 0.99Km transmitter diameter.

The impact of thermal constraints on system specific cost is indicated in Figure 26. Again, a peak thermal load of 3600 watts/m was assumed. For each throughput power the cost initially decreases with frequency, consistent with the decreasing system scale. However, subsystem inefficiencies and atmospheric losses combined with the thermal constraint on minimum transmitter size cause a reversal of this decreasing trend. The result is a series of minima which depend on the throughput power. For a 5GW system the minimum cost occurs very near 2.45 GHz and this has been selected as a reference point for the previous and succeeding cost comparisons.

It was mentioned in section 2.3.3 that system specific costs continually decrease with throughput power (at a particular frequency) even with a thermally limited transmitter. This trend is also indicated here. It was also mentioned in that section that the limit on this trend is the peak allowable power density at the receiver. And it was shown that the minimum cost system was realized when the transmitter and receiver power densities were simultaneously set at their maximum allowable values.

For a system designed with such an objective in mind, the

system throughput power would vary with frequency as shown in Figure 27. The trends are indicated for various receiver peak power densities. The reference 5GW system at 2.45 GHz is indicated, having a peak receive power density of 230 watts/m^2. The minimum cost throughput power rises very rapidly below 2.45 GHz.

Using the same strategy, the impact on system cost is shown in Figure 28, again for various peak receiver power densities. These curves suggest that the best frequency is the lowest possible frequency, in apparent contradiction to the previous development.

The fact is, the unconstrained and constrained systems do have opposite trends with frequency. However, it is important to note that the cost advantage of operating below 2.45 GHz is small for a given peak receiver power density. Therefore, it seems 2.45GHz is a reasonable selection from a cost viewpoint as well as from a spectrum impact viewpoint (see section 2.1.6).

2.4 ENERGY PAYBACK

For systems of this scale, it is appropriate to consider whether the energy payback justifies system production. A preliminary analysis was made to estimate the payback of one SPS.

The rationale on which this estimate was based was that energy input varied directly with the mass of the system. Thus there are two principal contributors to energy input. The first

is the energy to process and fabricate the mass of material for the SPS structures, components and devices. The second contributor is the energy to manufacture the propellant required to place the SPS in geosynchronous orbit. The assumptions used to scope the propellant requirements are in Table IX.

The energy cost to process materials is given in Table X. Cost of fabrication was assumed to be one-half the cost of processing the raw material. The cost of the receiving antenna is based on a material density of 4.5 Kg/m^2 for structure, reflecting screen, conductors and antenna elements.

The resulting apportionment of system mass is given for a 5GW SPS with a 1Km transmitter in Table XI. It is interesting to note that for this choice of transmitter size, the majority of total system mass is in the receiver.

All these factors can be incorporated into an energy cost model which is virtually identical to that developed for dollars cost in section 2.3. Consequently, one would expect system energy cost to be sensitive to transmitter size as was the case when accounting for dollars.

Figure 29 shows this effect for several delivered power levels. The energy expended in placing one SPS into operation is expressed as a fraction of the total energy recovered assumming a 30 year life time. Also shown is the period for payback of this energy.

Two factors are noteworthy. First, the payback period is relatively small even for a large range of transmitter sizes. Secondly, there is an optimum transmitter size, significantly larger than that based on dollars (1Km), which minimizes the payback period. However, as already mentioned, the payback period is relatively insensitive to transmitter size.

This conclusion is only preliminary since several factors were not included in the analysis. Sources of energy input that were not considered for this estimate are: Processing and fabrication scrap factors; materials processing and fabrication of launch vehicles, orbital assembly devices and stations, spare or backup power source, and ground support equipment and facilities; receiving antenna site preparation and erection;and items related to routine operation and maintenance.

3.0 CONCLUSIONS

3.1 MODELING RESULTS

In the conduct of this study it quickly became apparent that system specific cost should be the primary motivation for system optimization. Several parameters can be selected in a way which minimizes system specific cost.

An optimum transmit antenna can be derived which minimizes system cost when there are no constraints. This antenna size is very sensitive to the ratio of rectenna costs and transmitter costs. Using nominal estimates for component costs, the unconstrained optimum antenna size is approximately 1km in diameter.

Although the optimum antenna size is very sensitive to costs, system specific cost can be relatively insensitive to antenna diameter. That is, system specific cost can have a very broad minimum in the vicinity of the unconstrained optimum antenna diameter. This is especially true when the costs of prime power, transportation, and assembly overshadow the acquisition costs of the microwave system.

When constraints are imposed on the system model the optimization can produce significantly different results. The sensitivity of the system to biological and thermal limitations was tested by determining the system costs for a range of

possible limitations. The system was found to be relatively insensitive to thermal limitations but the biological limitation could have a very significant impact on the system cost effectiveness if this limitation were less than 100 watts/m.

There is an optimum interception efficiency and illumination taper for the MPTS system. This is obtainable for both the constrained and unconstrained cases. This optimum is somewhat sensitive to component costs and transportation. For the nominal cost and transportation estimates used in this study, system specific cost had a very broad minimum in the vicinity of optimum. Using the nominal cost parameters this optimum for a 5GW SPS included a 1Km transmitter, a 10 db taper, and a receiver sized for 93 per cent interception.

3.2 FEASIBILITY

In reference 7 and this study, there appeared to be no technical limitation which would prevent the implementation of an MPTS type system. Methods were identified to perform all the necessary tasks to implement such a system.

The economic feasibility of the concept, however, is at present uncertain. One of the objectives of this study was to bound this uncertainty where possible and test the sensitivity of system specific cost to various component costs, weights, and efficiencies.

The microwave system cost and weight has a small effect on

total system cost, especially for system power levels above 5GW and transmission frequencies above 1-2GHz. In this range of power and frequency, the microwave system affected system cost primarily through transmission efficiency. In fact, the economic feasibility of orbiting power stations depends in part on attaining a high efficiency microwave link.

Therefore, appropriate efforts should be directed toward improving component efficiencies in the microwave link, especially in the DC-RF converter and in the rectenna. Also, effort should be directed at attaining retro-directive modules that have low residual phase errors(less that 10 degrees rms). In addition, analytical and experimental work is appropriate to verify satisfactory performance of retro-directive schemes such as those suggested by JPL and Raytheon.

Two major elements that directly affect economic feasibility are transportation and on orbit assembly costs. The orbital power station will become economically attractive only if transportation costs are much lower than those projected for STS. For the SPS to be nominally competitive, the combination of transportation and on orbit assembly costs should be on the order of $100/Kg.

In regard to the cost and weight of prime power, a program is underway (ERDA) to produce low cost solar cells. The technology resulting from this program may lead to cells appropriate for the SPS application. In addition, NASA-sponsored

studies are currently being conducted to investigate the possibility of solar thermal conversion systems for this application. As a guideline, prime power costs of a few hundred dollars a kilowatt at a specific weight of a few kilograms/kilowatt will be required.

3.3 ENVIRONMENTAL IMPACT

In the conduct of this study and in reference 7 it appeared that the peak power density at the receive site for a cost effective orbital power system would be nominally 230 watts/m^2. Such a power density might be a hazard to animal and plant life. Therefore it would be appropriate to restrict the area of high flux density to only authorized and protected personnel. Metal skin aircraft flying through the beam may inherently provide adequate shielding for persons within. Aircraft communications would have to be protected or the aircraft diverted away from the receive site in the same way they are now diverted from military sites.

Outside the restricted area, animals and persons will be subjected to the sidelobe and scattered energy. Presumbably the illumination taper and power level can be selected to hold this exposure level to a safe value. At this time there is no official recommendation regarding this type of application. For the purpose of this study 1 watt/m^2 was assumed for the level outside the restricted area.

It was also shown that the receiver peak allowable power density can have a significant impact on system cost. This is somewhat true of the allowable continuous exposure level in the sidelobes as well. Therefore, it would be appropriate to establish acceptable exposure levels early, since projected cost competitiveness will play a role in the decision process.

The complete effect of the absorbed energy in the ionosphere is unknown at this time. Potentially non-linear effects could occur at the MPTS power density (200-300 watts/m^2). Experimental and theoretical work has been performed by others to produce and understand ionospheric modification (reference 28) by heating the ionosphere with high power HF transmissions. Significant changes in reflectivity of the ionosphere to frequencies as high as UHF were observed as well as significant electron density fluctuations.

Preliminary analyses (reference 7) indicate similar observable effects would occur in the ionosphere due to 2.45 GHz heating. Although these analyses indicate the effect on the beam would be insignificant, it would be appropriate to proceed with more study and possibly more experimentation to verify the absence of significant beam degradation at 2.45 GHz.

The RFI impact is somewhat uncertain due to unknowns regarding converter noise emissions and harmonic generation. It was shown that with suitable filtering an exclusion band can be defined outside of which interference is unlikely for other

spectral users. The impact of harmonic radiation is more uncertain than that of the noise emissions since the assessment is very sensitive to the assumptions used in conducting the analyses. Typically, 10-40 db of rejection of each harmonic will be necessary to prevent interference with satellite-to-earth communications. This is in addition to 80 db of rejection assumed to be provided by the fundamental filter and waveguide circuitry.

The need for accurate phase control on the transmitter was established. A total rms phase error, from all causes, of no more than 10 degrees is required to insure scattering losses will be less than 3 per cent.

REFERENCES

1. Dickinson, R. M.; and Brown, W. C.: Radiated Microwave Power Transmission System Efficiency Measurements. (JPL-TM-33-727, Jet Propulsion Lab.; NAS7-100) NASA CR-142986, 1975.

2. Dickinson, R. M.: Evaluation of a Microwave High-Power Reception-Conversion Array for Wireless Power Transmission. (JPL-TM-33-741, Jet Propulsion Lab.; NAS7-100) NASA CR-145625, 1975.

3. Glaser, Peter E.; et al.: Feasibility Study of a Satellite Solar Power Station. NASA CR-2357, 1974.

4. Dunn, Donald A.; and Loewenstern, W. Jr.: Economic Feasibility of Microwave Power Transmission in Circular Waveguide. Microwave Power Engineering, Vol. 1, E. C. Okress, ed., Academic Press, 1968, pp. 256-269.

5. Gaubau, George; Schwering, Felix: Free Space Beam Transmission. Microwave Power Engineering, Vol. 1, E. C. Okress, ed., Academic Press, 1968, pp. 241-255.

6. Ehricke, Krafft: Power Relay Satellite, A Means of Global Energy Transmission Through Space. Rep. E74-3-1, Rockwell International Corp., 1974.

7. Howell, J. M., et al: Microwave Power Transmission System Studies. Volume 1: Executive Summary. (ER75-4368-Vol-1, Raytheon Co.; NAS3-17835), NASA CR-134886-Vol-1, 1975.

   Maynard, O. E., et al: Microwave Power Transmission System Studies. Volume 2: Introduction, Organization, Environmental and Spaceborne Systems Analyses. (ER75-4368-Vol-2, Raytheon Co.; NAS3-17835), NASA CR-134886-Vol-2, 1975.

   Maynard, O. E., et al: Microwave Power Transmission System Studies. Volume 3, Section 8: Mechanical Systems and Flight Operations. (ER75-4368-Vol-3, Raytheon Co.; NAS3-17835), NASA CR-134886-Vol-3, 1975.

8. A National Plan for Energy Research, Development and Demonstration: Creating Energy Choices for the Future. Vol. 2: Program Implementation. ERDA-48, Energy Res. Develop. Adm., 1975.

9. Nathan, C. A.: Space-Based Solar Power Conversion and Delivery Systems (Study). (GAS-NSS-P-75-001, Grumman Aerospace Corp.; NAS8-31308), NASA CR-144252, 1975.

10. Goubau, George; and Schwering, F.: On Guided Propagation of Electromagnetic Wave Beams. IEEE Trans. Antennas Propag., vol. AP-9, no. 3, May 1961, pp. 248-256.

11. Heurtley, John C.: Maximum Power Transfer Between Finite Apertures. IEEE Trans. Antennas Propag., vol. AP-15, no. 2, March 1967, pp. 298-300.

12. Lansraux, Guy; and Boivan; Germain: Maximum of the Factor of Encircled Energy. Can. J. Phys.) vol. 39, 1961, pp. 158-188.

13. Sherman, John W., III: Properties of Focused Apertures in the Fresnel Region. IEEE Trans. Antennas Propag., vol. AP-10, no. 4, July 1962, pp. 399-408.

14. Goubau, G.: Microwave Power Transmission From an Orbiting Solar Power Station. J. Microwave Power, vol. 5, no. 4, Dec. 1970, pp. 223-231.

15. Skolnik, M. I.: Self-Phasing Array Antennas. IEEE Trans. Antennas Propag., vol. AP-12, no. 2, March 1964, pp. 142-149.

16. Sichelstiel, B. A.: Self-Focusing Array Research Model. IEEE Trans. Antennas Propag., vol. AP-12, no. 2, March 1964, pp. 150-154.

17. Pon, Chuck Y.: Retrodirective Array Using the Heterodyne Techniqe. IEEE Trans. Antennas Propag., vol. AP-12, no. 2, March 1964, pp. 176-180.

18. Roger, Robert S.; et al.: A Supersynthesis Radio Telescope for Neutral Hydrogen Spectroscopy at the Dominion Radio Astrophysical Observatory. Proc. IEEE, vol. 61, no. 9, Sept. 1973, pp. 1270-1276.

19. Ruze, John: Antenna Tolerance Theory - A Review. Proc. IEEE, vol. 54, no. 4, April 1966, pp. 633-640.

20. Feasibility Study of Large Space Erectable Antennas. Vol. 2: Study. (GDC-DCL-67-002-Vol-2, General Dynamics/Convair; NASW-1438) NASA CR-85268, 1967.

21. Crane, R. K.: Propagation Phenomena Affecting Satellite Communication Systems Operating in the Centimeter and Millimeter Wavelength Bands. Proc. IEEE, vol. 59, no. 2, Feb. 1971, pp. 173-189.

22. Falcone, V. J.,: Atmospheric Attenuation of Microwave Power." J. Microwave Power, vol. 5, no. 4, Dec. 1970, pp. 269-278.

23. Murahami, T; Wickizer, G. S.: Ionospheric Phase Distortion and Faraday Rotation of Radio Waves. RCA Review, vol. 30, Sept. 1969, pp. 474-503.

24. Stevens, Grady H.; Leninger, Gary: Statistics of the Radiated Field of a Space-To-Earth Microwave Power System. proposed TM.

25. Schanda, E.: The Effect of Random Amplitude and Phase Errors of Continuous Apertures. IEEE Trans. Antennas Propag., vol. AP-15, no. 3, May 1967, pp. 471-473.

26. Skolnik, Merrill I., ed.: Radar Handbook. McGraw-Hill Book Co., Inc., 1970, p. 29-6.

27. Blevis, B. C.: Losses Due to Rain on Radomes and Antenna Reflecting Surfaces. IEEE Trans. Antennas Propag., vol. AP-13, no. 1, Jan. 1965, pp. 175-176.

28. Utlaut, W. F.: Ionospheric Modification Induced by High-Power HF Transmitters - A Potential for Extended Range VHF-UHF Communications and Plasma Physics Research Proc. IEEE, vol. 63, no. 7, July 1975, pp. 1022-1043.

29. Skowron, John F.: The Continuous-Cathode (Emitting-Sole) Cross-Field Amplifier. IEEE Proc. vol. 61, no. 3, Mar. 1973, pp. 330-356.

30. Panter, Philip F.: Modulation, Noise, and Spectral Analysis. McGraw-Hill, 1965, pp. 429-431.

APPENDIX A

Calculation of Impact of Noise Emissions From DC-RF Converters

Currently, there is little data regarding noise emissions from amplitrons. A discussion of such emissions is found in reference 29, but the cited data were inferred from pulse measurements on the amplitrons. It is not clear that these data are applicable to continuous duty operation of amplitrons, but the data indicate noise levels of 100-110 db/Hz below the rated power output of the converters. Raytheon has indicated (reference 7) that for continous duty operation, -130db/Hz should be obtainable. In fact, their measurements on an oven type magnetron indicate the noise level may be even lower. For the klystron, Raytheon considers -150 db/Hz to be typical for this application.

The impact of these emissions is amplified to a degree when the DC-RF converters are used in cascade. Currently, this is the favored mode of operation for the amplitron since it makes double use of the waveguide for radiation and RF distribution. This is a useful weight saving feature.

There are probably many models for calculating noise impact. Two possible models will be discussed here. The basic difference in the models is the method of accounting for coherence between converter outputs.

Consider the cascade arrangement of converters as shown in Figure 30. Assume the cascade is excited by a noiseless source. This source is likely to be a TWT or klystron for which this assumption would be reasonable, given the much higher noise levels expected from the amplitron.

The output of the source is injected into the first amplitron. This amplitron synchronizes with this excitation but a small noise is added. The output of this first converter excites a section of slotted waveguide losing a major fraction of its output power. The remainder excites the following converter and so on.

Model I

Assume the additive noise is gaussian and of intensity p and amplitude e_{n_1}. Additive noise can be modeled as shown in Figure 31. A tone of amplitude E_1 is interfered with by a small signal, random in amplitude and phase, of amplitude $e_{n_1}(t)$. This approximation is reasonable whenever the application is very narrowband (reference 30), as is the case here. The resultant signal of amplitude E_2 is given by:

$$E_2 = \left[\sqrt{(E_1 + e_{n_1}\cos\psi_1)^2 + (e_{n_1}\sin\psi_1)^2}\right]\cos(\omega_0 t + \theta_2) \qquad (A-1)$$

where,

$$\theta_2 = \tan^{-1}\left[\frac{e_{n1}\sin\psi_1}{E_1 + e_{n1}\cos\psi_1}\right] \qquad (A-2)$$

Since $E_1 >> e_{n1}(t)$ equations (A-1) and (A-2) can be approximated with,

$$E_2(t) \doteq E_1 \cos(\omega_0 t + \theta_1(t)) \qquad (A-3)$$

and,

$$\theta_1(t) \doteq \frac{e_{n1y}(t)}{E_1} \qquad (A-4)$$

where $e_{n1y}(t)$ is the orthogonal component of $e_{n1}(t)$. Assuming the power is split evenly between the in-phase and quadrature components,

$$\overline{e_{n1y}^2(t)} = \frac{1}{2}\overline{e_{n1}^2(t)} \qquad (A-5)$$

Since the amplitron performs essentially as an injection locked oscillator, the oscillations will synchronize with the input excitation including the residual phase modulation produced by the additive noise of the previous stage.

Therefore, the output of the second tube will have a phase noise component which is perfectly coherent with the same component of the previous converter (We are ignoring the additive noise of this second converter in this model).

Since all the converters in a cascade will have coherent noise components, the effective radiation area is larger than a single section of slotted waveguide. The effective area is given by

$$A_e = \frac{\pi N P_o D_t^2}{4 \bar{P}} \qquad (A-6)$$

where D_t is the antenna diameter, P_o is the rated RF converter output, and $\bar{P}$ is the total radiated RF power. The effective gain of each such combination is

$$G_e = \frac{4\pi \Delta A_e}{\lambda^2} \qquad (A-7)$$

where $\Delta < 1$ accounts for possibility of outputs not being completely coherent (Separation in space is equivalent to separation in time. Therefore, the spatial correlation would have a similar appearance to the time correlation. For large separations, coherency of the noise components would disappear). The number of such combinations is given by

$$M = \frac{\bar{P}}{N P_o} \qquad (A-8)$$

The noise power density at the receive site, p_{no}, is then,

$$P_{no} = \frac{\Delta M}{2}\left(\frac{4\pi A_e}{\lambda^2}\right)\left(\frac{NP_n}{4\pi Z^2}\right) \qquad (A-9)$$

or,

$$P_{no} = \frac{\Delta N P_n A_t}{2\lambda^2 Z^2} \qquad (A-10)$$

where P_n is the noise power at the output of the first converter and the factor of 1/2 accounts for the splitting of the available noise power of the first converter into in-phase and quadrature components.

Model II

Including the noise contributions of the remaining N-1 converters in the N converter cascade has a significant effect on the calculated noise impact. The accounting for this additional effect follows.

The form of the output of the second converter was previously developed assuming the second converter noise was essentially zero. Allowing for a non-zero contribution, the output of the second converter can be visualized as shown in Figure 32. The orthogonal component introduced by the first converter, $e_{n_1 y}(t)$, is passed by the second converter with amplification to its original level. Added to this is the noise contribution of the second converter, $e_{n_2}(t)$.

The resultant signal at the output of the second converter can then be modeled as,

$$E_2 = \left[\sqrt{(E_1 + e_{n2}\cos\psi_2)^2 + (e_{n1y} + e_{n2}\sin\psi_2)^2}\right] \cos(\omega_o t + \theta_2) \qquad \text{(A-11)}$$

where,

$$\theta_2(t) = \tan^{-1}\left[\frac{e_{n1y}(t) + e_{n2y}(t)}{E_1 + e_{n2}\cos\psi_2(t)}\right] \qquad \text{(A-12)}$$

Since $E_1 >> e_{n2}$ and e_{n1} these equations can be approximated as,

$$E_2(t) \doteq E_1 \cos(\omega_o t + \theta_2(t)) \qquad \text{(A-13)}$$

where,

$$\theta_2(t) \doteq \frac{e_{n1y}(t) + e_{n2y}(t)}{E_1} \qquad \text{(A-14)}$$

By analogy, the output of the Lth converter is given by,

$$E_L(t) \doteq E_1 \cos(\omega_o t + \theta_L(t)) \qquad \text{(A-15)}$$

where,

$$\theta_L(t) \doteq \sum_{j=1}^{L} \frac{e_{njy}(t)}{E_1} \qquad \text{(A-16)}$$

Therefore the first converter will introduce a noise

component which is coherent over N converters, the second converter will introduce a noise component coherent over N-1 converters, etc. The effective radiation area varies for each component.

For the first noise component the effective radiation area is

$$A_{e_1} = \frac{\pi N P_0 D_t^2}{4 \bar{P}} \qquad \text{(A-17)}$$

the same as (A-6).

For the Lth noise component, the effective radiation area is

$$A_{eL} = \left(\frac{N-L+1}{N}\right) A_{e_1} \qquad \text{(A-18)}$$

The effective gain for the Lth component is given by,

$$G_{eL} = \frac{4\pi \Delta A_{eL}}{\lambda^2} \qquad \text{(A-19)}$$

and the number of such combinations with gain G_{eL} is

$$M_L = \frac{\bar{P}}{N P_0} \qquad \text{(A-20)}$$

Therefore, the noise power density at the receive site, p_{no}, is given by,

$$\rho_{no} = \sum_{L=1}^{N} \frac{M_L G_{eL} (N-L+1) P_n}{\lambda Z^2} \qquad \text{(A-21)}$$

or,

$$\rho_{no} = \frac{1}{12} \frac{\Delta A_t P_n (N+1)(2N+1)}{\lambda Z^2} \qquad \text{(A-22)}$$

This last equation made use of the rule,

$$\sum_{L=1}^{N} L^2 = \frac{L(L+1)(2L+1)}{6} \qquad \text{(A-23)}$$

This model is favored over model I because it is judged unreasonable to assume the first converter noise will dominate the noise level of the N tube cascade.

APPENDIX B

Cost Equations

This study made use of a cost model which is essentially the same as that suggested by Raytheon (reference 7). In this model the total cost of the system is structured as

$$Cost=C_{bs}+C_{wg}+C_t+C_{pc}+C_{at}+C_{rec}+C_{pwr}+C_{atpwr}+C_{xmtdis}+C_{gnddis}+C_{xcmd} \quad (B-1)$$

where each of the component costs are modeled as follows:

1) Backup structure-

$$C_{bs}=UC_{bs} \cdot UW_{bs} \cdot A_t + W_{jt} \cdot UC_{bs} \quad (B-2)$$

where UC_{bs} =cost of backup structure, \$/Kg

UW_{bs} =weight of backup structure, Kg/m^2

A_t =area of transmit antenna, m^2

W_{jt} =total weight of rotary joint, Kg

2) Waveguide-

$$C_{wg}=UC_{wg} \cdot A_t \quad (B-3)$$

where UC_{wg} =cost of waveguide, \$/m^2

3) DC-RF converters-

$$C_t = UC_t \cdot P_{RDC} / \eta_r \eta_{rf} \eta_{bm} \qquad (B-4)$$

where UC_t =cost of converter, \$/KW

P_{RDC} =total delivered ground power, KW

η_r =rectenna collection and conversion efficiency

η_{rf} =RF link efficiency including effects of atmosphere, scattering losses, and pointing errors.

η_{bm} =beam efficiency or fraction of available power intercepted by rectenna.

4) Phase control-

$$C_{pc} = UC_{pc} \cdot A_t / A_{sae} \qquad (B-5)$$

where UC_{pc} =cost of phase control, \$/subarray

A_{sae} =area of electrical subarray (may be different than mechanical subarray), m^2

5) Pointing control-

$$C_{pt} = UC_{pt} \cdot A_t / A_{sam} \qquad (B-6)$$

where UC_{pt} =cost of pointing, \$/subarray

A_{sam} =area of mechanical subarray

6) Assembly and transportation of transmit antenna-

$$C_{at}=UC_{at}\ W_{mpts} \tag{B-7}$$

where UC_{at}=cost of assembly and transport, \$/Kg

W_{mpts}=total weight of MPTS

7) Weight of MPTS-

$$W_{mpts}=W_{bs}+W_{wg}+W_t+W_{pc}+W_{pt}+W_{xmtdis}+W_{xcmd} \tag{B-8}$$

where

$$W_{bs}=UW_{bs}\cdot A_t + W_{jt} \tag{B-9}$$

$$W_{wg}=UW_{wg}\cdot A_t \tag{B-10}$$

$$W_{pc}=UW_{pc}\cdot A_t/A_{sae} \tag{B-11}$$

$$W_{pt}=UW_{pt}\cdot A_t/A_{sam} \tag{B-12}$$

$$W_{xmtdis}=UW_{xmtdis}\cdot\sqrt{P_{RDC}/\eta_{DC}} \tag{B-13}$$

$$W_t=UW_t\cdot P_{RDC}/\eta_r\eta_{rf}\eta_{bm} \tag{B-14}$$

and,

UW_{wg}=unit weight of waveguide, Kg/m^2

UW_{pc}=unit weight of phase control system, Kg/subarray

UW_{pt}=unit weight of subarray pointing control, Kg/subarray

UW_{xmtdis} =coefficient of distribution system weight, $Kg/(KW)^{\frac{1}{2}}$

UW_t =unit weight of converters, Kg/KW

η_{DC} =DC-DC system efficiency

W_{xcmd} =total weight of transmitter command control system, Kg

8) Rectenna-

$$C_{rec}=UC_{rec}\cdot A_r+UC_{prep}\cdot\frac{A_r}{\sin\theta}+\frac{4}{\pi}\frac{UC_{lnd}\cdot A_r\cdot(SLR)^2}{\sin\theta}+C_{gcmd} \qquad (B-15)$$

where UC_{rec} =unit cost of rectenna, $\$/m^2$

A_r =beam area normal to beam axis at receive site, m^2

UC_{prep} =unit preparation cost of land, $\$/m^2$

θ =incidence angle of beam

UC_{lnd} =unit cost of land, $\$/m^2$

SLR =ratio of fence diameter to rectenna diameter

C_{gcmd} =cost of ground command and pilot signal microwave system

9) Prime power-

$$C_{pwr}=UC_{pwr}\frac{P_{RDC}}{\eta_{DC}} \qquad (B-16)$$

where UC_{pwr} =unit cost of prime power, \$/KW

10) Assembly and transport of prime power-

$$C_{atpwr}=UC_{at}\ UW_{pwr}\ \frac{P_{RDC}}{\eta_{DC}} \qquad (B-17)$$

where UW_{pwr} =unit weight of prime power, Kg/KW

11) DC distribution on transmit antenna-

$$C_{xmtdis}=UC_{xmtdis}\sqrt{\frac{P_{RDC}}{\eta_{DC}}} \qquad (B-18)$$

where UC_{xmtdis} =coefficient of distribution system cost, $\$/(KW)^{\frac{1}{2}}$

12) DC collection and conversion at rectenna-

$$C_{gnddis}=UC_{Gnddis}\sqrt{P_{RDC}} \qquad (B-19)$$

where UC_{gnddis} =unit cost of distribution system, $\$/KW^{\frac{1}{2}}$

13) Transmitter command control system-

$$C_{xcmp}=\text{Fixed Cost/System}$$

These equations can be simplified somewhat by combining terms. One such combination results in,

$$Cost = F_1 A_t + F_2 A_r + F_3 \sqrt{P_{RDC}} + F_4 P_{RDC} + F_5 \qquad \text{(B-20)}$$

where,

$$F_1 = UC_{bs} \cdot UW_{bs} + UC_{wg} + \frac{UC_{pc}}{A_{sac}} + \frac{UC_{pt}}{A_{sam}} + UC_{at} \cdot \left(UW_{bs} + UW_{wg} + \frac{UW_{pc}}{A_{sac}} + \frac{UW_{pt}}{A_{sam}} \right)$$

$$F_2 = UC_{rec} + \frac{UC_{preamp}}{\sin\theta} + \frac{4}{\pi} \frac{UC_{Ind} \cdot (SLR)^2}{\sin\theta}$$

$$F_3 = \frac{UC_{xmtdis} + UC_{at} \cdot UW_{xmtdis} + UC_{gnddis}}{\eta_{DC}}$$

$$F_4 = \frac{(UC_t + UC_{at} \cdot UW_t)}{\eta_r \eta_{rf} \eta_{bm}} + \frac{(UC_{pwr} + UC_{at} \cdot UW_{pwr})}{\eta_{DC}}$$

$$F_5 = W_{jt} \cdot UC_{bs} + UC_{at} \cdot W_{jt} + C_{gcmd} + C_{xcmd}$$

The system specific cost, Γ, can then be written as,

$$\Gamma = \frac{F_1 A_t + F_2 A_r + F_5}{P_{RDC}} + \frac{F_3}{\sqrt{P_{RDC}}} + F_4 \qquad \text{(B-21)}$$

The specific cost can be optimized with respect to transmit antenna diameter by substituting,

$$A_r = \frac{(\lambda z \tau)^2}{A_t} \qquad \text{(B-22)}$$

into equation (B-21) and differentiating with respect to A_t. Setting the result equal to zero and solving for A_t

$$A_t^{opt} = \lambda z \tau \sqrt{\frac{F_2}{F_1}} \qquad \text{(B-23)}$$

gives a minimum for Γ since the second derivative is positive.

Cost Equations With Constraints

Limitations on peak axial density at the transmitter (thermal effects) and the rectenna (biological effects) can be included in equation (B-21). With these constraints it will be shown that no optimum antenna area exists except when these constraints are considered simultaneously.

Thermal Constraints

The effects of maximum converter packing density and maximum allowable structural temperature are discussed in section 2.1.3. Each of these effects establishes a maximum allowable peak RF power density on the transmit antenna and the dominant limitation is identified by the value of the ratio (section 2.1.3),

$$\gamma = \frac{\eta_t}{1-\eta_t} \frac{k_{mat}}{k_{tube}} \qquad \text{(B-24)}$$

where η_t is the converter DC-RF conversion efficiency, k_{mat} is the peak allowable thermal flux density due to structural temperature limitations, and k_{tube} is the maximum converter packing density, watts /m^2.

The peak axial density at the transmitter can be related to the total transmitted power as

$$P_t(0) = \frac{P_t}{A_t} \left(\frac{V}{F}\right)^2 \qquad \text{(B-25)}$$

where V and ζ are dimensionless parameters. Empirical values for these parameters can be found in section 2.1.3.

The transmitted power and the delivered DC ground power are related by,

$$P_{RDC} = \eta_{rf}\,\eta_{bm}\,\eta_r\,P_t \tag{B-26}$$

Combining (B-25) and (B-26),

$$\mathcal{P}_t(0) = \left(\frac{V}{\zeta}\right)^2 \frac{P_{RDC}}{\eta_{rf}\,\eta_{bm}\,\eta_r\,A_t} \tag{B-27}$$

It can be seen from (B-27) that placing a limit on peak transmitter power density in no way limits the delivered DC ground power. The transmitter area and beam geometry can be manipulated to vary the delivered power.

Substituting (B-27) into (B-21), and using

$$A_r = \frac{(\lambda z \tau)^2}{A_t}$$

gives the system specific cost as,

$$\Gamma = \frac{(F_1 A_t + F_2 (\lambda z \tau)^2/A_t + F_5)\cdot(\zeta/V)^2}{\eta_{rf}\,\eta_{bm}\,\eta_r\,A_t\,\mathcal{P}_t(0)} + \frac{F_3\,(\zeta/V)}{\sqrt{\eta_{rf}\,\eta_{bm}\,\eta_r\,A_t\,\mathcal{P}_t(0)}} + F_4 \tag{B-28}$$

which can be written as

$$\Gamma = \frac{F_8}{A_t^2 p_t(0)} + \frac{F_9}{A_t p_t(0)} + \frac{F_{10}}{\sqrt{A_t p_t(0)}} + \frac{F_{11}}{p_t(0)} + F_4 \qquad \text{(B-29)}$$

where,

$$F_8 = F_2 \frac{(\lambda z \tau / V)^2}{\eta_{rf}\, \eta_{bm}\, \eta_r}\, \xi^2$$

$$F_9 = F_5 \frac{(\xi / V)^2}{\eta_{rf}\, \eta_r\, \eta_{bm}}$$

$$F_{10} = F_3 \frac{(\xi / V)}{\sqrt{\eta_{rf}\, \eta_{bm}\, \eta_r}}$$

$$F_{11} = F_1 \frac{(\xi / V)^2}{\eta_{rf}\, \eta_{bm}\, \eta_r}$$

It can be seen from (B-29) that the specific cost decreases monotonically with increasing A_t, for fixed $p_t(0)$. Therefore, with the thermal limit considered alone, there is no optimum A_t. That is, the larger the value of A_t, the lower the system cost.

Ultimately the cost model will become invalid if A_t is made much larger than 1Km. Data supplied by Raytheon (reference 7) suggests the cost model is valid up to approximately 2Km for a transmit antenna diameter.

Biological Constraint

The effect of an environmental regulation on the maximum allowable power density at the receive site is discussed in section 2.3.3.

The delivered ground DC power is related to the peak density at the receive site by

$$P_{Roc} = \frac{\eta_r \eta_{bm} (\lambda z \rho)^2 p_r(0)}{A_t} \qquad \text{(B-30)}$$

Substituting this and equation (B-22) into (B-21) gives the relation,

$$\Gamma = \frac{(F_1 A_t + F_2 (\lambda z \tau)^2 / A_t + F_5) \cdot A_t}{\eta_r \eta_{bm} (\lambda z \tau)^2 p_r(0)} + F_3 \left[\frac{A_t}{\eta_r \eta_{bm} (\lambda z \tau)^2 p_r(0)} \right]^{1/2} + F_4 \qquad \text{(B-31)}$$

which can be rewritten as

$$\Gamma = F_{12} \cdot \sqrt{\frac{A_t}{p_r(0)}} + F_{13} \cdot \frac{A_t}{p_r(0)} + F_{14} \cdot \frac{A_t^2}{p_r(0)} + \frac{F_{15}}{p_r(0)} + F_4 \qquad \text{(B-32)}$$

where,

$$F_{12} = \frac{F_3}{\lambda z \rho \sqrt{\eta_r \eta_{bm}}}$$

$$F_{13} = \frac{F_5}{(\lambda z \rho)^2 \eta_r \eta_{bm}}$$

$$F_{14} = \frac{F_1}{(\lambda z \rho)^2 \eta_r \eta_{bm}}$$

$$F_{15} = \frac{F_2 (\tau/\rho)^2}{\eta_r \eta_{bm}}$$

It can be seen from (B-32) that the specific system cost decreases monotonically as A_t decreases. Therefore, with $p_r(0)$ fixed no optimum A_t can be established. That is, the smaller A_t is made, the less the system specific cost.

This point and the relation developed for a fixed peak transmitter power density may seem contradictory. However, these equations are simply indicating valid methods for reducing system

costs within certain constraints.

Remember that (B-21) indicated that system specific cost decreases monotonically with P_{RDC}. Therefore, given one or more constraints, efforts should be made to adjust system parameters to make P_{RDC} as large as possible.

With a fixed transmitter peak power density, P_{RDC} can be increased by increasing the transmitter area. Also, for a fixed receive peak power density, P_{RDC} can be increased by decreasing the transmitter antenna area (this spreads the beam at the receive site requiring a larger rectenna). If both constraints are satisfied simultaneously, only one transmitter area is possible (if a solution exists at all). Since the rectenna area is related to the transmitter area by (B-22), the rectenna area is also determined by these constraints.

For a given P_{RDC} and maximum allowable $p_t(0)$, equation (B-25) and (B-26) can be used to establish the minimum antenna area,

$$A_t^{min} \geq \frac{(\nu/f)^2 P_{RDC}}{\eta_{rf}\,\eta_{bm}\,\eta_r\,p_t(0)} \qquad \text{(B-33)}$$

Also, for a given P_{RDC} and maximum allowable $p_r(0)$, equation (B-30) can be used to establish the maximum allowable antenna area,

$$A_t^{max} \leq \frac{(\lambda z \xi)^2 \eta_r \eta_{bm} \rho_r(\omega)}{P_{ADC}} \qquad \text{(B-34)}$$

The conditions for simultaneous solution of (B-33) and (B-34), if a solution exists, can be found from

$$A_t^{min} = A_t^{max} \qquad \text{(B-35)}$$

Solving for P_{ADC},

$$P_{ADC} = \frac{\lambda z \eta_r \eta_{bm} \xi^2}{V} \sqrt{\eta_{rf} \rho_t(\omega) \rho_r(\omega)} \qquad \text{(B-36)}$$

Therefore, the transmit antenna area that satisfies both constraints can be found from,

$$A_t = (\lambda V z) \sqrt{\frac{\rho_r(\omega)}{\eta_{rf} \rho_t(\omega)}} \qquad \text{(B-37)}$$

APPENDIX C

Cost and Weight Parameters

At this time, estimates for various cost and weight parameters for the MPTS reflect the judgements of people working in the respective technology areas. Devices appropriate to this application do not yet exist. For this reason it would be inappropriate to use the cost model to generate a "number". It would be appropriate to use the model to test the MPTS sensitivity to various parameters. In this way, one can quickly identify critical technology areas where uncertainties significantly affect system cost.

In this study the sensitivity of a MPTS to variations in geometrical parameters such as beam efficiency, taper, etc was determined. A more extensive sensitivity analysis, including cost parameters, was performed as a part of the Raytheon effort (reference 7).

Values for all microwave system cost and weight parameters used in this study were supplied by Raytheon and are tabulated in Tables C-I and C-II. Power system, transportation and orbital assembly parameters used in this study are tabulated in Table C-III. The third column of this table has been highlighted and this column represents values that have been identified in the literature and used in other study efforts (references 8,9). Note that there are several values for each of these parameters

included in the table. The highlighted values have been treated as reference values. System sensitivity was determined by using 1/2 these values (second column) and twice these values (fourth column). Also shown for purposes of comparison are values designated as current which are either achievable now or expected to be achieved in the near term. All values in this table are rounded to two significant figures. Note that the current data for transportation and assembly only includes the cost of transportation. No current data is available for assembly of large structures in space.

The relative sensitivity of total system capital cost to various parameters was determined and the results are shown in Figure 33. The (1/2,1,2) sequence used in Table C-III was also applied to power level and frequency. Figure 33 indicates the largest sensitivities to be those due to power source, power level, transportation and assembly. Note that the sensitivity to power level decreases rapidly above 5 Gw.

The relative ranking of subsystem costs and sensitivities was also determined and the results are shown in Figures 34-38. In each case displayed, the drivers of total system cost are the power source and/or transportation and assembly. Consequently, variations in these parameters produced the greatest variation in total system cost.

Figure 34 shows subsystem sensitivity to frequency. Because of the thermal limit on minimum transmitter size and decreasing

efficiency with frequency, the transmitter has a minimum size with respect to frequency and the power source increases with frequency. The total impact is relatively small over the range considered.

Figure 35 shows subsystem sensitivity to power source cost and Figure 36 shows the sensitivity to transportation and assembly. The power source variation only impacts the power source contribution but the impact is very significant. Costs of transportation and assembly impact the transmitter and receiver as well since the optimum size is a function of this cost.

The amount of power delivered by the receiver (power level) affects only the less expensive subsystems as shown in Figure 37. Therefore the effect of power level on total system cost decreases as power level increases.

Figure 38 shows the subsystem sensitivity to power source weight. This variation only affects the cost of transport and assembly of the power source, but the variation is significant.

It should be noted that a second order effect could have been included in performing the analysis regarding the power source parameters. The minimum cost beam interception is a function of the relative cost between the microwave link and power source. Hence for high power source cost the interception efficiency should be higher than the 90 per cent used in Figures 34-38 and vice versa. Consequently, a more detailed analysis would have displayed a small sensitivity for the transmitter and

receiver due to changes in power source costs and weights. Although not shown explicitly here, this result is implicit in the analysis in section 2.3.3 and the results displayed in Figures 22 and 23.

TABLE I

CONTENDERS FOR SUBARRAY

Antenna Type	Estimated Efficiency	Comments
1. Deployable cluster of rigid paraboloids	20%	Spillover, blockage, mechanical alignment, and power distribution major impediments to high efficiency.
2. Large erectable paraboloid	50-60%	Spillover and blockage major impediments to high efficiency. Cassegrain type feeds may boost efficiency to 80%.
3. Large erectable horn array	10-80%	Power distribution major impediment to high efficiency. 80% may be obtainable if the horns are driven individually, 10-70% if driven in parallel. Grating lobes may be a problem.
4. Array of slotted waveguide sections with all sections driven in parallel	50-90%	Practical only with high power tube (100 KW and higher).
5. Array of slotted waveguide sections with integral cross-field amplifiers (SSPS).	80-90%	Cascading of cross field amplifiers may produce coherence of tube noise over the subarray, possibly creating a severe RFI impact.
6. Array of dipoles driven in parallel	15%	Distribution losses high.
7. Array of dipoles driven individually	30-80%	Low power amplitrons (100 W) not cost effective. Solid state amplifiers relatively inefficient.
8. Dielectric lens	70-80%	Heavy, non-deployable.
9. Metal lens	70-80%	Lighter than dielectric lens but heavier than other antenna types. Possibly deployable.
10. Array of helices driven individually	55%	Insensitive to polarization shifts in ionosphere. Requires circularly polarized receive elements.

TABLE II

TRANSMITTER CONCEPT AND REQUIRED CONVERTER EFFICIENCY
FOR MAXIMUM CONVERTER DENSITY

Concept	Minimum Converter Efficiency
Amplitron/Aluminum Structure	0.86
Amplitron/Epoxy Composite	0.86
Amplitron/Polyimide Composite	0.73
Klystron/Aluminum Structure	0.93
Klystron/Epoxy Composite	0.93
Klystron/Polyimide Composite	0.85

TABLE III

PARAMETERS OF OPTIMAL ILLUMINATIONS

TAPER, DB	ν	ε^2
0	1.000	1.000
5	1.303	1.027
10	1.627	1.103
15	1.958	1.213
20	2.289	1.346

TABLE IV

IMPACT OF UNFILTERED CONVERTER NOISE

Number of Converters in Cascade, N	Noise Power Density at Receiver, DBW/M^2/HZ
10	-154
20	-148
40	-143
80	-147

TABLE V

FILTERED NOISE IMPACT FOR N = 20

Service	Typical Interference Level, DBW/M^2/HZ	Required Exclusion Bandwidth, MHZ
Satellite-Earth Communications	-188	60
Radio Astronomy	-240	236
Terrestrial Radar	-142	23

TABLE VI

HARMONIC OUTPUT OF CONVERTERS IN DB BELOW FUNDAMENTAL (REFERENCE 26)

Harmonic / Converter	2	3	4	5	6	7	8
Magnetron:							
Mean	78.1	71.7	77.7	86	87.2	91.9	99.3
Range	57/103	45/100	62/93	67/114	76/96	81/96	83/114
Samples	77	59	34	23	17	7	5
Klystron:							
Mean	71.3	78.2	76.9	73.9	82.3	87.2	
Range	38/119	57/105	56/101	59/111	73/89	72/97	
Samples	44	27	21	8	7	4	

TABLE VII

IMPACT OF HARMONIC RADIATION, DBW/M^2

Harmonic	Coherence Area 20 M x 20 M	Coherence Area 1 M x 1 M
2	-178	-204
3	-167	-193
4	-169	-195
5	-174	-201
6	-173	-199
7	-176	-202
8	-182	-208

TABLE VIII

SENSITIVITY OF 5 GW OPTIMUM SYSTEM

TO COST PARAMETERS

COSTS	TAPER DB	BEAM EFF. %	TRANSMITTER DIAMETER KM	5/10 DB COST DIFF. %
1/2 x Reference	5/10	85.5/88.5	1.000/1.029	0.9
Reference	5/10	88.5/92.5	.952/1.007	2.0
2 x Reference	5/10	90.5/95.0	.887/0.993	3.0

TABLE IX

ASSUMPTIONS IN DETERMINATION OF PROPELLANT

MASS REQUIREMENTS

DESTINATION	SYSTEM	PROPELLANT PER LAUNCH			NO. LAUNCHES
		10^6 KG		10^6 LB	
		1.36	SOLID	3	
LEO	SHUTTLE				1120*
		.73	O_2+H_2	1.6	

*Includes transport of: assembly equipment, assembly crew rotation and resupply, advanced ion stage (to GEO) and propellant, assembly propellants and tanks, crew space stations, all SPS equipment. Total 23×10^6 kg at 75% packing density.

TABLE X

ENERGY COST TO PROCESS MATERIALS

MATERIAL	ENERGY COST, THERMAL KW-HR/KG
SILICON	6.61
PLASTICS	3.31
INORGANICS	7.72
ALUMINUM	72.8*
SOLID PROPELLANT	3.31
LIQUID HYDROGEN AND OXYGEN	16.2

*100% PRIMARY METAL, NO SCRAP USED TO PRODUCE

TABLE XI

MASS PROPERTIES OF A 5 GW SPS

SUBSYSTEM/COMPONENT	WEIGHT	
	10^6 KG	10^6 LB
Power Source	12.8	28.2
Transmitter	7.0	15.4
o DC-RF Converters	2.37	5.22
o Waveguide	3.38	7.44
o Power Distribution	0.52	1.15
o Phase Control	0.18	0.40
o Structure	0.55	1.21
Receiver	331	729

TABLE C-I

RECTENNA COST ELEMENTS

COMPONENT	COST
UC_{REC}	10 $/M^2$
UC_{PREP}	0.40 $/M^2$
UC_{LND}	0.25 $/M^2$
C_{GCMD}	26 M $/SYSTEM
UC_{GNDDIS}	10 $/(KW)^{\frac{1}{2}}$

TABLE C-II

TRANSMITTER COSTS

SUBSYSTEM	COMPONENT	COST		WEIGHT	
		ALUM	GREP	ALUM	GREP
Structure	UC_{BS}	2.1	32\$/m^2	---	---
	UW_{BS}	---	---	.26	.16 Kg/m^2
	W_{jt}	---	---	2.3×10^5	1.7×10^5 Kg/system
Subarrays	UC_{WG}	130	560\$/m^2	---	---
	UW_{WG}	---	---	4.3	2.6 Kg/m^2
	UC_T(amplitron)	25 \$/KW		---	
	UC_T(klystron)	39 \$/KW		---	
	UWT(amplitron)	---		.32 Kg/KW	
	UWT(klystron)	---		1.0 Kg/KW	
	UC_{PC}	92×10^3 \$/Subarray		---	
	UW_{PC}	---		75 Kg/Subarray	
	UC_{PT}	3×10^4 \$/Subarray		---	
	UW_{PT}	---		70 Kg/Subarray	
Power Distribution	$UC_{XMITDIS}$	3.0×10^4 \$/$(KW)^{\frac{1}{2}}$*		---	
	$UW_{XMITDIS}$	---		18 Kg/$(KW)^{\frac{1}{2}}$*	
Command Control	C_{XCMD}	5.1×10^6 \$/System		---	
	W_{XCMD}	---		760 Kg/System	

*Total DC Power Delivered to Transmit Antenna

TABLE C-III

SATELLITE POWER SYSTEM PARAMETERS

		CURRENT	R/2	REFERENCE	2R
POWER SOURCE COST	- $/KW	100,000+	250	500 (3)	1,000
POWER SOURCE WEIGHT	- KG/KW	12.6 (1)	0.75	1.5 (4)	3.0
TRANSPORTATION AND ORBITAL ASSEMBLY	- $/KG	3,300 (2)	100	200 (4)	400

(1) COMMUNICATIONS TECHNOLOGY SATELLITE (CTS) ARRAY

(2) SHUTTLE/TUG

(3) REFERENCE 8

(4) REFERENCE 9

SPACE TO EARTH MICROWAVE BEAM GEOMETRY

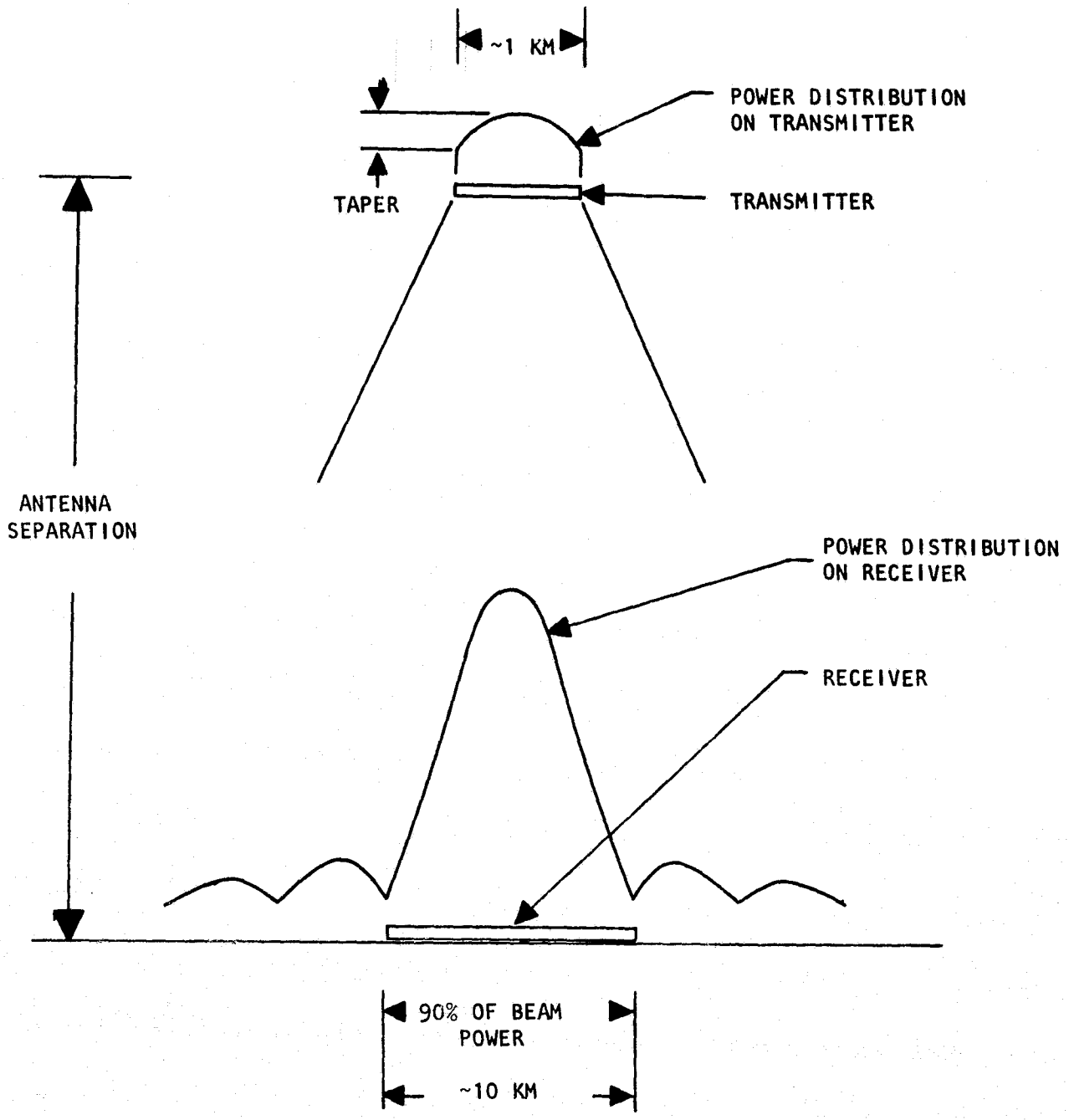

FIGURE 1 - TYPICAL GEOMETRY FOR A SPACE-TO-EARTH MICROWAVE POWER TRANSMISSION SYSTEM SHOWING A 1 KM TRANSMITTER AND A 10 KM RECEIVER WITH WHICH 90% OF THE TRANSMITTED POWER IS INTERCEPTED.

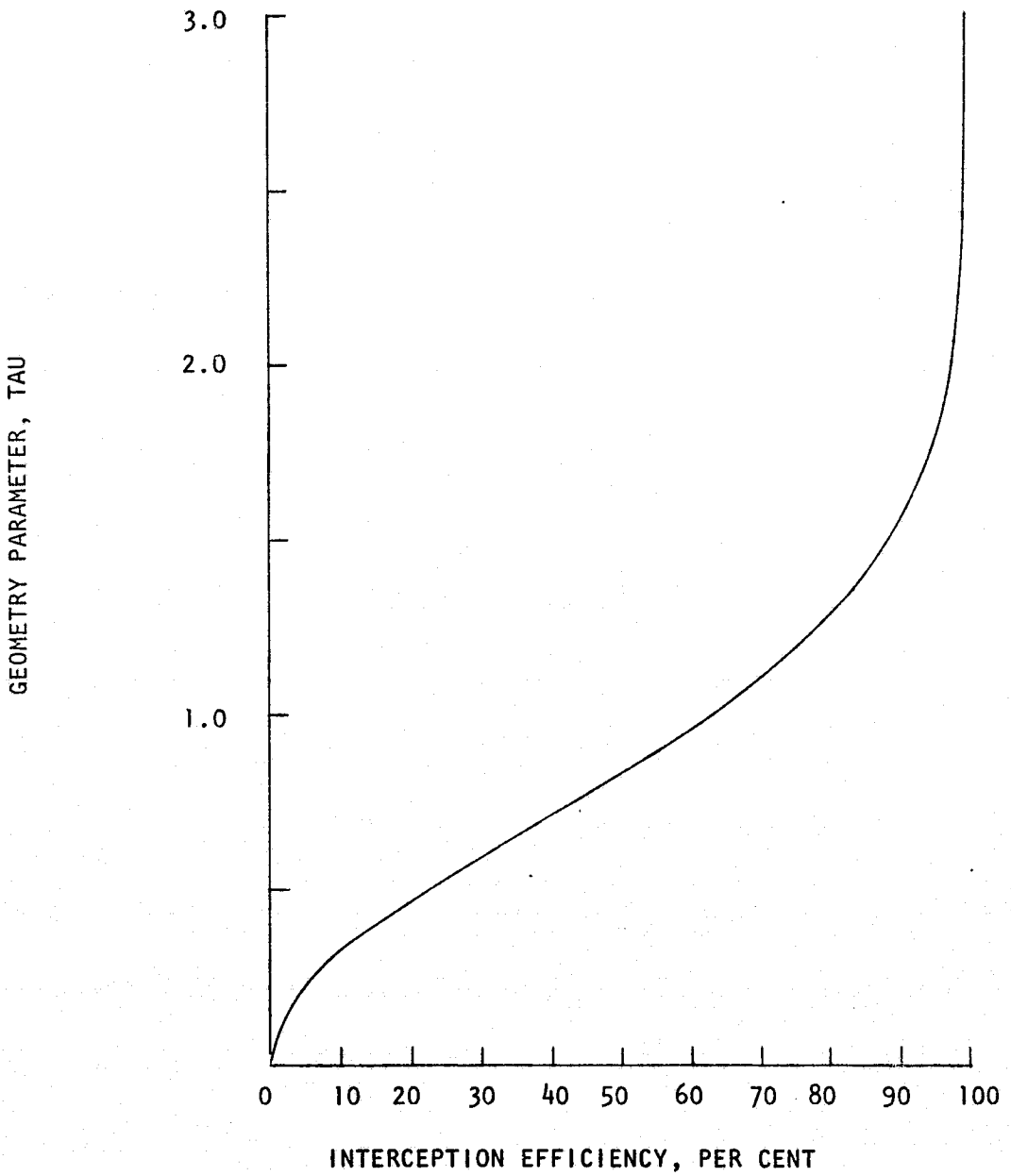

FIGURE 2 - Unconstrained optimum geometry factor, tau, as a function of interception efficiency. Illumination taper is constantly adjusted to provide a minimum tau at each interception efficiency.

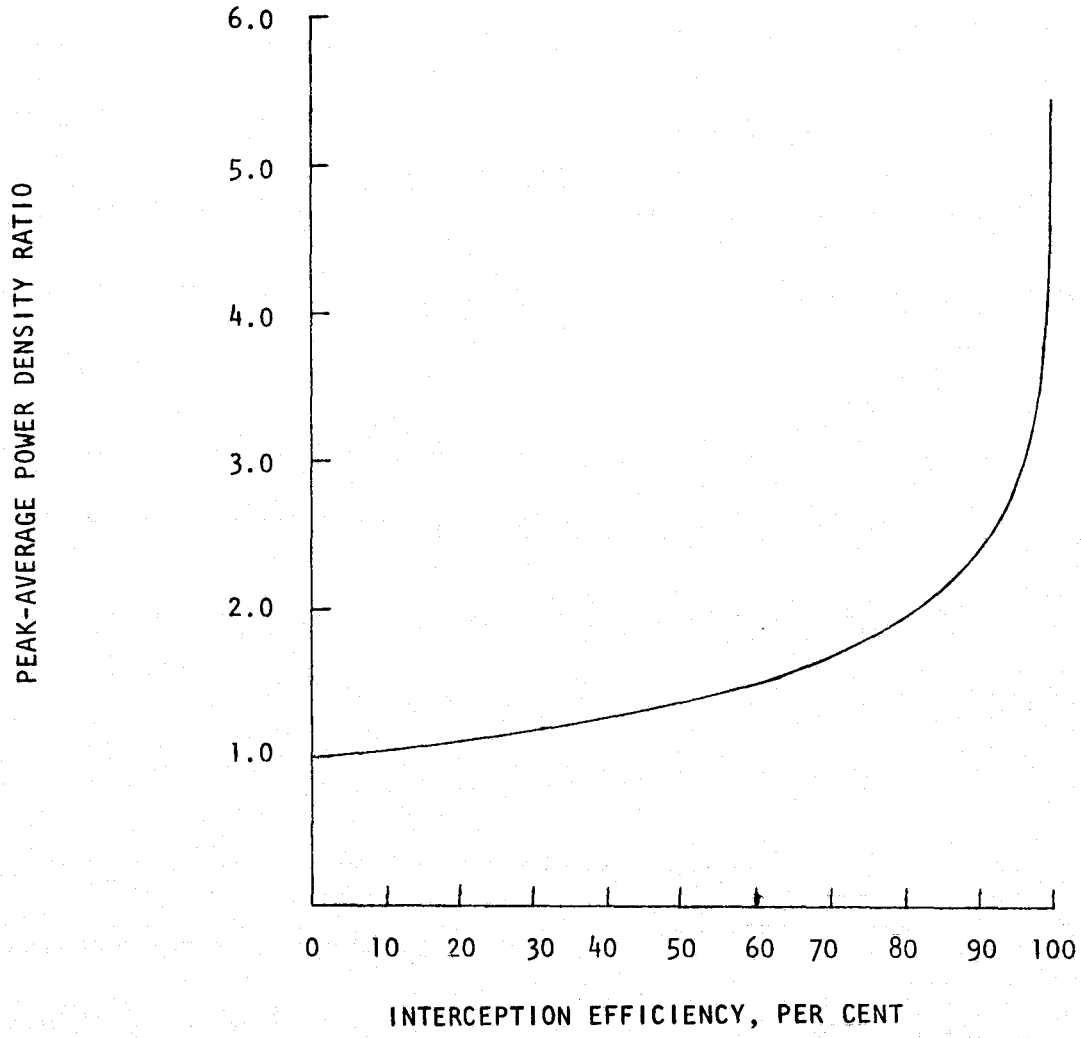

FIGURE 3 - Unconstrained optimum peak-average power density ratio on transmit antenna as a function of interception efficiency.

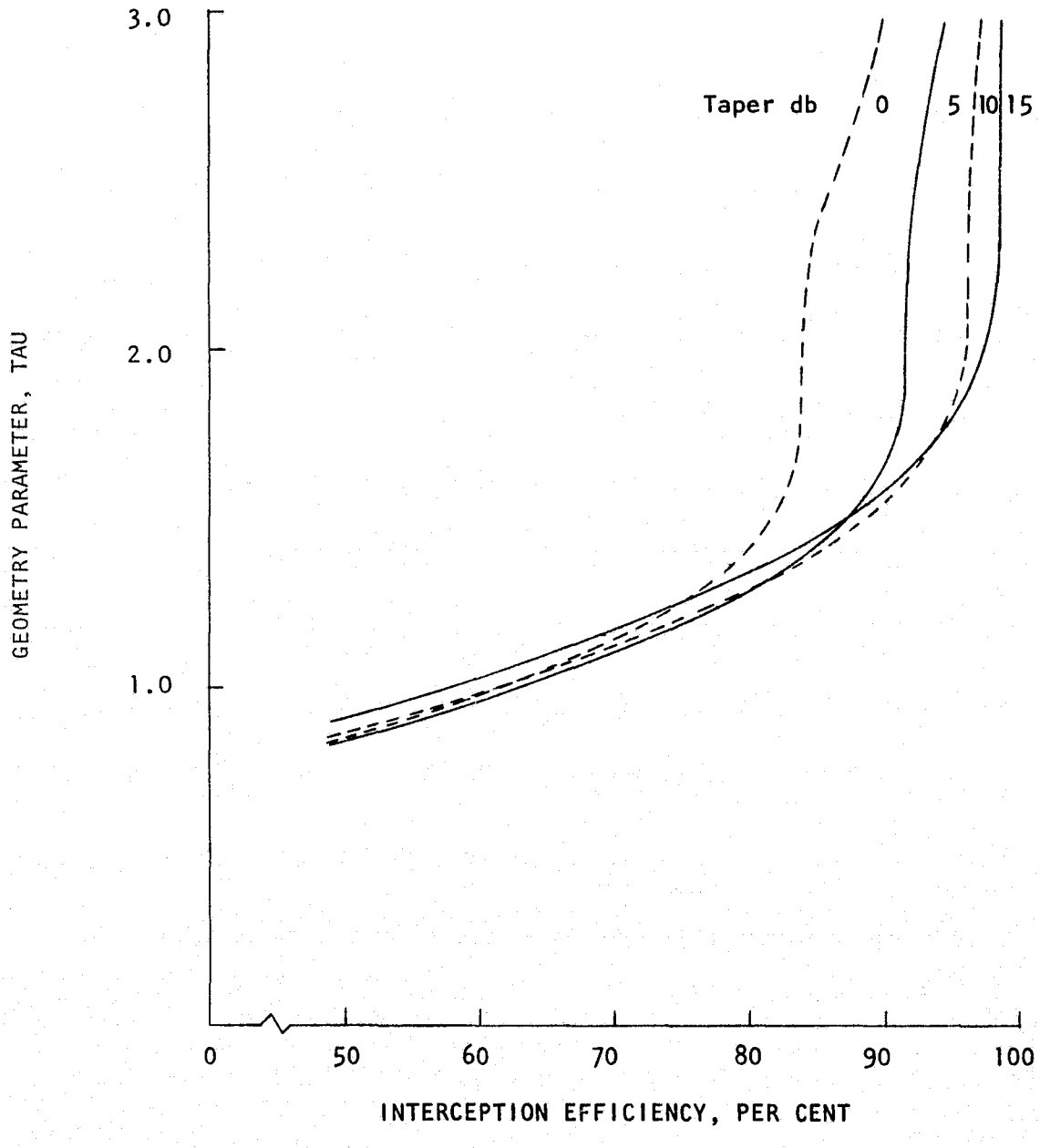

FIGURE 4 - Geometry factor, tau, as a function of interception efficiency for various fixed illumination tapers.

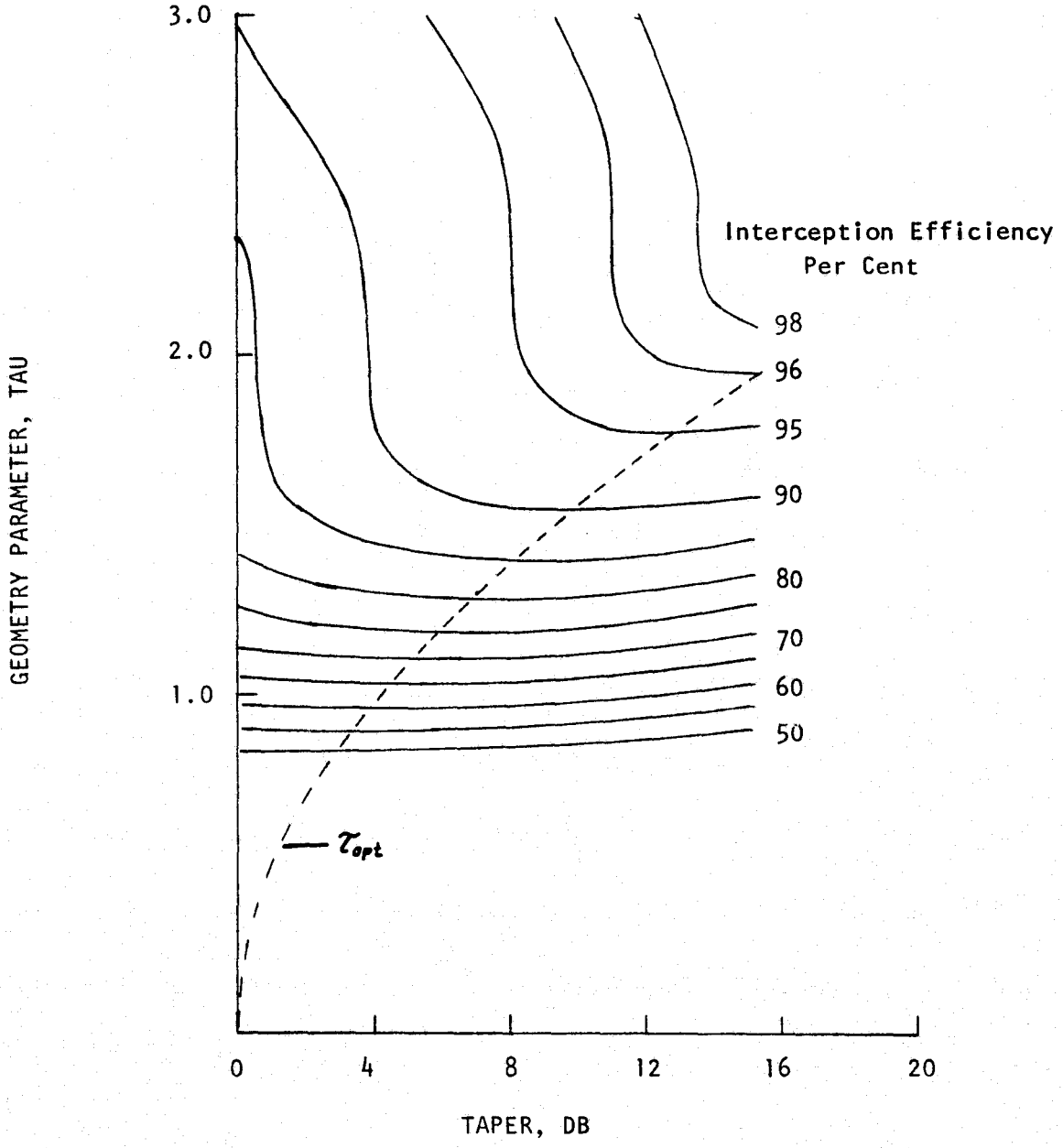

FIGURE 5 - Tau as a function of taper for various interception efficiencies. Also shown is the locus of τ_{opt} (Gaubau relation).

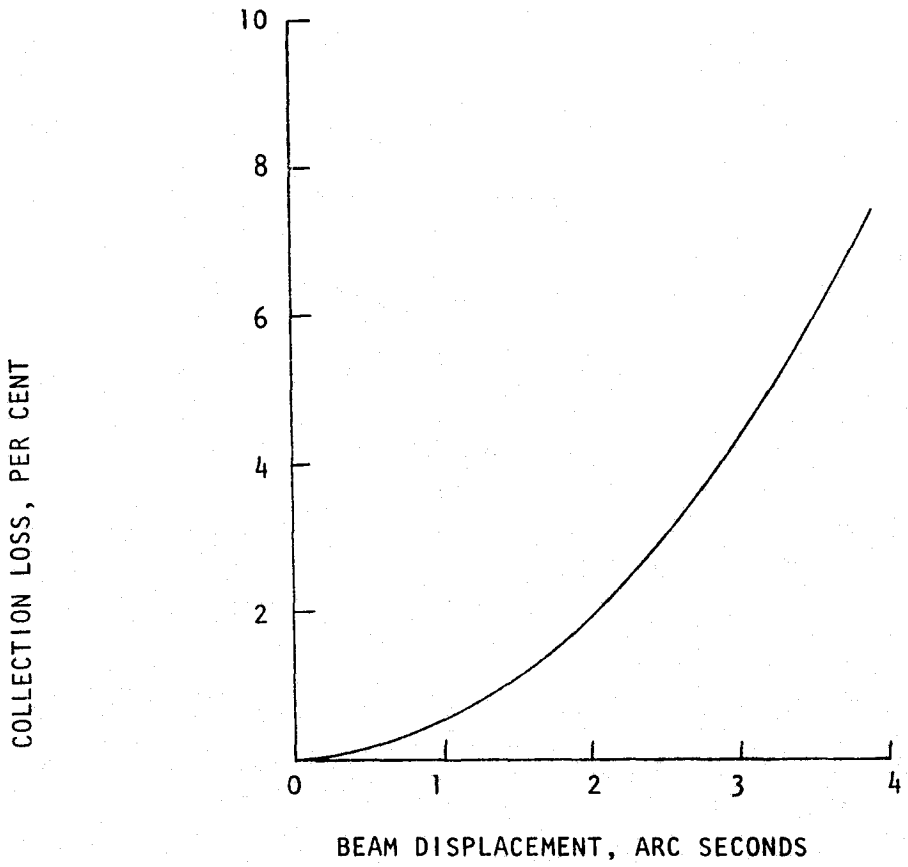

FIGURE 6 - Collection loss versus beam displacement from receive antenna axis. Receive antenna sized to nominally collect 90 per cent of beam energy.

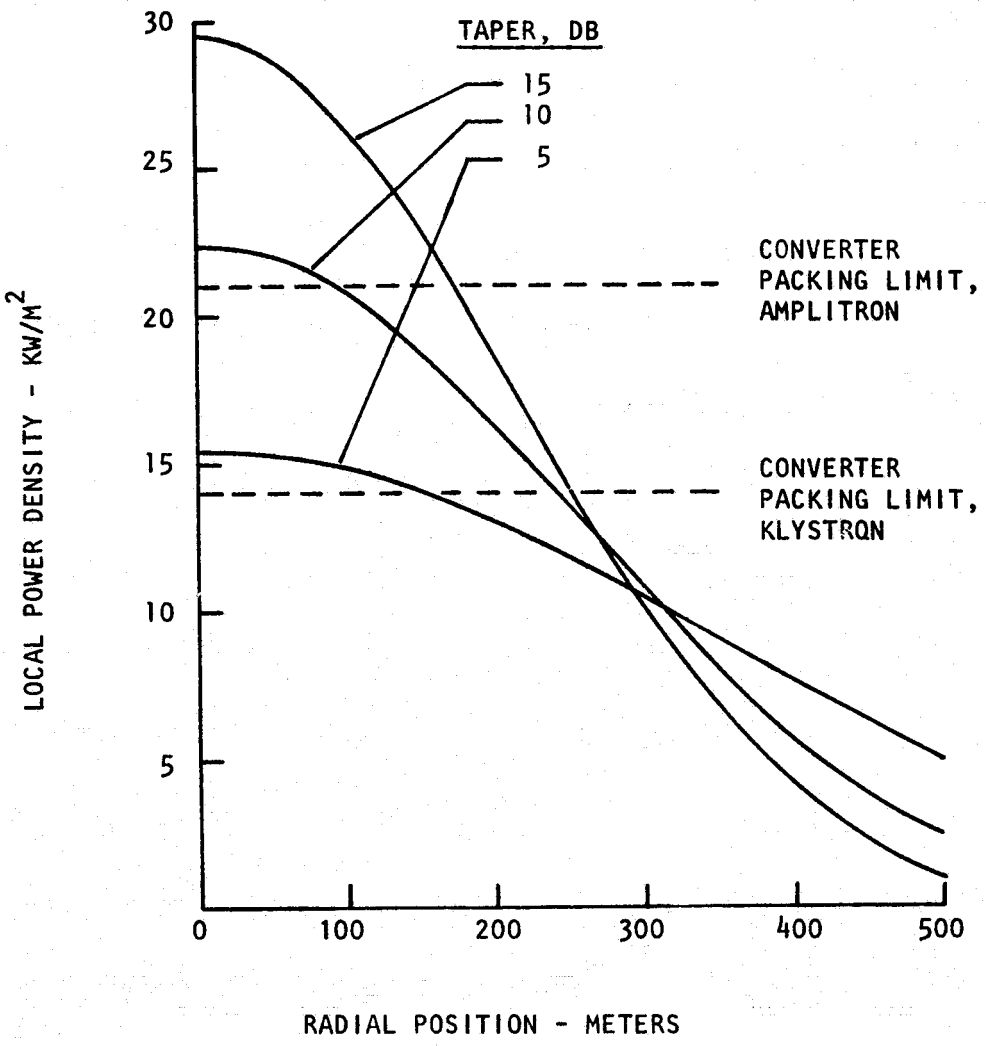

FIGURE 7 - REQUIRED POWER DENSITY ON TRANSMITTER AS A FUNCTION OF RADIAL POSITION FOR VARIOUS ILLUMINATION TAPERS. SYSTEM IS SIZED TO DELIVER 5 GW DC WITH A 1 KM TRANSMITTER. CONVERTER EFFICIENCY IS ASSUMED TO BE 85 PER CENT WITH A NET LINK EFFICIENCY OF 68 PER CENT.

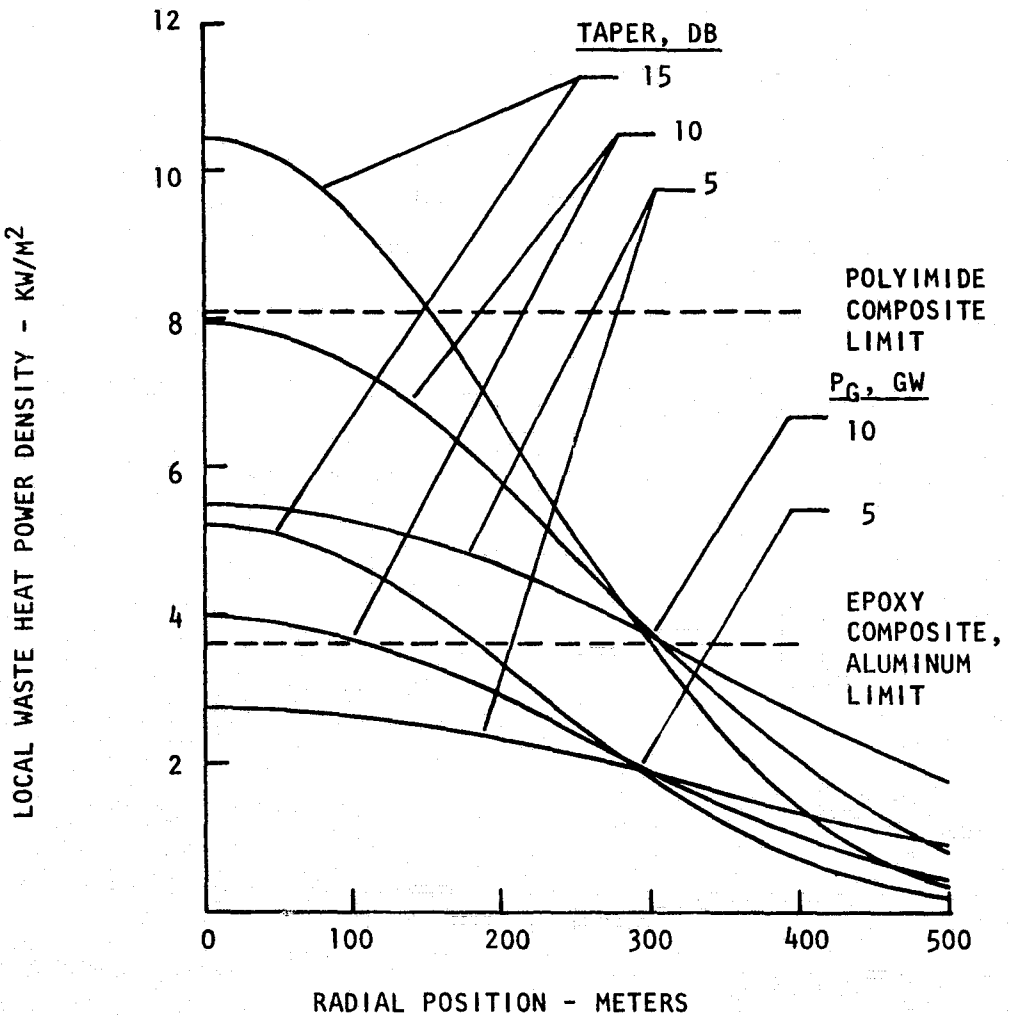

FIGURE 8 - RESULTING THERMAL POWER DENSITY AS A FUNCTION OF RADIAL POSITION FOR VARIOUS ILLUMINATION TAPERS AND DELIVERED DC GROUND POWER LEVELS. TRANSMITTER IS 1 KM. THE CONVERTER EFFICIENCY IS ASSUMED TO BE 85 PER CENT WITH A NET LINK EFFICIENCY OF 68 PER CENT.

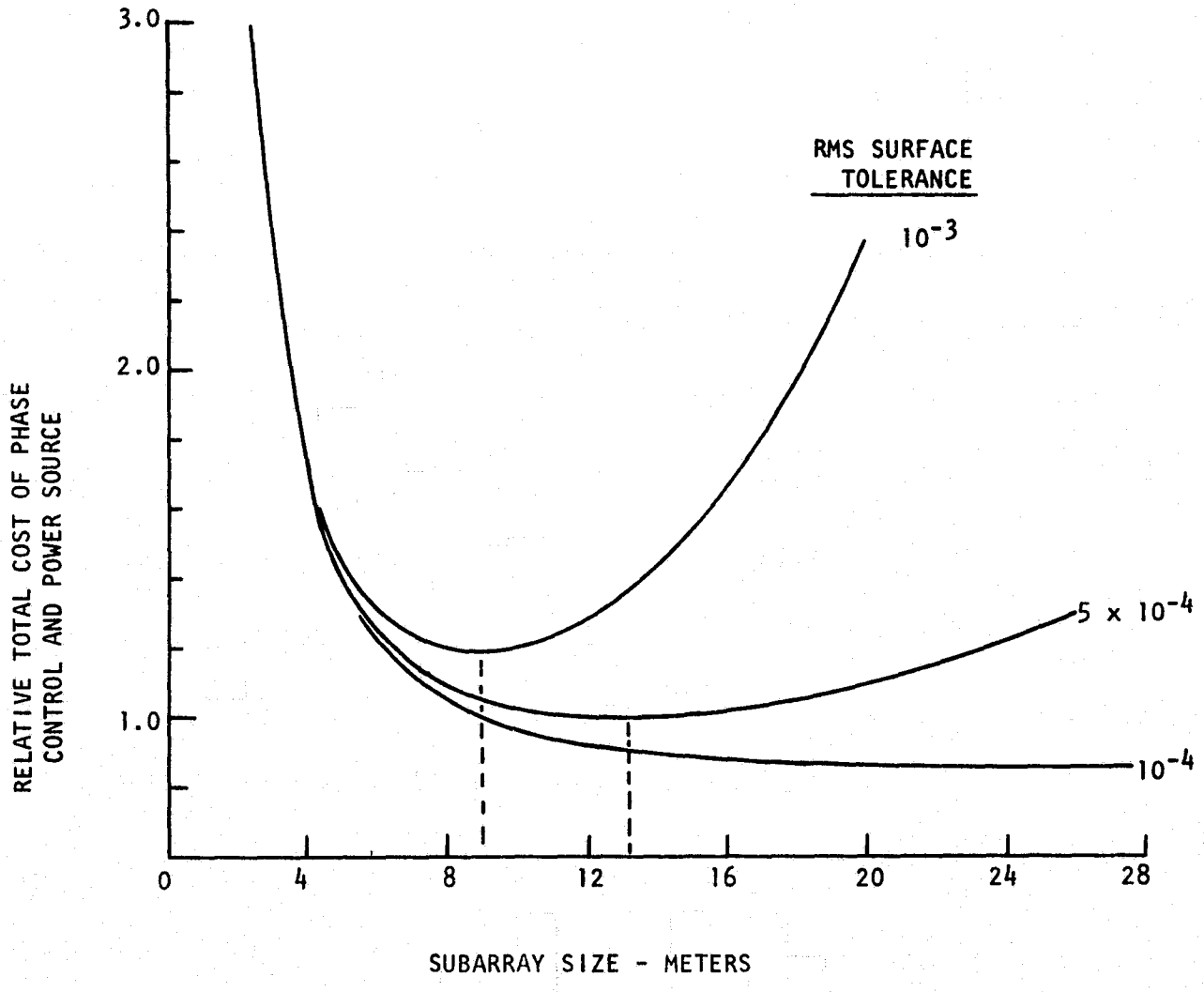

FIGURE 9 - TOTAL COST PENALTY, INCLUDING PHASE CONTROL ELECTRONICS AND PRIME POWER AS A FUNCTION OF SUBARRAY SIZE FOR VARIOUS SUBARRAY SURFACE TOLERANCES.

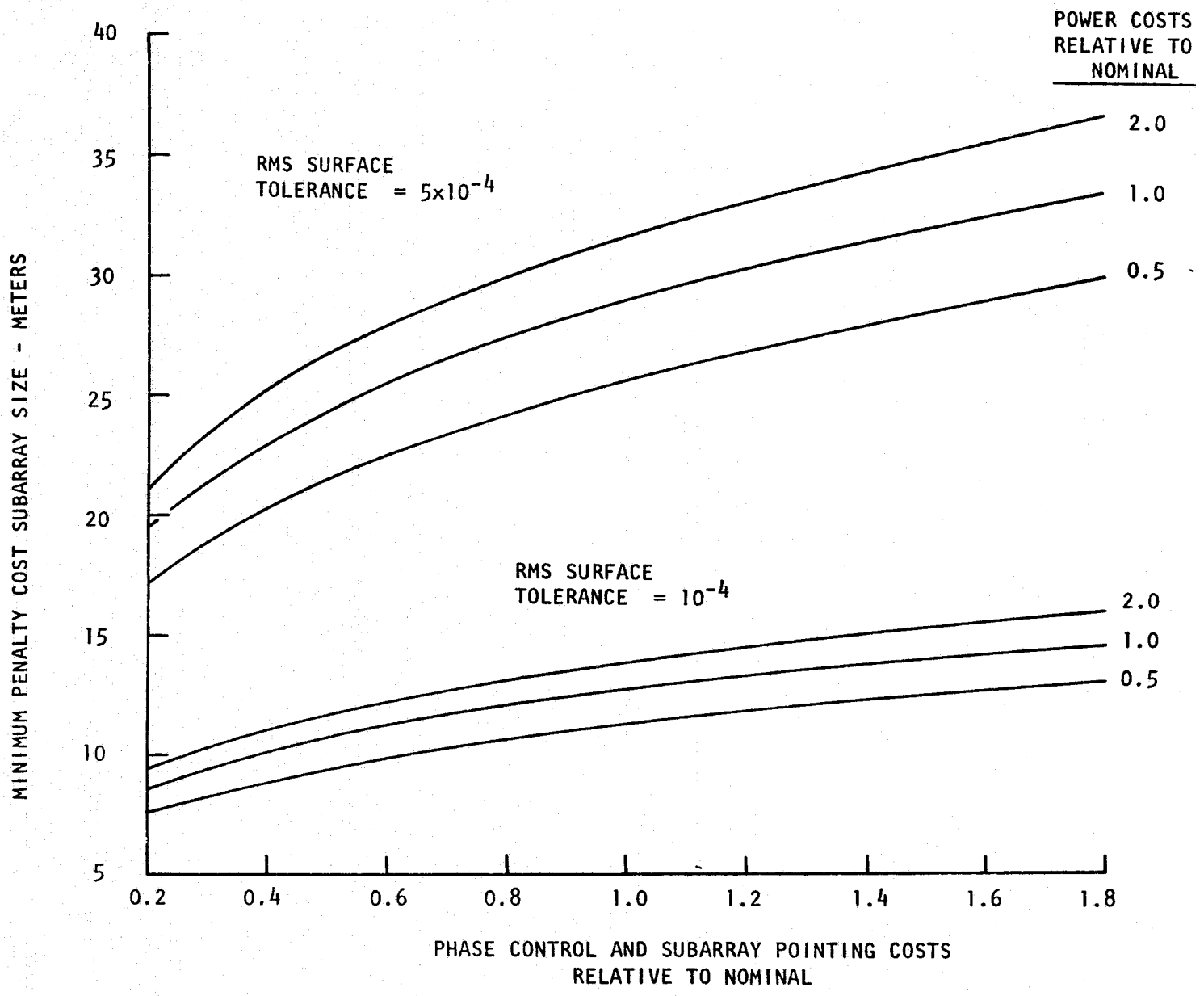

FIGURE 10 - OPTIMUM SUBARRAY SIZE AS A FUNCTION OF PHASE CONTROL COSTS FOR VARIOUS POWER COSTS AND TWO POSSIBLE VALUES OF SUBARRAY SURFACE TOLERANCE.

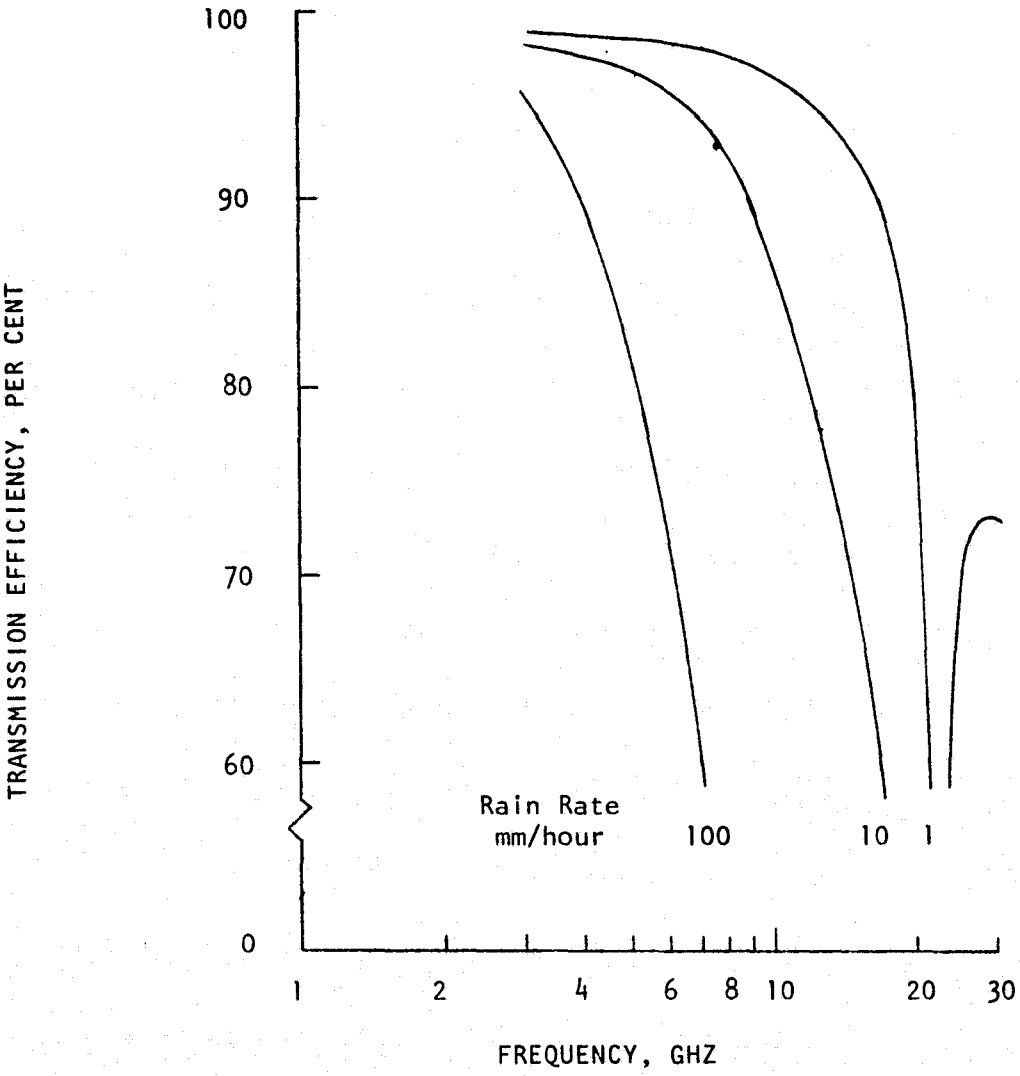

FIGURE 11 - Transmission efficiency of a 45^{o} incidence path through the atmosphere, including rain, versus frequency of emission.

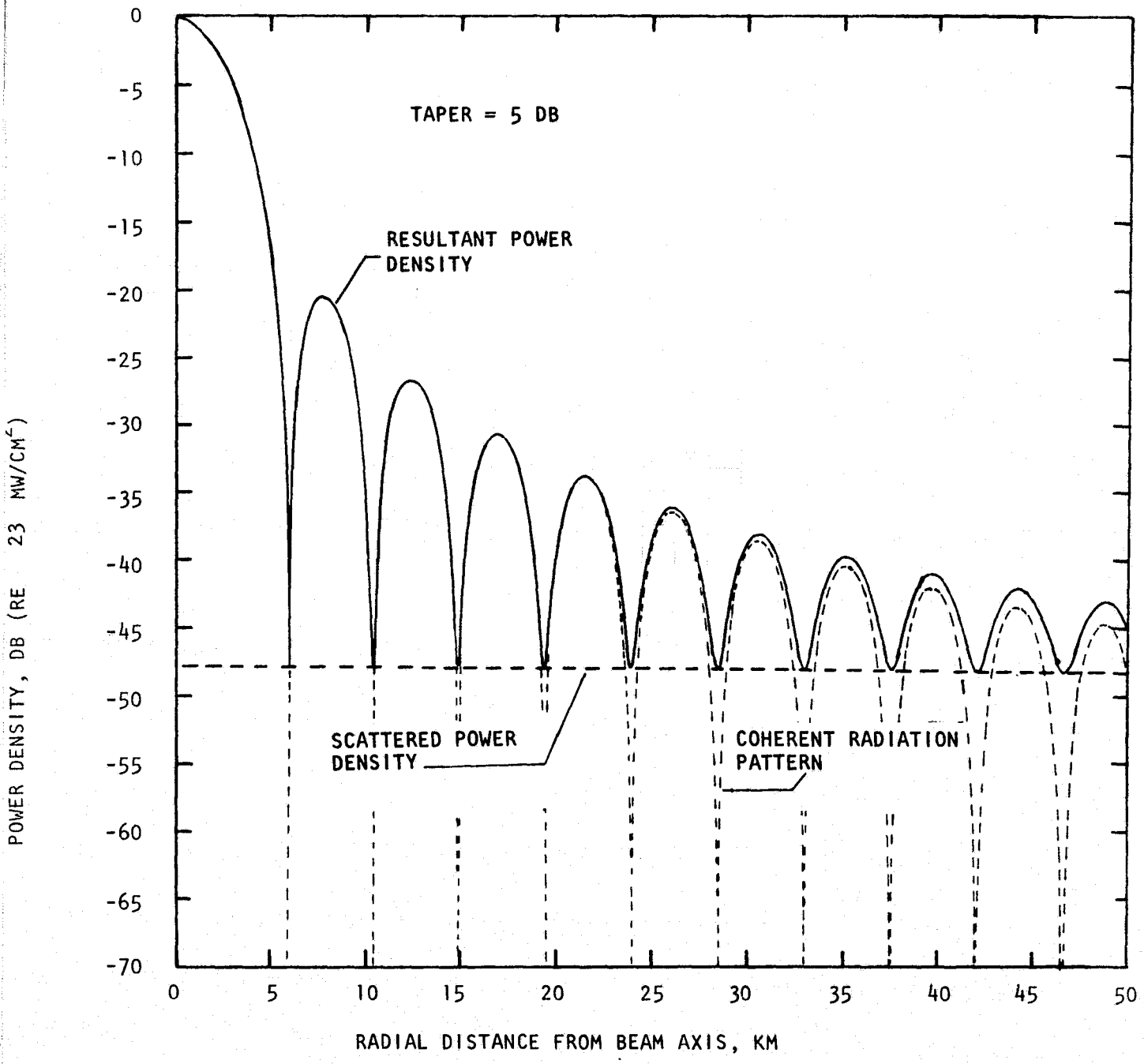

Figure 12 - Average composite receive power density pattern including effects of random amplitude and phase errors.
$\phi = 10^{o}$, k = 0.01

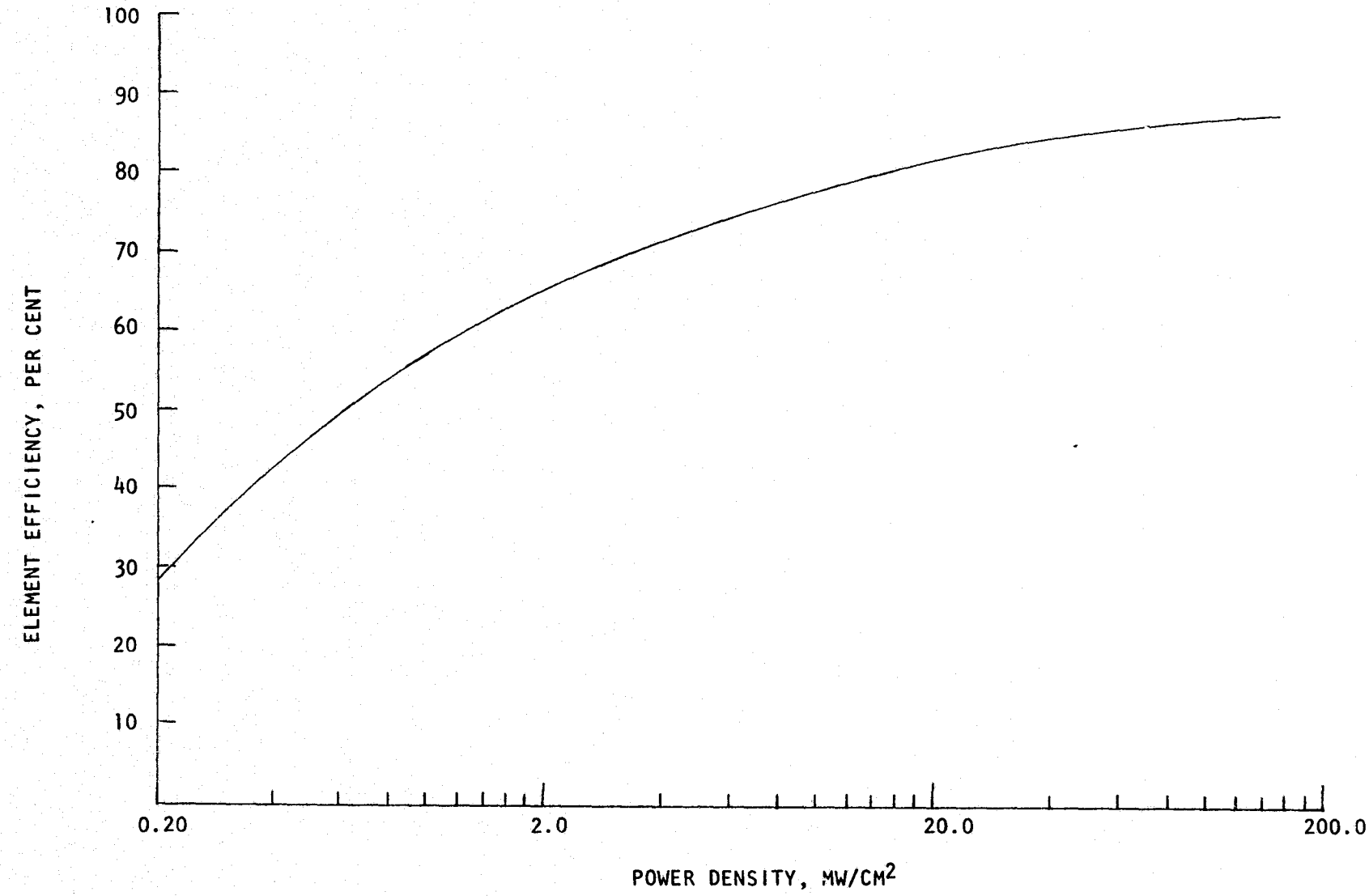

FIGURE 13 - Rectenna element efficiency as a function of local power density.

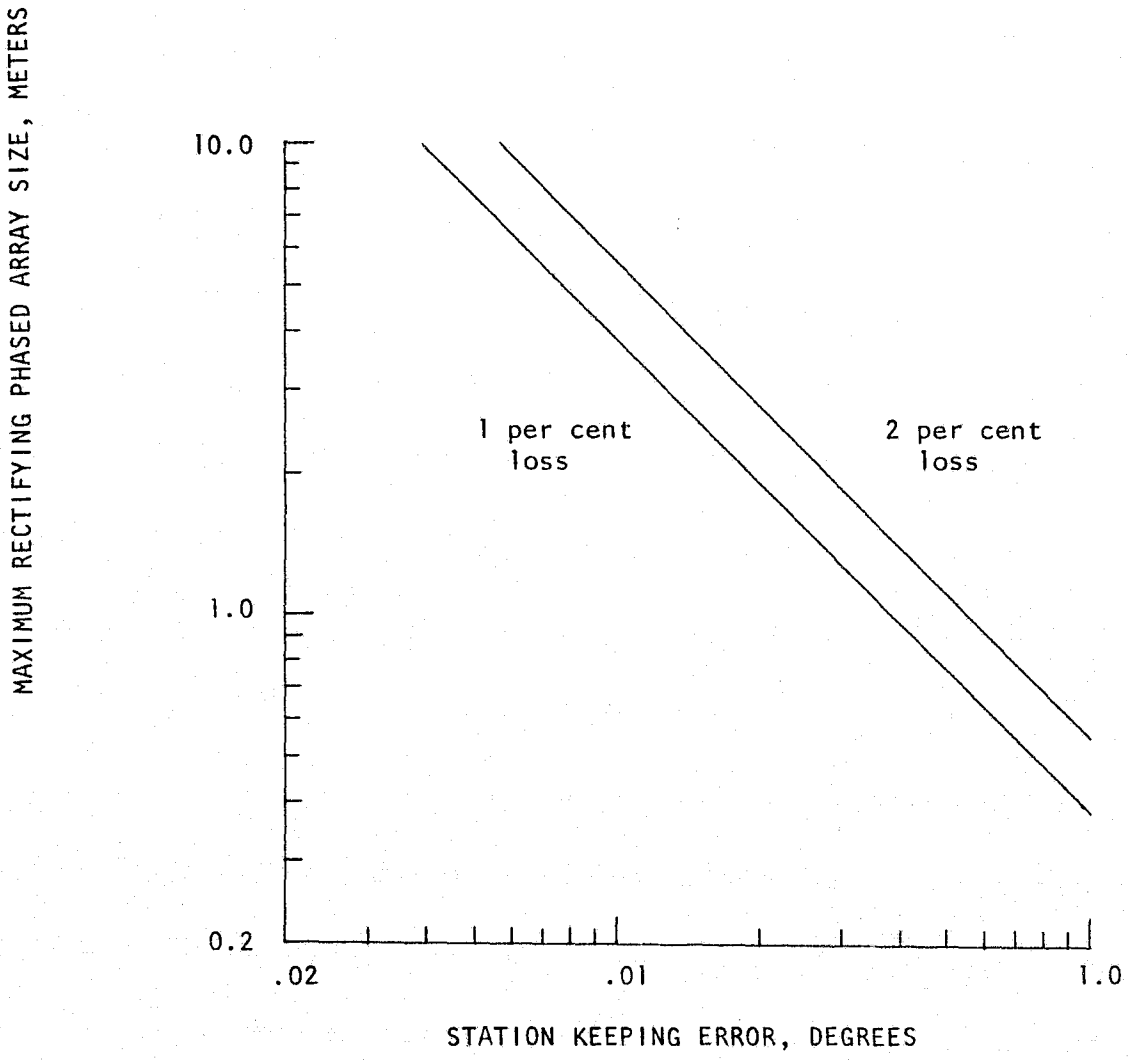

FIGURE 14 - Maximum rectifying phased array size as a function of orbital system station keeping error for various pointing error losses.

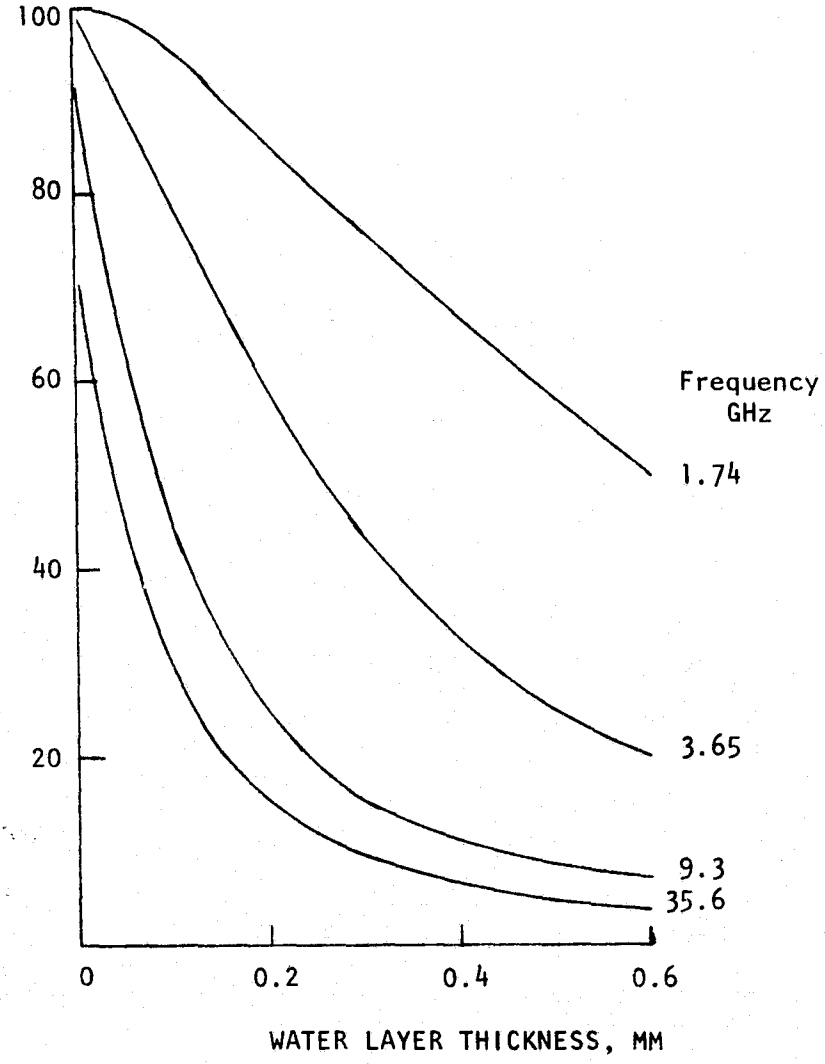

FIGURE 15 - Transmission efficiency of dielectric protective cover versus water layer thickness on cover. Frequency of emission is shown as a parameter (reference 24).

TRANSMIT/RECEIVE ANTENNA SIZE CONSIDERATIONS

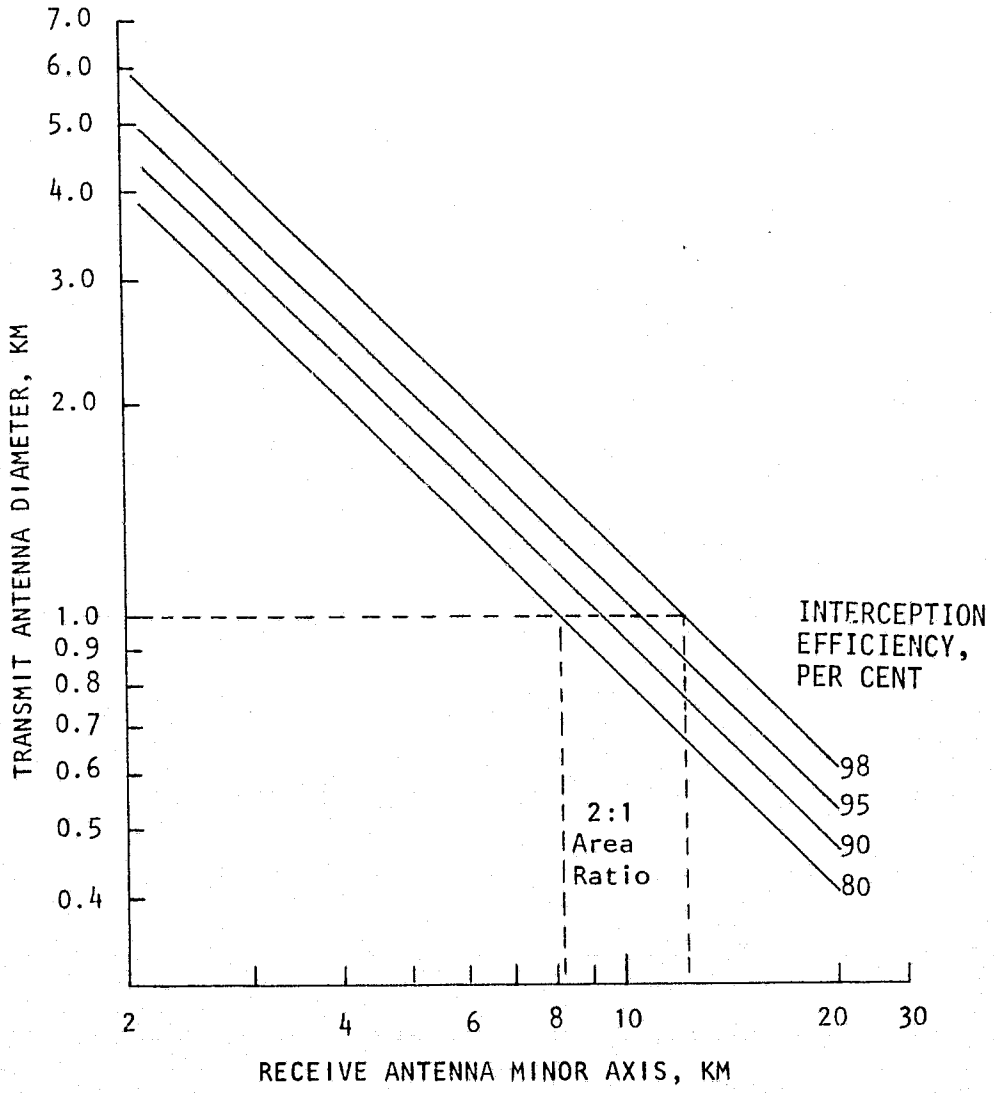

FIGURE 16 - REQUIRED TRANSMITTER DIAMETER AS A FUNCTION OF RECEIVER DIAMETER FOR VARIOUS INTERCEPTION EFFICIENCIES.

UNCONSTRAINED CAPITAL COSTS VS. PEAK POWER DENSITY
AT RECEIVER FOR VARIOUS LEVELS OF DELIVERED DC POWER

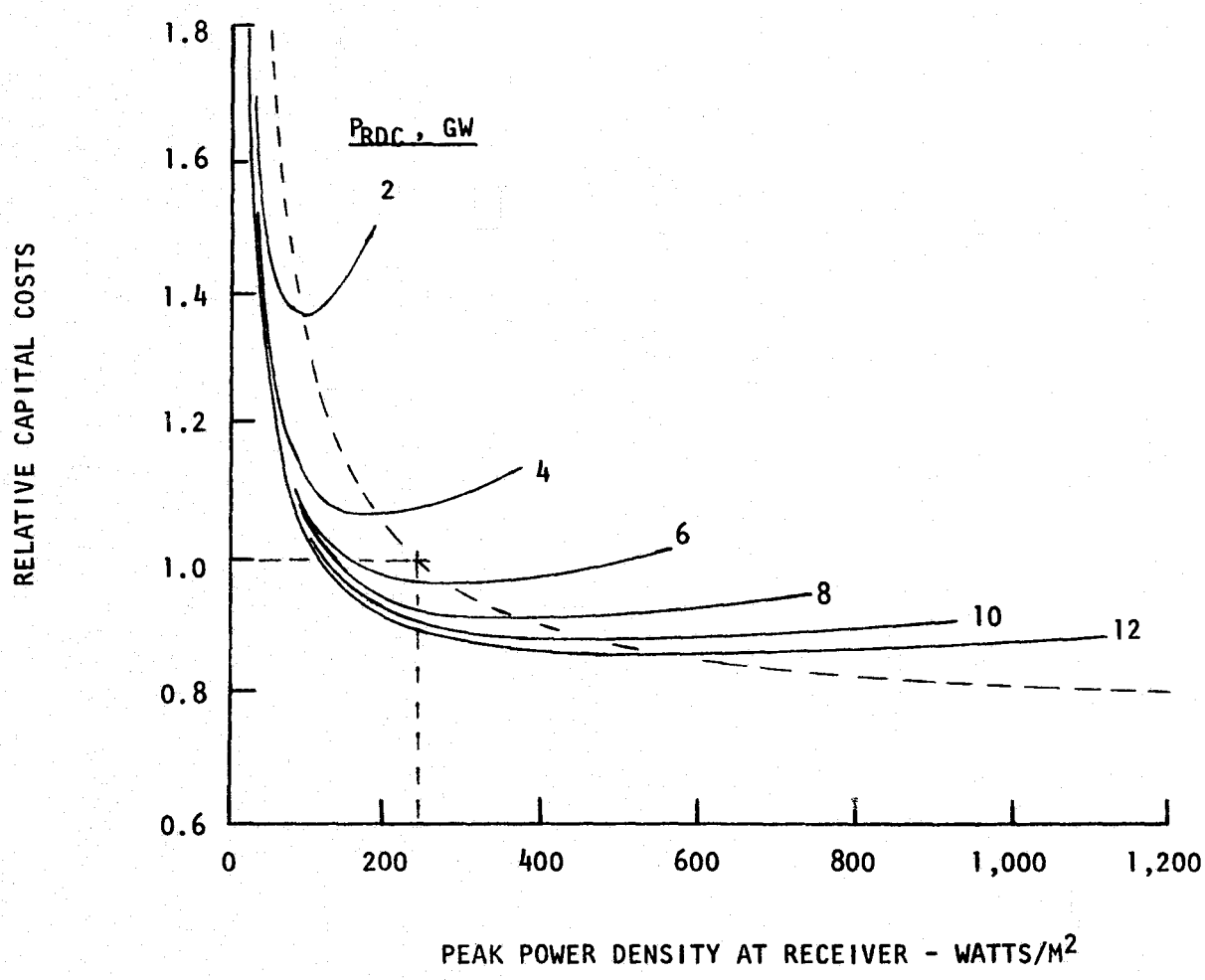

FIGURE 17 - UNCONSTRAINED SYSTEM SPECIFIC COSTS AS A FUNCTION OF PEAK POWER DENSITY AT RECEIVER WITH DELIVERED DC POWER AS A PARAMETER.

TOTAL SYSTEM CAPITAL COSTS VS. PEAK POWER DENSITY
AT RECEIVER FOR VARIOUS RECEIVER COST PARAMETERS
P_{RDC} = 5 GW

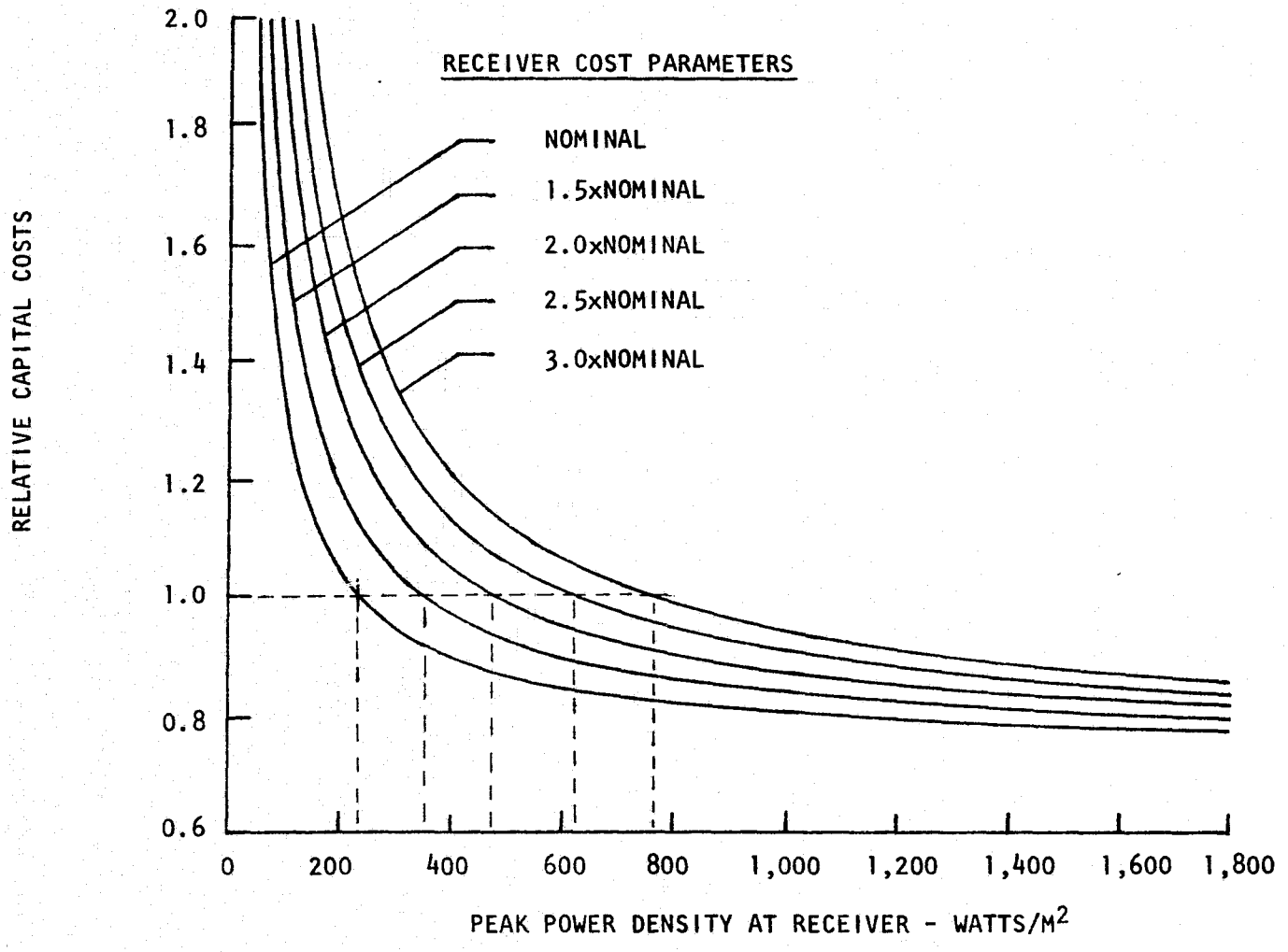

FIGURE 18 - SYSTEM COSTS AS A FUNCTION OF RECEIVER PEAK POWER DENISTY
FOR VARIOUS ASSUMPTIONS REGARDING RECEIVER COSTS.

TOTAL SYSTEM CAPITAL COSTS VS. TRANSMITTER
DIAMETER WITH NO THERMAL OR BIOLOGICAL CONSTRAINTS

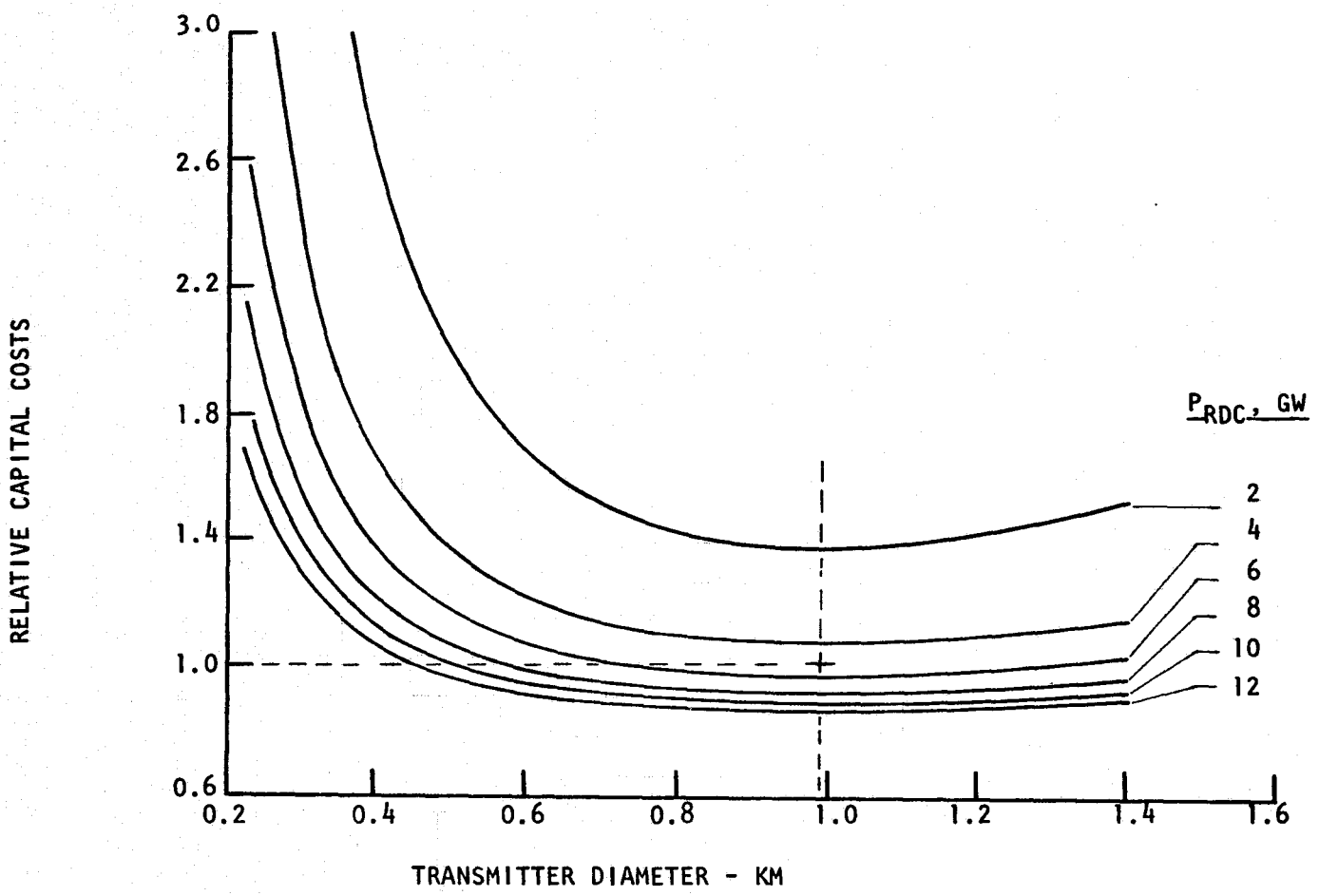

FIGURE 19 - UNCONSTRAINED SYSTEM SPECIFIC COSTS AS A FUNCTION OF TRANSMITTER DIAMETER FOR VARIOUS LEVELS OF DELIVERED DC POWER.

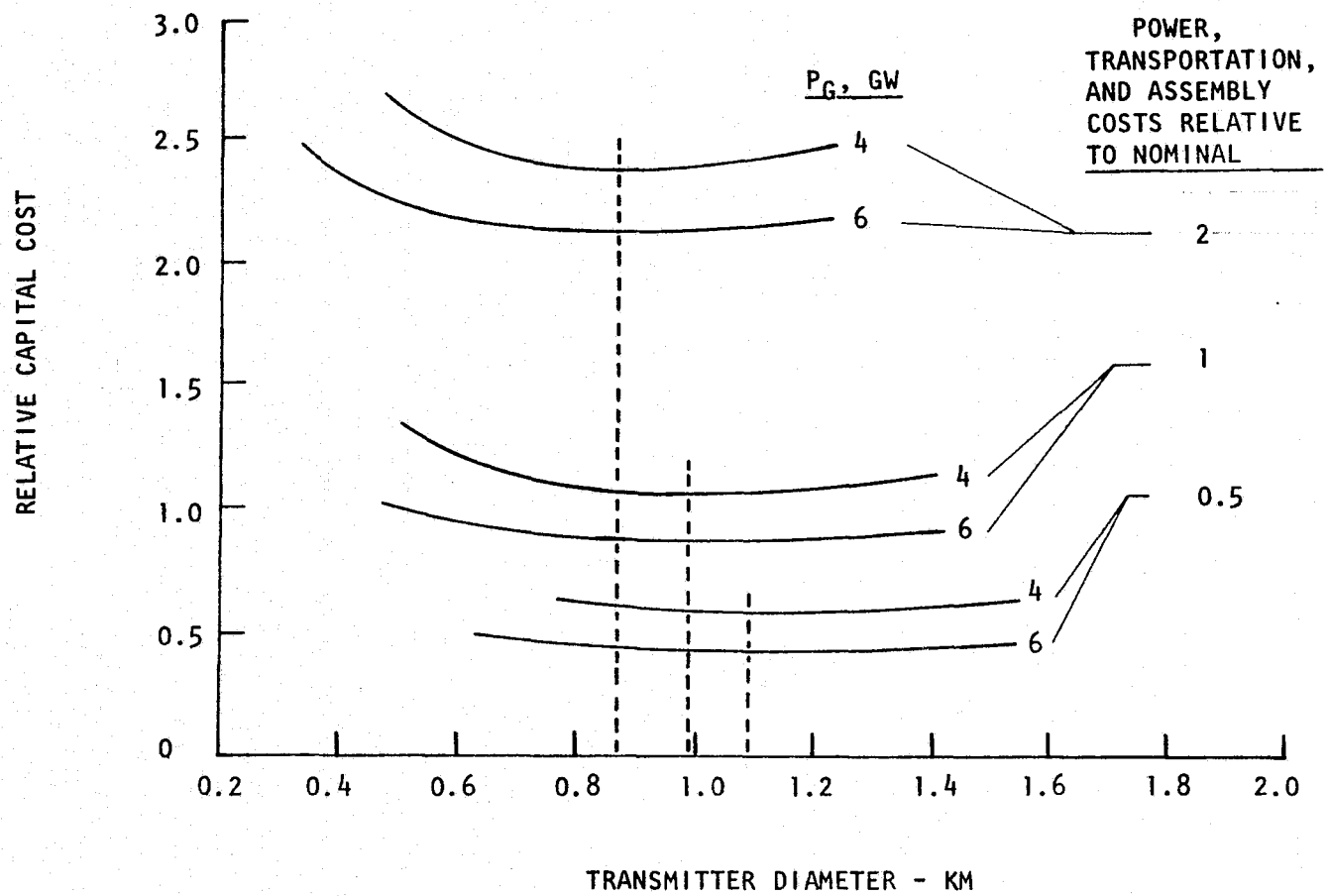

FIGURE 20 - SENSITIVITY OF UNCONSTRAINED SYSTEM COSTS TO ASSUMPTIONS REGARDING COSTS OF POWER, TRANSPORTATION, AND ASSEMBLY.

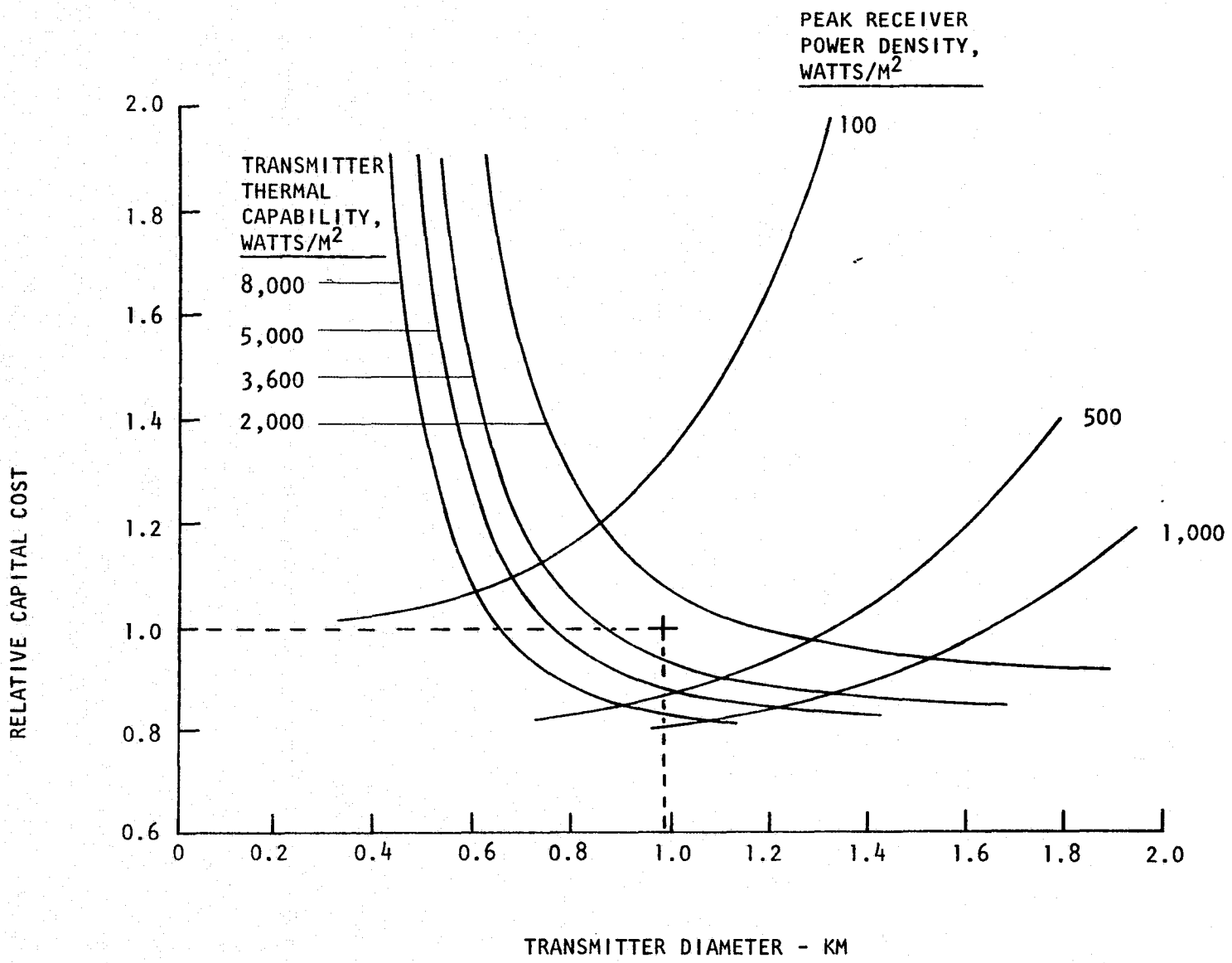

FIGURE 21 - SENSITIVITY OF CONSTRAINED SYSTEM COSTS AND TRANSMITTER DIAMETER TO VARIOUS CHOICES OF THERMAL CAPABILITIES AND PEAK ALLOWABLE RECEIVER POWER DENSITY. ALSO INDICATED IS THE TRANSMITTER DIAMETER OF THE REFERENCE 5 GW SYSTEM.

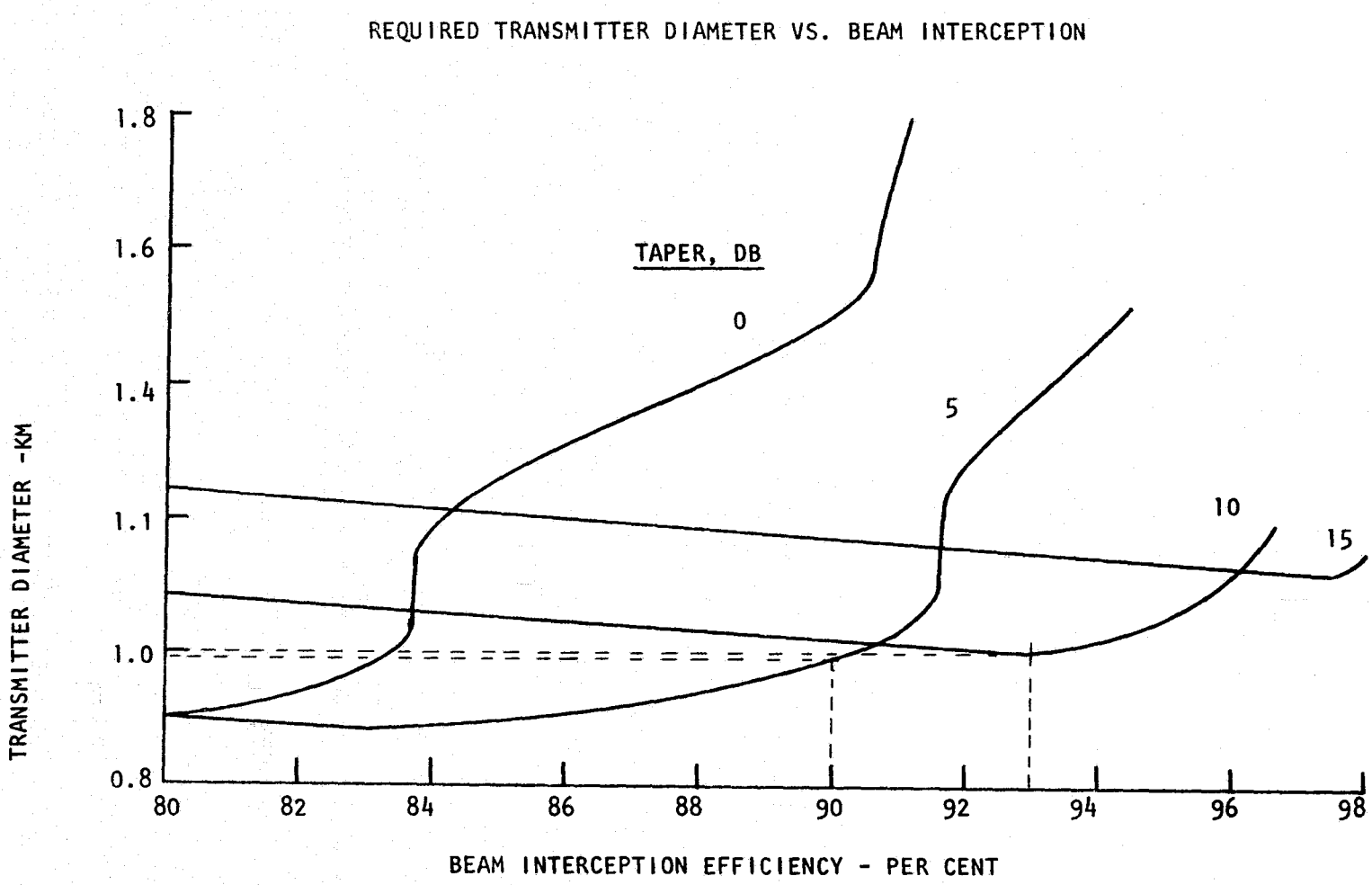

FIGURE 22 - REQUIRED TRANSMITTER DIAMETER AS A FUNCTION OF BEAM INTERCEPTION FOR VARIOUS TAPERS. SYSTEM IS SIZED TO DELIVER 5 GW DC. SLOPE DISCONTINUITIES AT 83 PER CENT/5 DB TAPER AND 93 PER CENT/10 DB TAPER INDICATE A SHIFT TO A THERMALLY LIMITED SYSTEM. OTHER DISCONTINUITIES INDICATE EFFECT OF SIDELOBE INTERCEPTION.

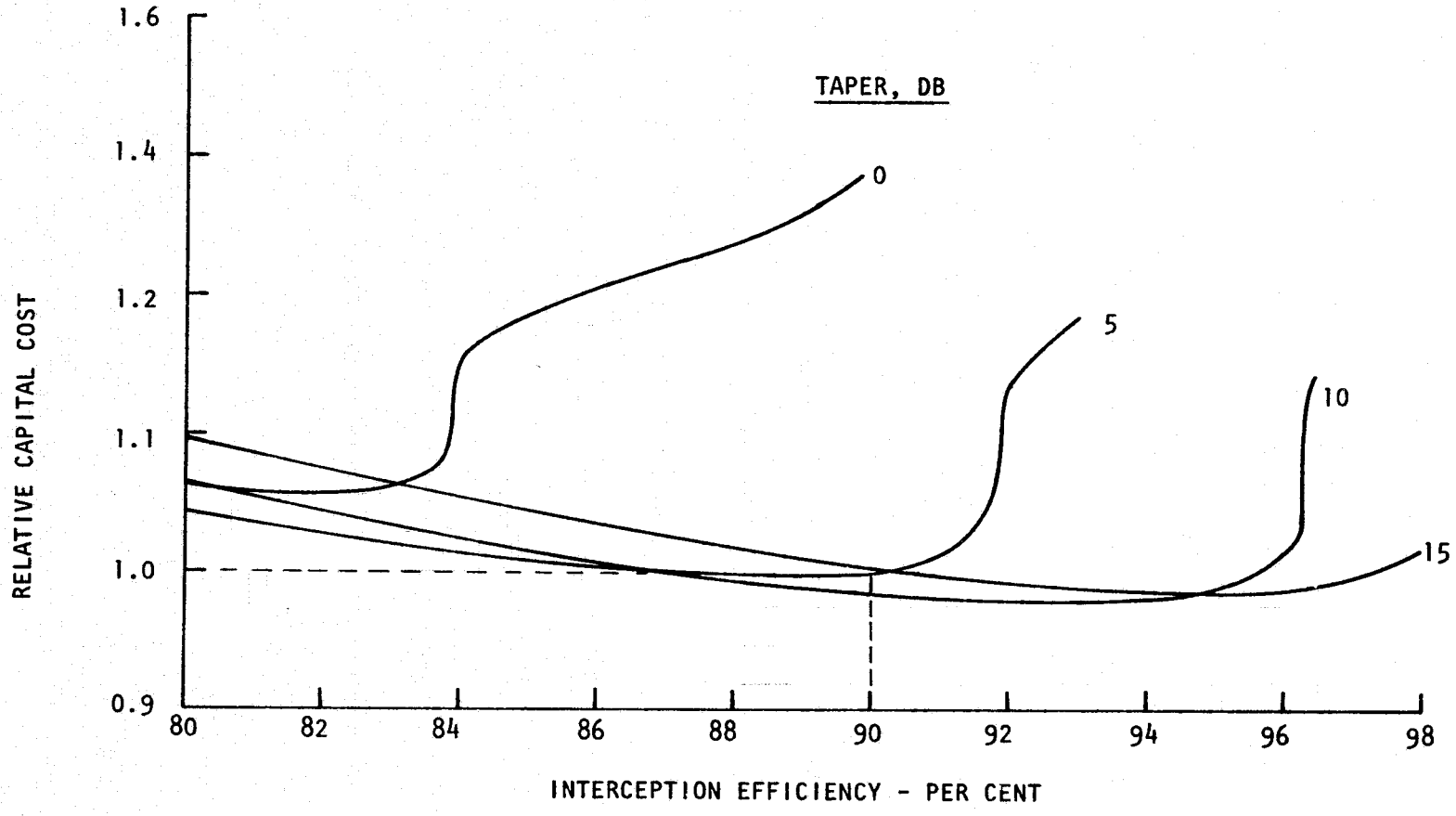

FIGURE 23 - CAPITAL COST AS A FUNCTION OF BEAM EFFICIENCY FOR VARIOUS TAPERS WITH A SYSTEM SIZED TO DELIVER 5 GW. THE REFERENCE 5 DB TAPER/90 PER CENT INTERCEPTION SYSTEM IS INDICATED.

TOTAL SYSTEM CAPITAL COSTS VS. INTERCEPTION EFFICIENCY
FOR A 10 GW SPS

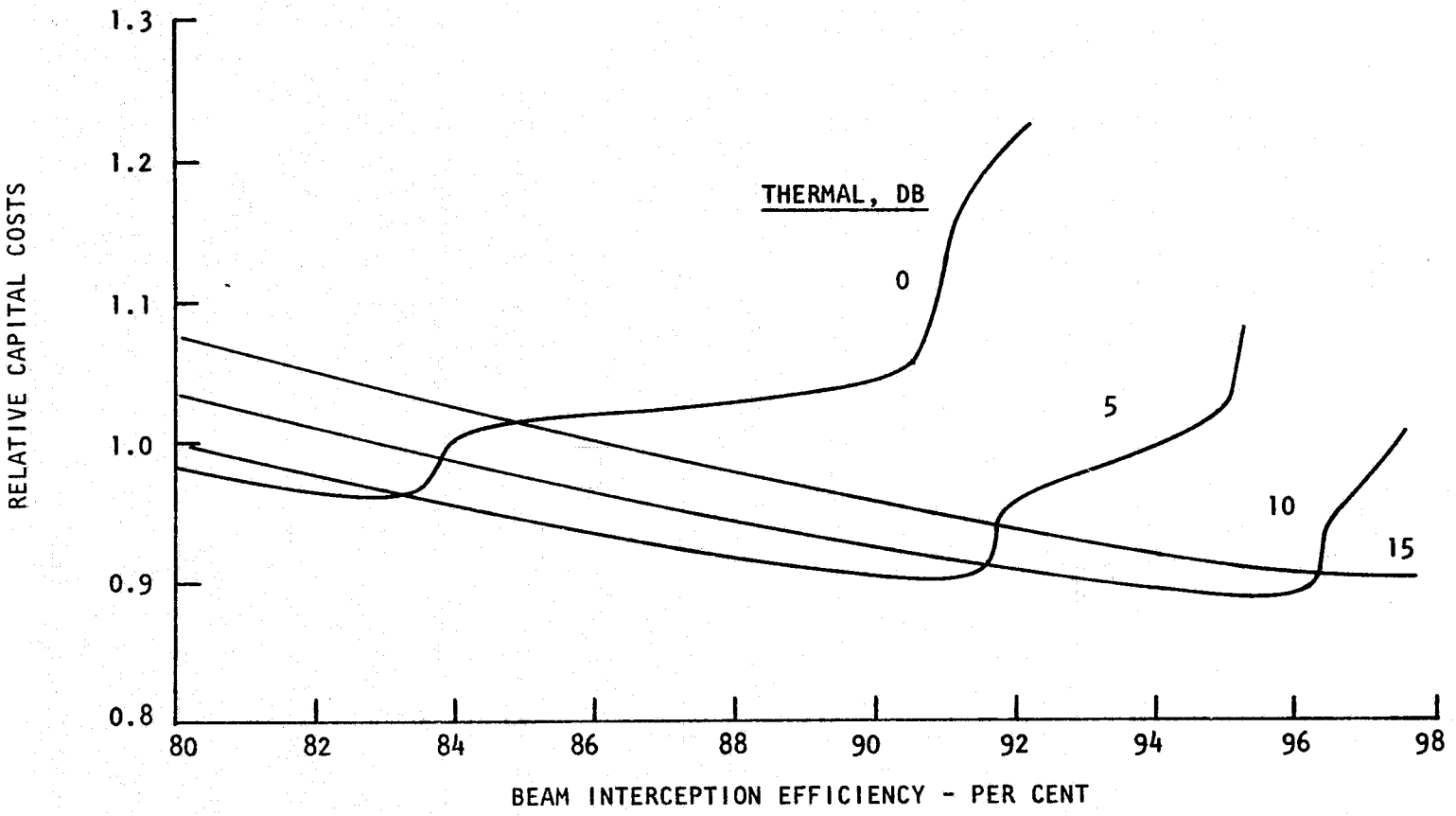

FIGURE 24 - CAPITAL COST AS A FUNCTION OF INTERCEPTION FOR VARIOUS TAPERS WITH A SYSTEM SIZED TO DELIVER 10 GW.

REQUIRED TRANSMITTER DIAMETER VS. FREQUENCY
FOR A PARTICULAR THERMAL CONSTRAINT

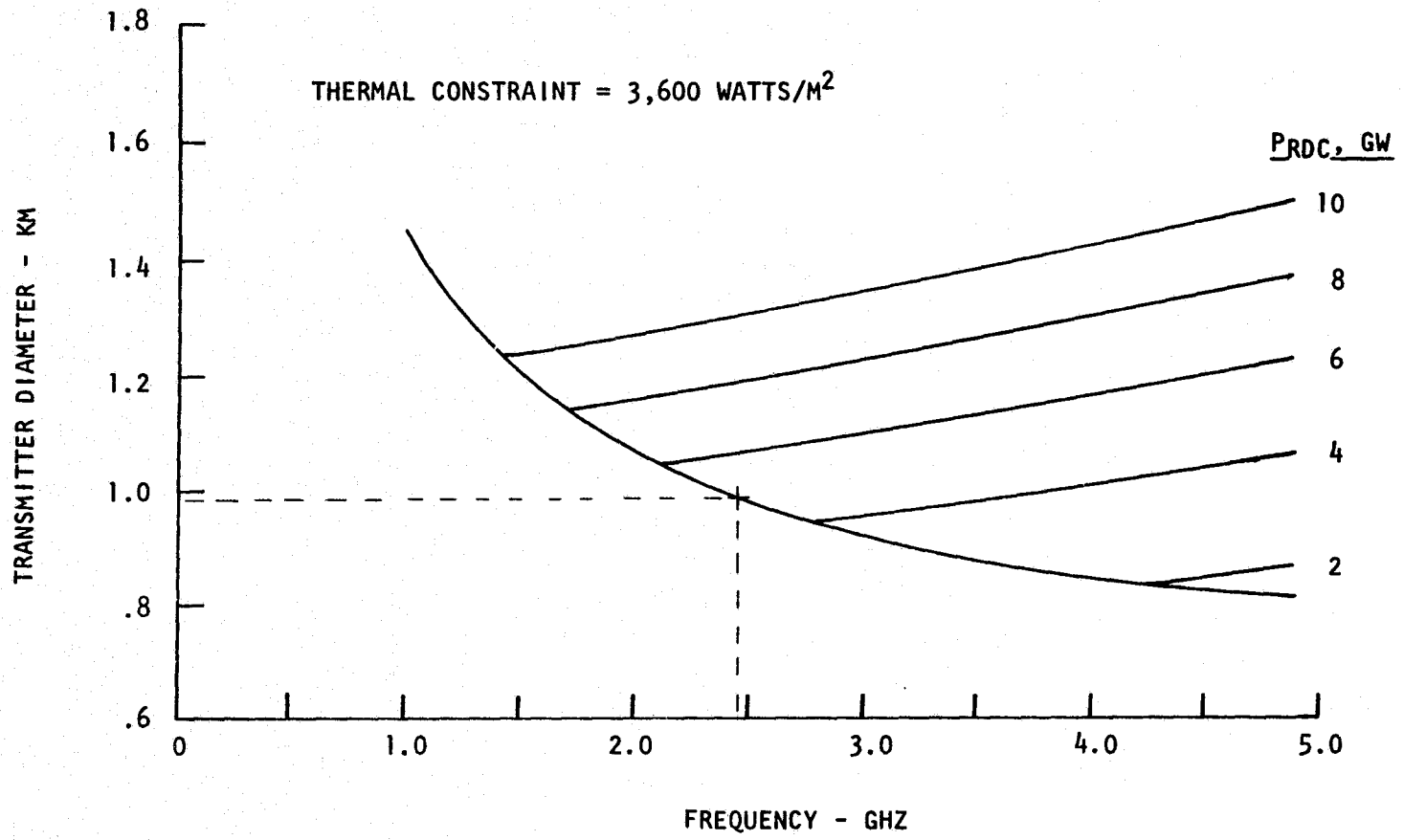

FIGURE 25 - REQUIRED TRANSMITTER DIAMETER AS A FUNCTION OF FREQUENCY FOR VARIOUS DELIVERED DC POWER LEVELS WITH THE THERMAL CONSTRAINT INDICATED. ALSO SHOWN IS THE REFERENCE 5 GW SYSTEM.

TOTAL SYSTEM CAPITAL COSTS VS. FREQUENCY
FOR A FIXED THERMAL CONSTRAINT

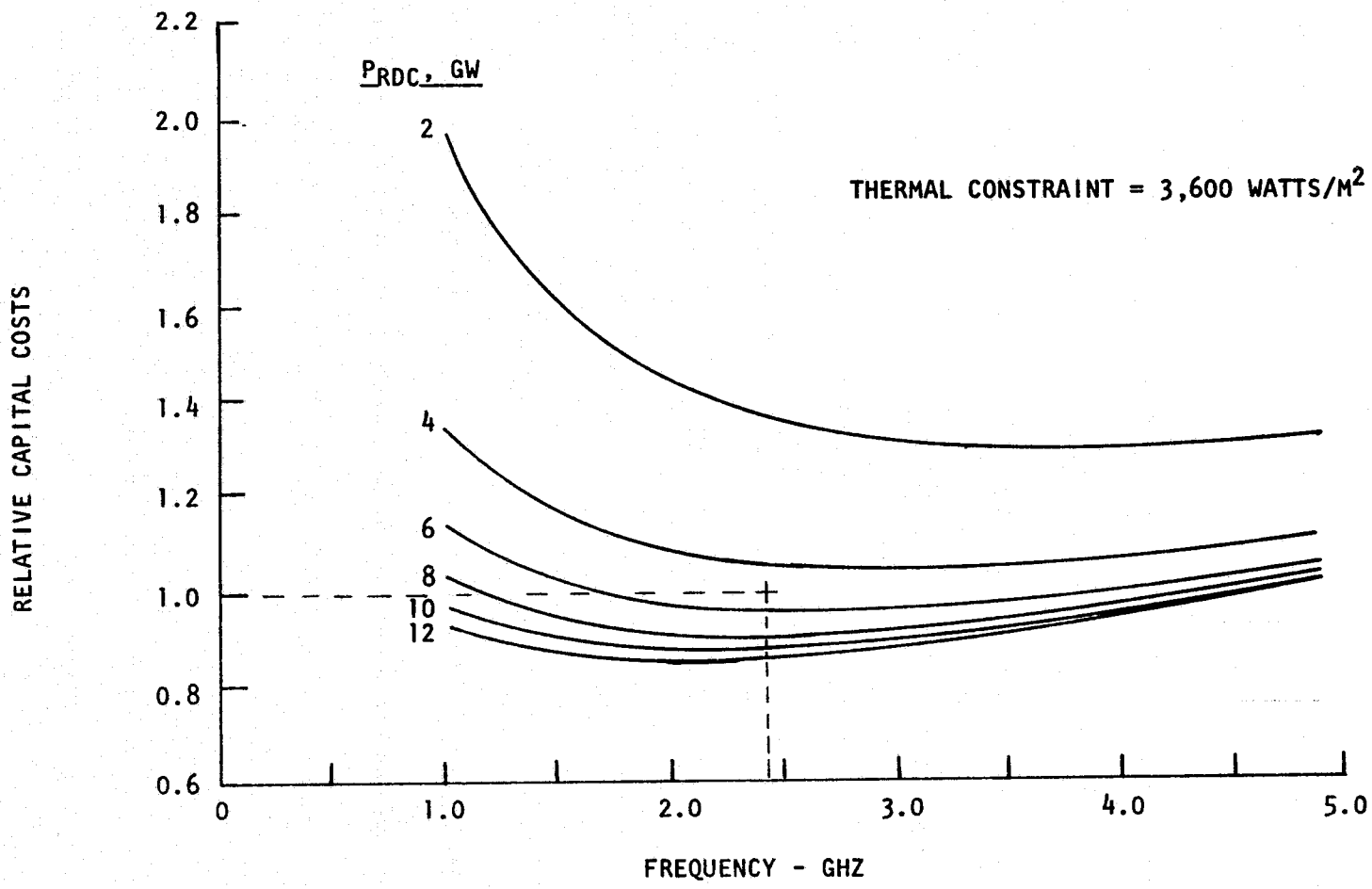

FIGURE 26 - CAPITAL COSTS AS A FUNCTION OF FREQUENCY FOR VARIOUS DELIVERED DC POWER LEVELS WITH THE THERMAL CONSTRAINT INDICATED. ALSO SHOWN IS THE REFERENCE 5 GW SYSTEM.

P_G CAPABILITY VS. FREQUENCY FOR A FIXED THERMAL CONSTRAINT AND VARIOUS BIOLOGICAL CONSTRAINTS

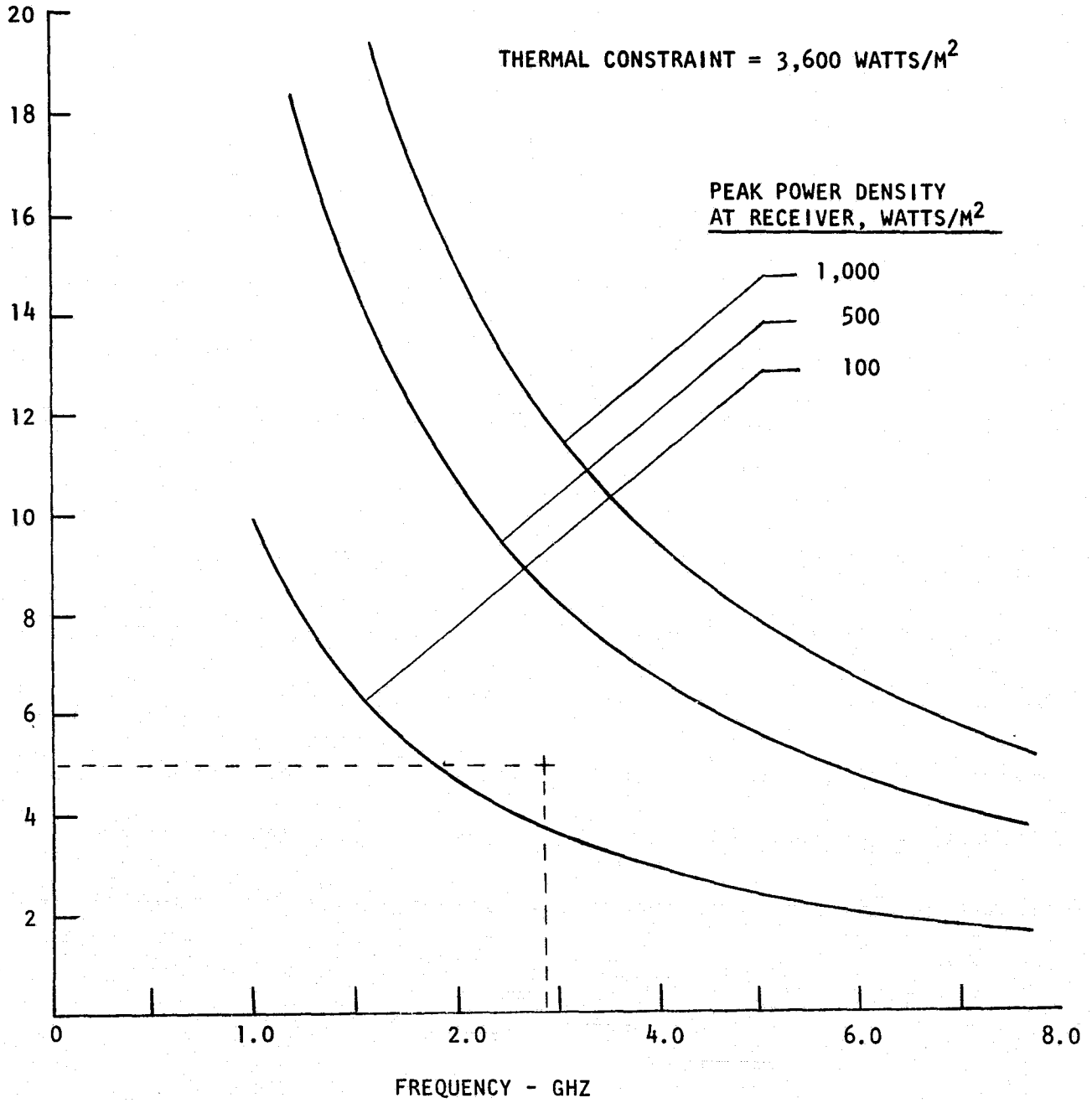

FIGURE 27 - MAXIMUM THROUGHPUT POWER CAPABILITY AS A FUNCTION OF FREQUENCY FOR VARIOUS CONSTRAINTS ON PEAK POWER DENSITY AT THE RECEIVER AND FOR THE PARTICULAR THERMAL CONSTRAINT INDICATED. ALSO SHOWN IS THE REFERENCE 5 GW SYSTEM.

TOTAL SYSTEM CAPITAL COSTS VS. FREQUENCY
WITH THERMAL AND BIOLOGICAL CONSTRAINTS

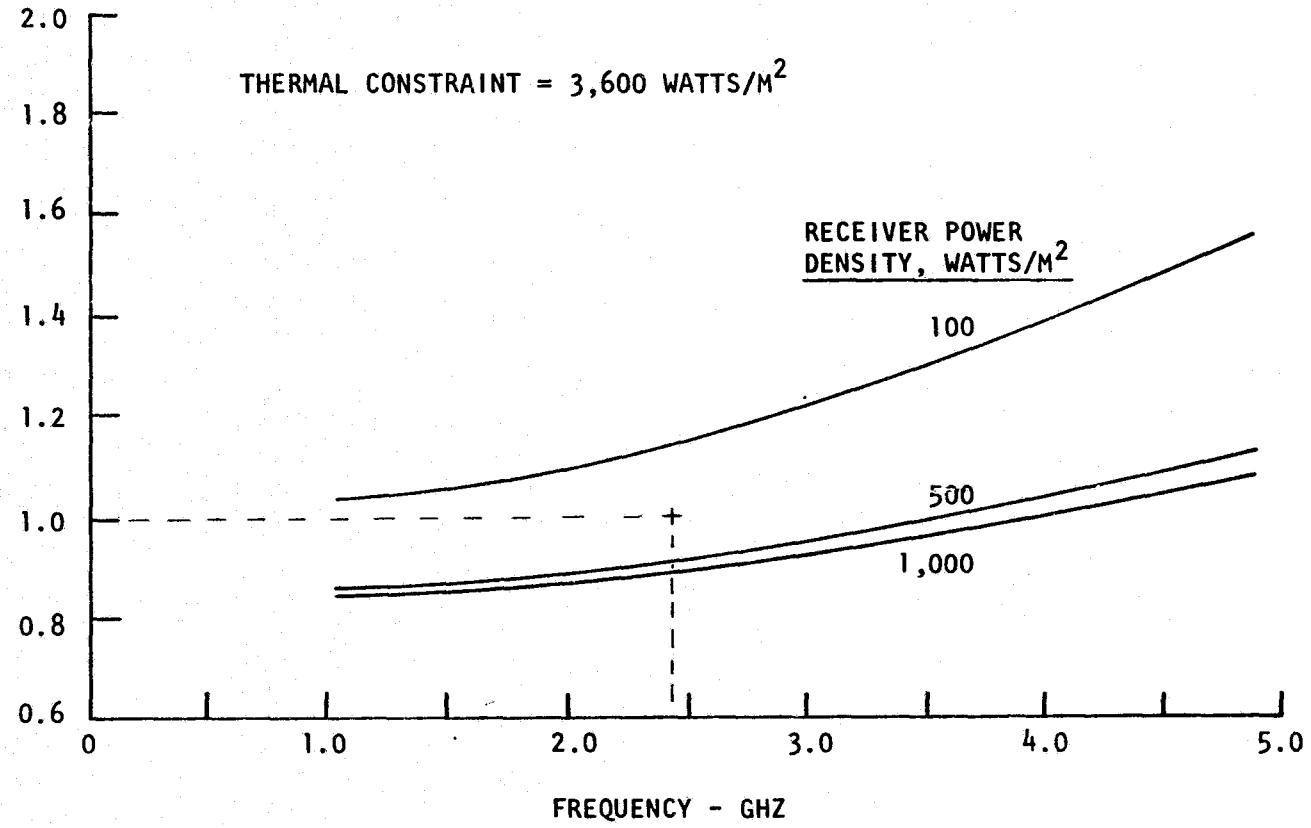

FIGURE 28 - MINIMUM CAPITAL COST AS A FUNCTION OF FREQUENCY FOR VARIOUS CONSTRAINTS ON PEAK POWER DENSITY AT THE RECEIVER AND FOR THE PARTICULAR THERMAL CONSTRAINT INDICATED. ALSO SHOWN IS THE REFERENCE 5 GW SYSTEM.

ENERGY PAYBACK CONSIDERATION

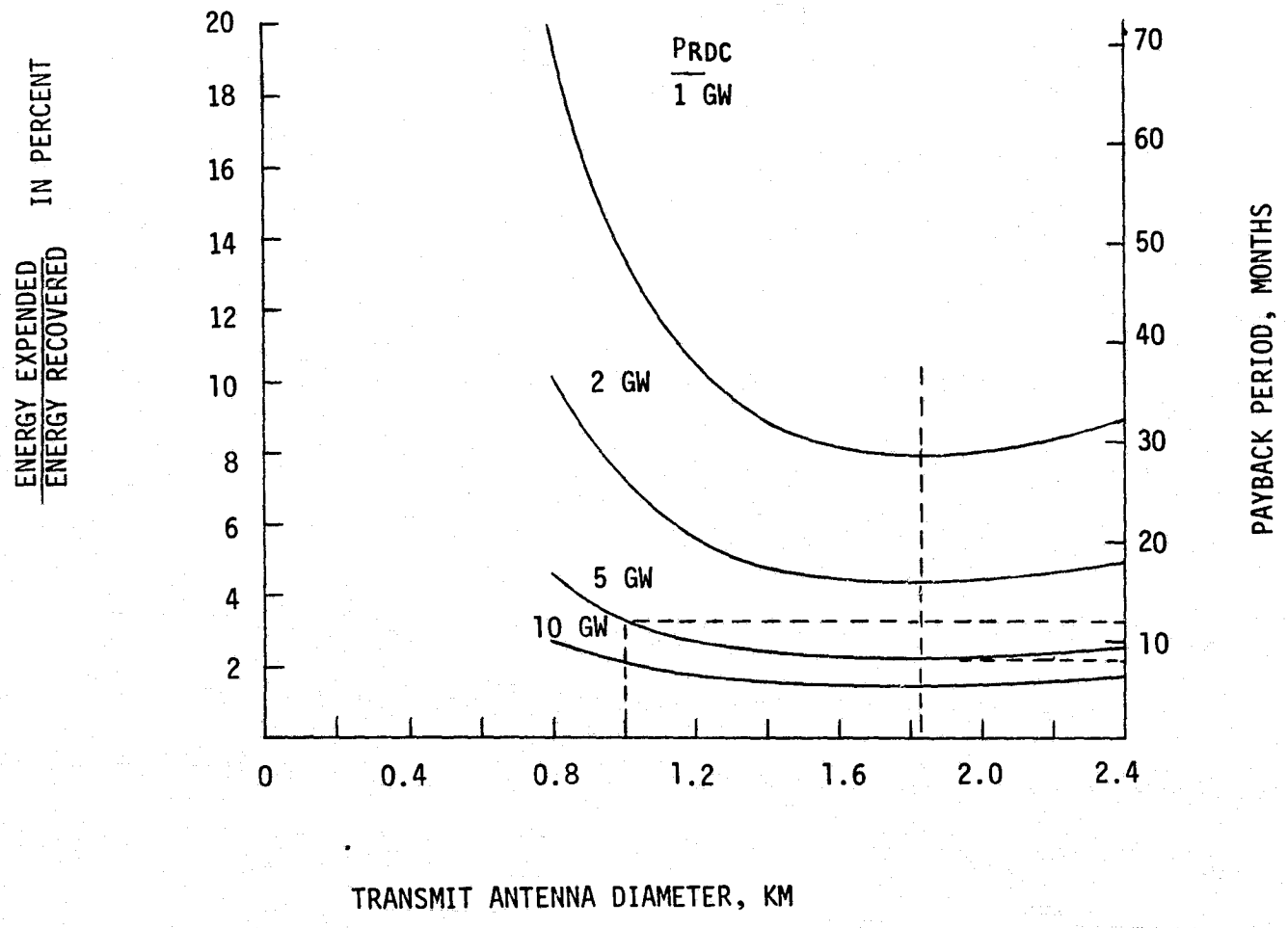

FIGURE 29 - ENERGY EXPENDED IN PLACING ONE SPS INTO OPERATION EXPRESSED AS A PER CENT OF THE ENERGY RECOVERED BY THE SYSTEM (30 YEARS) AS A FUNCTION OF TRANSMITTER DIAMETER. ALSO SHOWN IS THE PAYBACK PERIOD IN MONTHS. THE OPTIMUM BASED ON ENERGY PAYBACK IS SIGNIFICANTLY LARGER THAN THAT BASED ON DOLLARS COST (~1 KM).

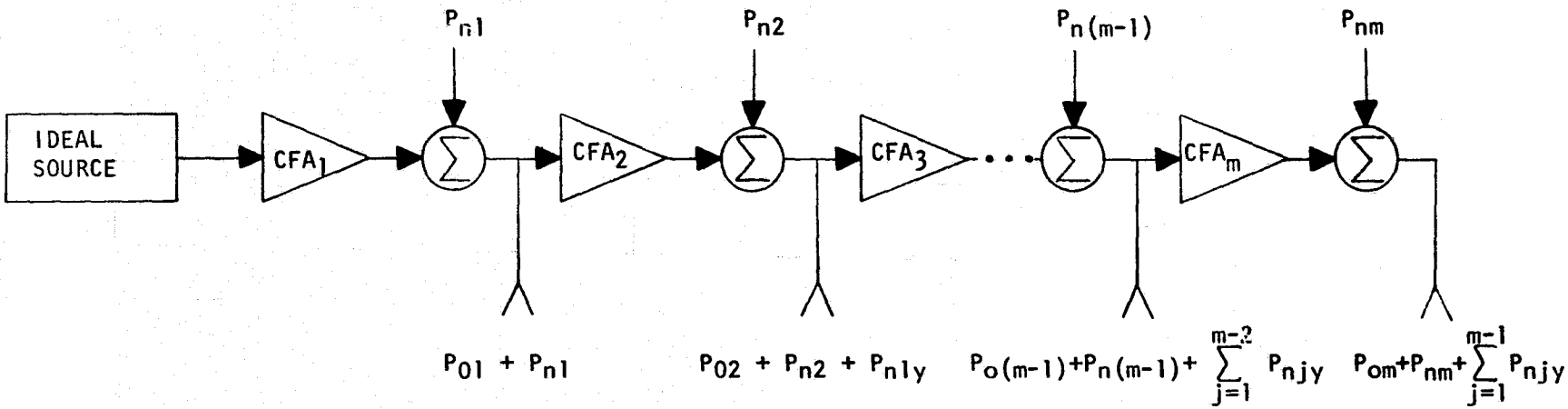

FIGURE 30 - TYPICAL N TUBE CASCADE CONFIGURATION SHOWING COUPLING OF DESIRED SIGNALS THROUGH CHAIN AND UNDESIRED NOISE SIGNALS.

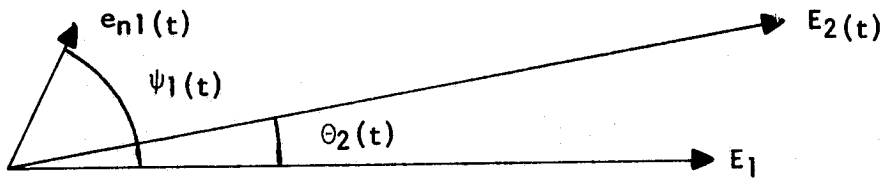

FIGURE 31 - PHASOR ADDITION OF CONVERTER OUTPUT, E_1, WITH A RANDOM DISTURBANCE, en1(t).

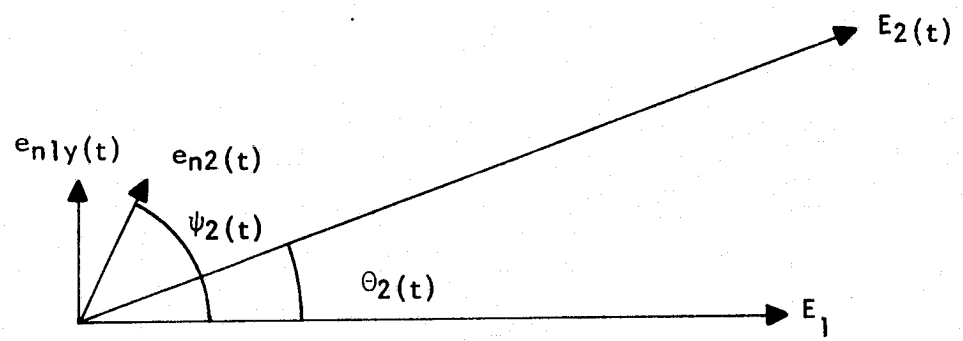

FIGURE 32 - PHASOR ADDITION OF CONVERTER OUTPUT, E_1, WITH RANDOM DISTURBANCE en2(t) AND ORTHOGONAL DISTURBANCE $e_{n1y}(t)$.

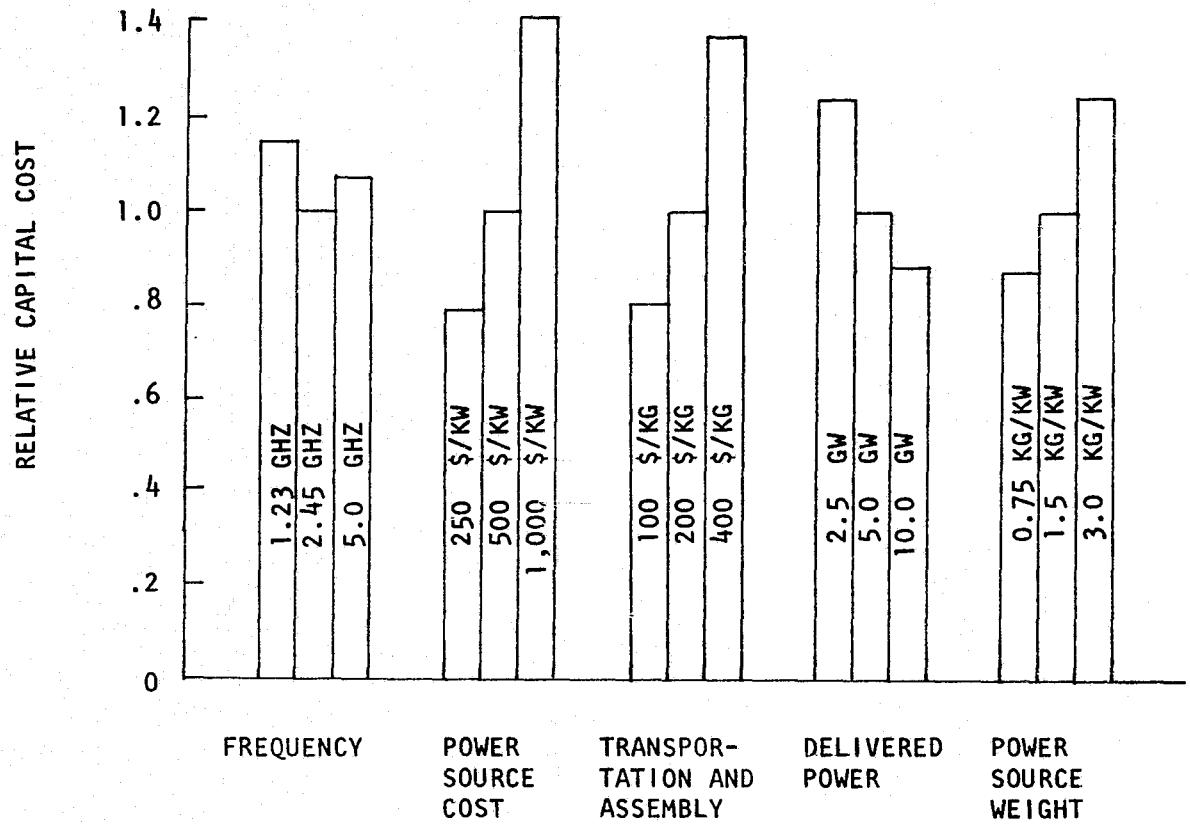

FIGURE 33 - SENSITIVITY OF TOTAL SPS CAPITAL COST TO VARIATION IN SEVERAL KEY PARAMETERS.

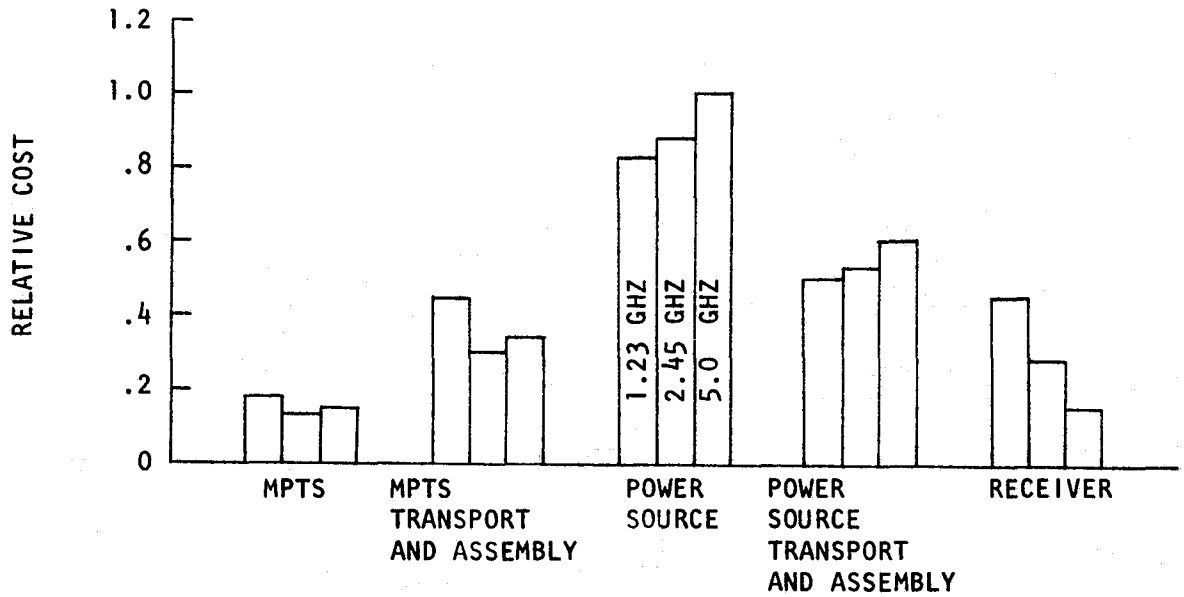

FIGURE 34 - RELATIVE RANKING OF SUBSYSTEM COSTS AND SENSITIVITY TO VARIATION IN FREQUENCY.

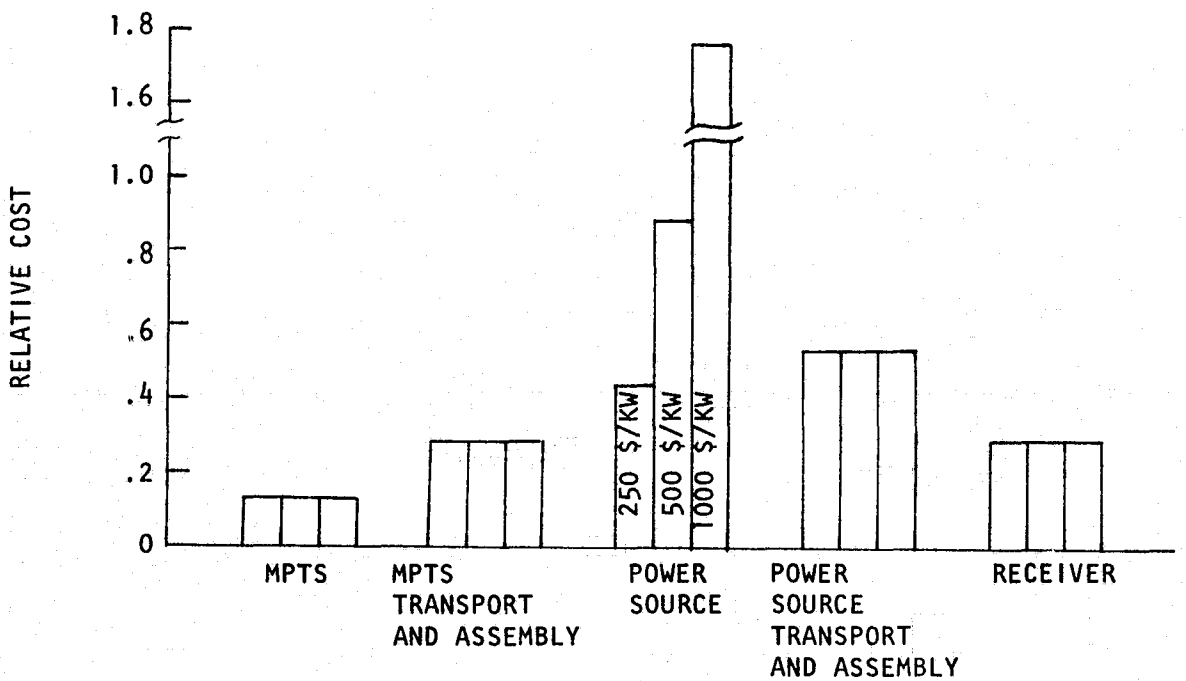

FIGURE 35 - RELATIVE RANKING OF SUBSYSTEM COSTS AND SENSITIVITY TO POWER SOURCE COST.

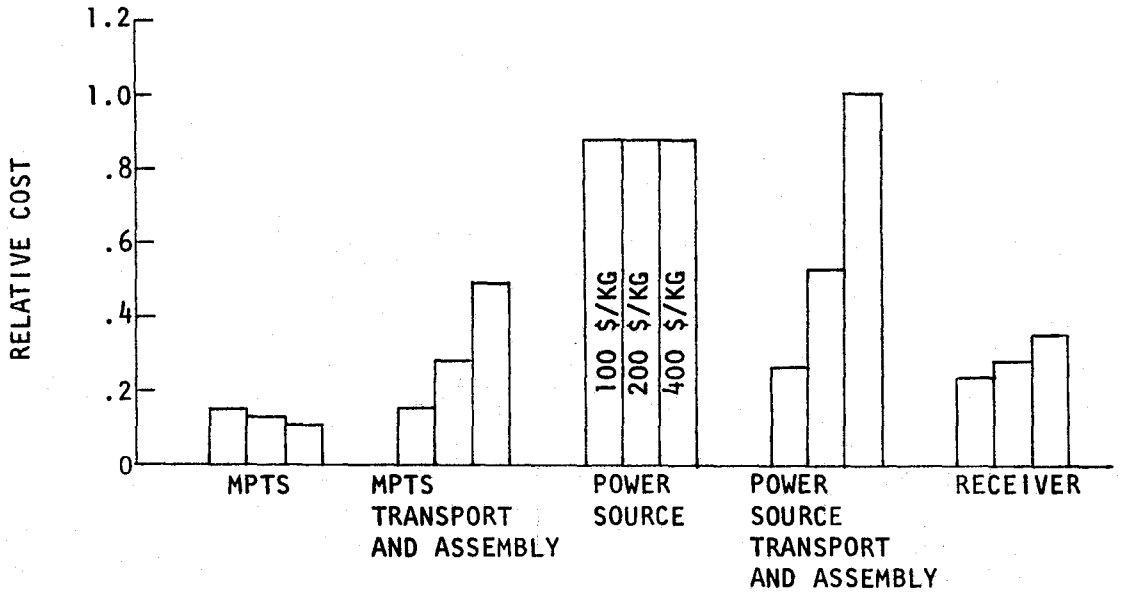

FIGURE 36 - RELATIVE RANKING OF SUBSYSTEM COSTS AND SENSITIVITY TO TRANSPORTATION AND ASSEMBLY COSTS.

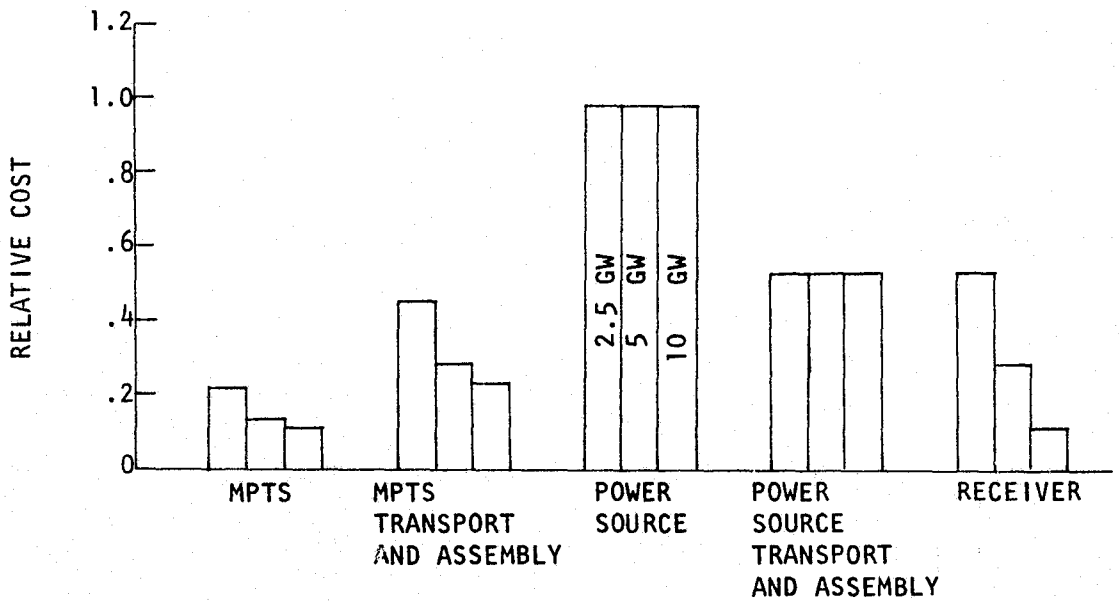

FIGURE 37 - RELATIVE RANKING OF SUBSYSTEM COSTS AND SENSITIVITY TO LEVEL OF DELIVERED POWER.

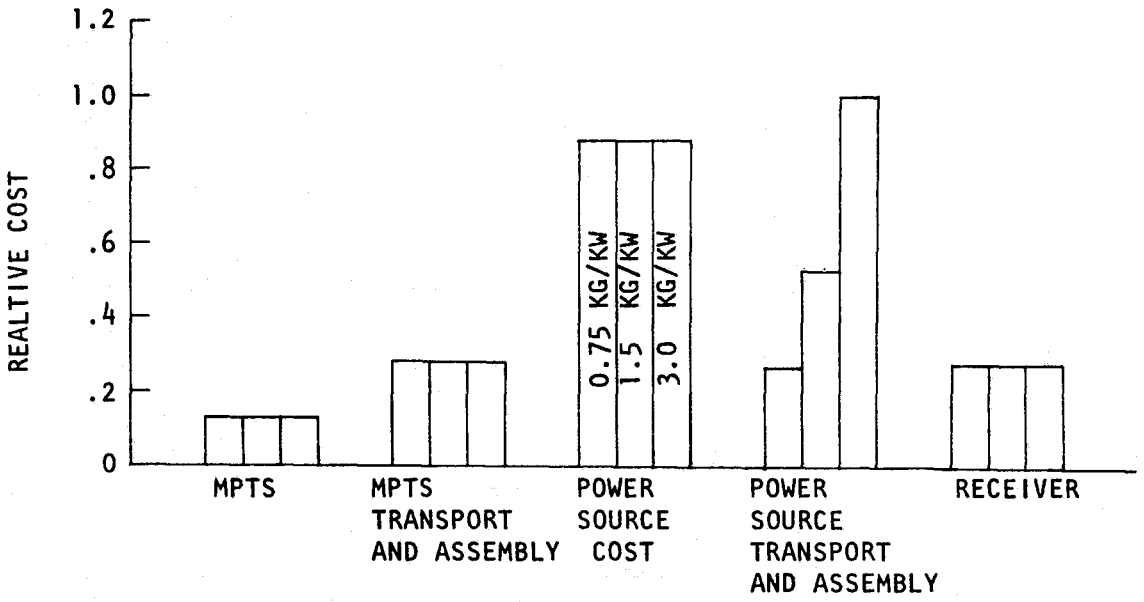

FIGURE 38 - RELATIVE RANKING OF SUBSYSTEM COSTS AND SENSITIVITY TO POWER SOURCE WEIGHT.